

2010

 TU Delft

 Materials
innovation
institute

Tailoring the Mechanical Properties of Titanium Alloys via Plasticity Induced Transformations

Tailoring the Mechanical Properties of Ti Alloys via Plasticity Induced Transformations

Suresh Neelakantan

Invitation
to attend the public
defence of my
Ph.D. dissertation

Tailoring the Mechanical Properties of Titanium Alloys
via Plasticity Induced Transformations

Time: **12:30 PM**

Date: **July 7 (Wednesday)**, 2010

Venue: Senaatszaal, Aula, TU Delft
Mekelweg 5, 2628 CD,
Delft, The Netherlands

*Prior to the defence there will be a short presentation (@ 12:00 noon)
on the contents of the thesis. A reception will be given after the defence.*

Suresh Neelakantan

Suresh Neelakantan
vnsuresh@gmail.com

ISBN 978-90-77172-57-5



9 789077 172575 >

Propositions belonging to the PhD thesis

Tailoring the mechanical properties of Ti alloys via plasticity induced transformations

by Suresh Neelakantan

1. The translation of design principles for TRIP effect in steels into those for PiTTi effect in metastable β titanium alloys is not straight forward. (this thesis)
2. The Mo equivalence for predicting the β phase stability in titanium alloys and the Andrews' equation for the M_s temperature in steels suggests a simple additivity rule to hold. However the M_s in multicomponent Ti alloys is not captured by such a rule. (Chapter 4, this thesis)
3. The Mo equivalence only gives a measure for the stability of β , from which the likelihood of martensitic transformation can be estimated. However, a physical model may lead to an accurate prediction of the M_s temperature. (this thesis)
4. Modelling metastable phase transformations remains a challenging task, especially in titanium alloys.
5. Metastable β alloy behaviour can broaden the application of titanium alloys from the typical high temperature and corrosive environments to complex shaped structural products.
6. Employing physical reasoning is the best way to understand a problem; however this does not necessarily mean the problem can be solved.
7. The increased usage of software programs to acquire experimental data simplifies work and reduces time, but at the risk of a reduced understanding of underlying principles of the apparatus and overconfidence in the reported data by the software.
8. The complexity involved in an Indian arranged marriage is no less than that of a doctoral research.
9. The open-mindedness and tolerant nature of Dutch people contradicts their attachment to traditional values.
10. Deformation (i.e. successive small step developments) and transformations (i.e. radical changes) are common phenomena in PiTTi alloys and PhD research.

These propositions are regarded as opposable and defensible, and have been approved as such by the supervisor Prof. dr. ir. Sybrand van der Zwaag

Stellingen behorende bij het proefschrift

Tailoring the mechanical properties of Ti alloys via plasticity induced transformations
van Suresh Neelakantan

1. De vertaling van de ontwerpregels voor TRIP staalsoorten naar die voor metastabiele β titanium legeringen die het PiTTi effect vertonen, is niet eenvoudig. (dit proefschrift)
2. Het Molybdeen equivalentiegetal voor de beschrijving van de stabiliteit van β titanium legeringen en de Andrew's vergelijking voor de martensiet start-temperatuur in staal suggereren een eenvoudig additiegedrag voor de effecten van de legeringselementen. De martensiet start-temperatuur van titanium legeringen met meerdere elementen wordt echter niet door dit additiegedrag beschreven. (dit proefschrift)
3. Het Molybdeen equivalentiegetal is een maat voor de stabiliteit van de β fase, van waaruit de waarschijnlijkheid van het optreden van een martensitische transformatie geschat kan worden. Een fysisch model kan echter tot nauwkeuriger schattingen van de martensiet start-temperatuur leiden. (dit proefschrift)
4. Het modelleren van het transformatiegedrag van metastabiele legeringen blijft moeilijk, in het bijzonder voor titanium legeringen.
5. Metastabiele β titanium legeringen kunnen het toepassingsgebied van titanium uitbreiden van dat voor hoge temperatuur en corrosieve toepassingen naar dat voor producten met een complexe vorm.
6. Het gebruik van fysische argumenten verbetert het begrip van veel problemen, maar leidt niet altijd tot een oplossing.
7. Het toegenomen gebruik van software programma's om experimentele data te verkrijgen leidt tot meer gemak en snelheid maar heeft het risico van een beperkter begrip van de werking van de apparatuur. Het kan daardoor leiden tot een overmatig vertrouwen in de door de software gepresenteerde meetresultaten.
8. De complexiteit van een gearrangeerd Indiaas huwelijk doet niet onder voor die van een promotieonderzoek.
9. De 'open' houding en tolerantie van 'de' Nederlander staat haaks op diens gehechtheid aan traditionele normen en waarden.
10. Ontwikkeling (d.w.z. een opeenvolging van kleine stappen) en transformaties (d.w.z. een radicale verandering) zijn beide gebruikelijke verschijnselen in zowel PiTTi legeringen als een promotieonderzoek.

Bovengenoemde stellingen zijn zowel opponeerbaar als verdedigbaar en zijn als zodanig goedgekeurd door de promotor, Prof. dr. ir. Sybrand van der Zwaag

**Tailoring the mechanical properties of Titanium
alloys via plasticity induced transformations**

Ph.D. Thesis
July 2010

Suresh Neelakantan

Cover designed by Suresh Neelakantan

The cover in the background shows the microstructure with α laths in the prior β grain boundaries and within the β grains of the above β solutionized followed by annealing in the below β regime of β -Cez alloy



This research was carried out as part of the innovation program of the Materials innovation institute (M2i) (formerly, the Netherlands Institute for Metals Research(NIMR)) on "Design of highly formable and ultra-strong alloys through Plasticity Induced Transformations in Titanium alloys (PiTTi)", project number: MC5.05206.

**Tailoring the mechanical properties of Titanium
alloys via plasticity induced transformations**

Proefschrift

ter verkrijging van de graad van doctor
aan de Technische Universiteit Delft,
op gezag van de Rector Magnificus Prof. ir. K.Ch.A.M. Luyben,
voorzitter van het College voor Promoties, in het
openbaar te verdedigen op woensdag 7 juli 2010 om 12:30 uur

door

Suresh NEELAKANTAN

Master of Science in Metallurgical Engineering
Indian Institute of Science, Bangalore, India
geboren te Chengalpattu, Provincie Tamilnadu, India

Dit proefschrift is goedgekeurd door de promotor:

Prof. dr. ir. S. van der Zwaag

Copromotor:

Dr. P.E.J. Rivera Díaz del Castillo

Samenstelling promotiecommissie:

Rector Magnificus,	voorzitter
Prof. dr. ir. S. van der Zwaag,	Technische Universiteit Delft, promotor
Dr. P.E.J. Rivera Díaz del Castillo,	University of Cambridge, UK, copromotor
Prof. dr. E. Gautier,	Ecole des Mines de Nancy, Nancy-Université, France
Prof. dr. W. Sha,	The Queen's University of Belfast, UK
Prof. dr. ir. J. Sietsma,	Technische Universiteit Delft
Prof. dr. E.H. Brück,	Technische Universiteit Delft
Prof. dr. ir. R. Benedictus,	Technische Universiteit Delft

Keywords: Titanium alloys, M_s temperature model, Alloy design, Thermodynamics, Martensitic transformation, Metastable β alloys, Mechanical properties

ISBN: 978-90-77172-57-5

Copyright © 2010 by Suresh Neelakantan

vnsuresh@gmail.com

All rights reserved. No part of the material protected by this copyright notice may be reproduced or utilized in any form or by any means, electronic or mechanical, including photocopying, recording or by any information storage and retrieval system, without appropriate permission from the author.

Printed by: Ipskamp Drukkers, Rotterdam, The Netherlands

To my family...

Contents

1	Introduction	1
1.1	Current trends in titanium alloys	1
1.2	Deformation induced martensite formation	5
1.3	Potential improvements	7
1.4	Scope and outline of the thesis	8
2	Experiments to verify PiTTi effect in β Ti alloys	11
2.1	Materials	12
2.2	Experimental Procedure	14
2.3	Solution treatment schemes	17
2.4	Characterization of the alloys	20
2.4.1	$\beta - \text{Ce}z$	20
2.4.1.1	Microstructure formation	20
2.4.1.2	Evaluation of mechanical properties	23
2.4.2	$Ti - 1023$	26
2.4.2.1	Microstructure kinetics	26
2.4.2.2	Evaluation of mechanical properties	30
2.4.2.3	X-ray structural analysis	34

2.5	Further characterization of properties in <i>Ti</i> – 1023	35
2.5.1	Nano indentation	35
2.5.2	Tribological properties	38
2.6	Conclusions	40
3	Defining factors of PiTTi effect in β <i>Ti</i> – 1023 alloy	41
3.1	Solute partitioning	42
3.2	Microstructural features	46
3.2.1	Grain size	46
3.2.2	α phase fraction	48
3.3	Deformation temperature	50
3.3.1	Experimental procedure	50
3.3.2	Compression testing results	51
3.3.3	Discussion	51
3.4	Conclusions	54
4	Thermodynamic prediction of M_s temperature in β Ti alloys	57
4.1	Need for thermodynamic based models	58
4.2	Ghosh-Olson model	59
4.3	Martensite formation in Ti alloys	61
4.4	Application of modified Ghosh-Olson model	63
4.4.1	β Ti-binary systems	63
4.4.2	Validation of M_s predictions	66
4.5	Extension to β Ti multicomponent systems	66
4.5.1	Development of M_s equation	67
4.5.2	Validation of M_s equation	69
4.6	Application of M_s model for <i>Ti</i> – 1023 experimental conditions . .	70
4.7	Conclusions	73

5	Design and characterization of the newly developed Ti alloys	75
5.1	Design of new alloy compositions	76
5.1.1	Design approach	76
5.1.2	Results and discussion	76
5.2	Alloy fabrication	81
5.3	Experimental details	84
5.4	Characterization of the new <i>Ti1023 – B</i> alloy	86
5.4.1	Results	86
5.4.1.1	Microstructure	86
5.4.1.2	Mechanical property evaluation	88
5.4.2	Discussion	90
5.4.2.1	Structural analysis	90
5.4.2.2	Comparison with <i>Ti – 1023</i>	90
5.5	Characterization of <i>Ti10551</i> alloy	92
5.5.1	Results	92
5.5.1.1	Microstructure	92
5.5.1.2	Mechanical property evaluation	96
5.5.2	Discussion	96
5.5.2.1	Structural analysis	96
5.5.2.2	Sub-ambient temperature compression testing	97
5.5.2.3	Optimization of <i>Ti10551</i> microstructures	99
5.6	Characterization of <i>Ti β – 21S</i> commercial alloy	102
5.7	Discussion	106
5.8	Conclusions	107

6 Comparison of TD and NN model M_s predictions in Ti alloys	109
6.1 Artificial neural network model	110
6.2 Application of ANN model	112
6.2.1 ANN predictions and validation of M_s	112
6.3 Comparison between thermodynamic and NN model predictions .	113
6.4 Identification of solute interactions	115
6.4.1 Method	115
6.4.2 Results and discussion	116
6.5 Conclusions	119
Summary	121
Samenvatting	127
Bibliography	131
Acknowledgements	141
Curriculum Vitae	145
List of Publications	147

Chapter 1

Introduction

1.1 Current trends in titanium alloys

Titanium and its alloys are relatively new in commercial applications; however, they slowly and steadily start to gain a unique position amongst other structural materials, like Fe-, Ni- and Al-based alloys. Being light weight, *i.e.* displaying a density between that of Al and Fe, highly corrosion resistant and thermally stable at high temperatures, Ti possesses superior structural efficiency in application areas such as airframes and aero-engines. Emerging lower cost processing technologies, along with strategies for improved strength-ductility relations, would aid in developing new Ti alloy grades that offer great potential as futuristic materials, fulfilling commercial demands.

Titanium alloys are commonly categorized as α , β and $\alpha + \beta$ based on predominant crystallographic phases present at room temperature [1]. The alloying elements, responsible for the stability of phases and their influence on the β -transus temperature, are classified as α -stabilizers, β -stabilizers and neutral [1, 2]. Each alloy category exhibits different mechanical properties as they differ in the individual properties of β (austenite) and α phases, their volume fraction and arrangement [1, 3]. Table 1.1 summarizes the range of properties for different Ti alloys and their dominant microstructural characteristics.

Table 1.1: Comparison of the different categories of Ti alloy properties, applications and microstructural features [1, 2, 3]. T_β is the β -transus temperature; YS is Yield Strength; UTS is Ultimate Tensile Strength; EI is Elongation.

	T_β ($^{\circ}C$)	YS (MPa)	UTS (MPa)	EI %	Applications	Critical microstructure features
α alloys	890-950	170-655	240-740	15-24	chemical, processing and Bio-medical	α morphology and colony size
$\alpha + \beta$ alloys	890-995	800-1200	900-1300	8-19	aircraft structures and aero-engines	Bi-modal and lamellar distribution of α and β
metastable β alloys	700-940	800-1200	800-1400	6-20	aerospace structures, landing gears	ω , β' , α' and α'' metastable phases, β grain size and grain boundary α

Low density α alloys, due to their single (stable) phase character, are insensitive to heat treatment, and hence offer little opportunities for strength improvement. They exhibit moderate tensile strength in the range of 240 to 740 MPa at room temperature, but possess excellent corrosion behaviour and formability. Being predominantly single phase alloys, they have good weldability and cold formability, but lack on toughness and age hardenability [4, 5]. Commercially pure (cp-) titanium with a range of oxygen levels is a popular α alloy, along with Ti-5Al-2.5Sn and Ti-3Al-2.5V alloys, which are mainly used in chemical and petrochemical industries [6, 7, 8, 9]. $\alpha + \beta$ alloys, especially Ti-6Al-4V, are by far the most popular type of titanium alloy. More than 50 % of all titanium alloys applications are of this type [2, 10, 11, 12]. These alloys are sensitive to heat treatment, and thus the combination of a wide range of possible microstructures offer the potential for tuning strength and ductility. However, the meticulous control of the α phase morphology for certain conditions is required. Having a two phase microstructure with different morphologies, they possess an exceptionally good balance of strength (900 to 1300 MPa), ductility, fatigue and fracture properties [13, 14, 15, 16, 17, 18, 19, 20, 21]. An advantage of these alloys is the superplastic formability for complex sheet metal applications [1, 22]. Common alloys in use are Ti-6Al-6V-2Sn, *Ti-6242* and *IMI-834* in particular for aircraft structural parts and aero-engines, in sporting goods and automobiles [5, 13]. Recent trends in $\alpha + \beta$ alloys focuses on grain refinement using Boron (B) or Nitrogen (N) additions for improved properties [23, 24, 25, 26].

β alloys are arguably the most versatile in the titanium family. They exist in two forms as metastable β alloys (in between β_c and β_s) and stable β alloys (beyond β_s) based on the β stabilizing content as shown in Figure 1.1 [27]. The β_c and β_s correspond to the critical β and stable β stabilizer content, respectively. The schematic pseudo binary phase diagram (Figure 1.1) reveals the importance of the β stabilizing elements on the stability level of β . In general, β alloys have a number of advantages over other Ti-alloy systems. Perhaps the most important one relates to their high cold formability, higher fatigue strength and improved bio-compatibility. Metastable β alloys possess processing advantages over the $\alpha + \beta$ alloys, owing to their low flow stress at elevated temperature. They offer the highest strength-to-weight ratio for engineering alloys, excellent hardenability and heat treatability, and hence provide significant improvements in both strength and

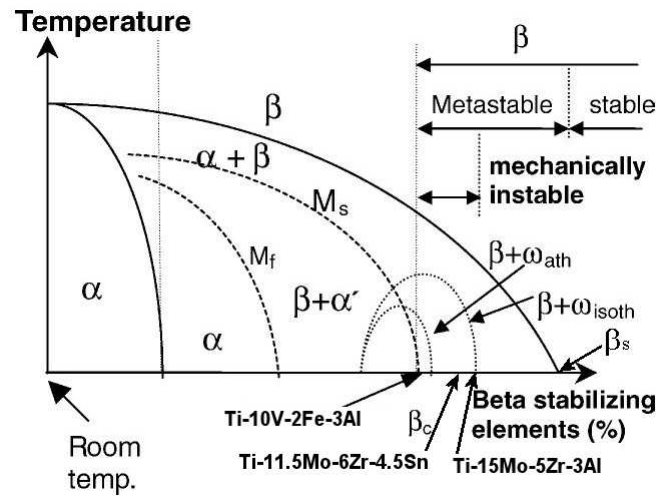


Figure 1.1: Pseudo-binary phase diagram of Ti with regions highlighting the different alloy categories and the decomposition products of β alloys.

toughness with enhanced uniform properties throughout the forgings [28, 29, 30, 31]. Some of the most commonly used metastable β alloys are Ti-10V-2Fe-3Al (*Ti-1023*), Ti-5Al-2Sn-2Cr-4Mo-4Zr-1Fe (β -*Cez*), Ti-15V-3Cr-3Al-3Sn (*Ti-15-3*), Ti-15Mo-2.6Nb-3Al-0.2Si (β -21S), Ti-11.5Mo-6Zr-4.5Sn (*Beta III*) and Ti-3Al-8V-6Cr-4Mo-4Zr (*Beta C*).

The importance of metastable β alloys has steadily increased over the last few decades, mainly because the wide range of complex microstructures enable the designer to optimize for both high strength and toughness [32, 33, 34, 35]. These alloys can be taken to extremely high strength levels beyond 1400 MPa, and can be improved further by effective control of the metastable phase formation. Metastable β alloys, in general, decompose into α (hcp), α' (hcp) martensite, α'' (orthorhombic) martensite and ω (hcp) metastable phases based on the cooling rate, initial alloy composition and β solute content Fig. 1.1 [27, 36, 37, 38, 39, 40, 41, 42]. The strength-ductility improvements mainly stem from the formation of martensite, while the other metastable phase, ω , is more detrimental to ductility [32, 43, 44, 45, 46, 47, 48]. Martensite formation can be tailored mainly by the heat treatment parameters that control the β stabilising contents in the range of me-

mechanically unstable β alloys as shown in Fig. 1.1. With increasing solute content the hexagonal (α' martensite) structure loses its symmetry and distorts to an orthorhombic (α'' martensite) structure [49, 50, 51, 52, 53, 54, 55, 56, 57, 58, 59, 60]. Such alteration of β stability by alloying helps in achieving an attractive range of properties. Wide spread application of β alloys is, however, limited by their relatively high specific weight, modest weldability, poor oxidation behaviour, high cost and complex microstructure.

1.2 Deformation induced martensite formation

Phase transformations resulting from the elasto-plastic deformation of metals or alloys have been known for a long time, for some systems they are intentionally used to improve properties. The formation of martensite under externally applied load is a well established deformation mode of several type of alloys resulting in Transformation Induced Plasticity (TRIP) mechanical effects [61, 62, 63, 64, 65]. The primary mechanism behind TRIP is the low temperature stress assisted transformation of a retained high temperature phase into martensite. Martensite is characterized by superior hardness and strength in steels [66]. The transformation upon deformation proceeds in the ductile phase progressing to a high strength crystal structure. Technological applications have been established in copper and equi-atomic titanium-nickel based systems, in which shape memory characteristics are exploited [67, 68]; and in TRIP steels, where relatively high ductility has been obtained [69, 70].

The TRIP effect, *i.e.* the mechanically induced martensitic transformation of metastable austenite, has been demonstrated to contribute very effectively to the deformation process in a large variety of fully austenitic iron-based alloys [71, 72, 73, 74]. Numerous studies have shown that the TRIP effect improves the strength-ductility balance by helping to maintain a high work-hardening rate during later stages of straining [61, 69, 70, 71]. This phenomenon is commonly ascribed to two different mechanisms: i) stress-assisted nucleation of martensitic variants favourably oriented with respect to the applied stress and ii) plastic straining of the surrounding phases due to the volume and shape changes associated

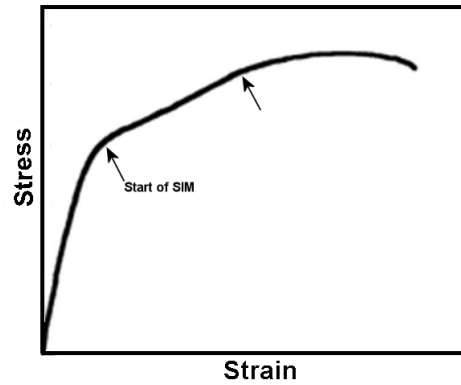


Figure 1.2: Schematic stress-strain characteristics of martensite formation in Ti alloys.

with the transformation, and due to the deformation itself. However, it should be pointed out that the martensite in Ti alloys is much softer than the martensite in ferrous alloys mainly because the interstitial oxygen atoms only cause a small elastic distortion of the hexagonal lattice of the martensite in Ti [1, 2]. Hence the stress-assisted martensite nucleation is the predominant mechanism in Ti alloys, which increases their ductility substantially above that of similar Ti alloys with other microstructures. The characteristics of martensite formation and the role played by stress have been reviewed by Grosdidier *et al.* [75].

In Ti alloys, when the martensite is stress induced, the stress-strain curve shows a double-yield effect as highlighted by the arrows in the schematic diagram shown in Fig. 1.2. The first yielding at low stress levels corresponds to the onset of stress-induced martensite (SIM) nucleation, after which an initial region of low work hardening rate associated with the progression of martensite throughout the gauge length is observed until the second yield point, where slip deformation initiates [76]. Plastic strain results from the deformation strain of the martensite together with subsequent slip accommodation in the parent β phase. Studies on Ti-Ta [36], Ti-V [44, 50, 77], Ti-Mo [49, 50], *Ti* – 1023 [29, 78], β – *Cez* [75], *Ti* – 10 – 12 [79] and *Ti* – 10 – 14 [80] alloys show the deformation characteristics are those of stress induced orthorhombic α'' martensite, which is associated with a shape strain of $\sim 7 - 8 \%$ [29, 48, 79, 80]. Such a TRIP like effect in Ti alloys

is further-on referred to in this thesis as Plasticity induced Transformation in Ti (PiTTi) alloys.

From an applications point of view, the strengthening behaviour of β titanium alloys by stress-induced martensite transformation at room temperature is a promising feature rapidly gaining importance for many potential applications in various fields. Detailed studies, upon tensile testing, on β -Cez and Ti-1023 have shown that the heat treatment parameters and sequence determine the deformation mechanism by α'' martensite formation [28, 75, 81, 82, 83, 84]. Indications on the dependence of prior β grain size, interaction of ω phase, athermal martensite start temperature (M_s) and solute concentration on formation of martensite have also been observed [28, 75, 76, 81, 85]. An important difference in titanium alloys, as compared to the ferrous systems, is the intrusion of ω phase, and the associated negative role of interstitials upon the deformation products [45].

1.3 Potential improvements

Over the past two decades, the strength-ductility increase in high strength steels has been a major research topic. Success has been achieved with ductility improvement through the TRIP effect as an additional strengthening mechanism in addition to solid solutioning, precipitation hardening and dual phase structures (see Fig. 1.3). Such improvements resulted in very strong and ductile yet cheap TRIP steel grades, for the production of intricate morphologies of automotive components.

Applying such concepts to Ti metallurgy would address the ductility levels while retaining their high strength levels. The potential of observing PiTTi effects for strength improvements is high in metastable β alloys as they exhibit a homogeneous and stable high temperature β regime, which can be retained in a metastable state to room temperature and thus have the potential to undergo martensite transformation upon loading. Optimizing the PiTTi effect for potential strength-ductility improvement depends mainly on tailoring various factors, athermal M_s temperature, β grain size, α phase fraction and β solute partitioning, through different thermo-mechanical treatment. However, no attempts to effectively control the factors in order to achieve an optimal mechanical performance

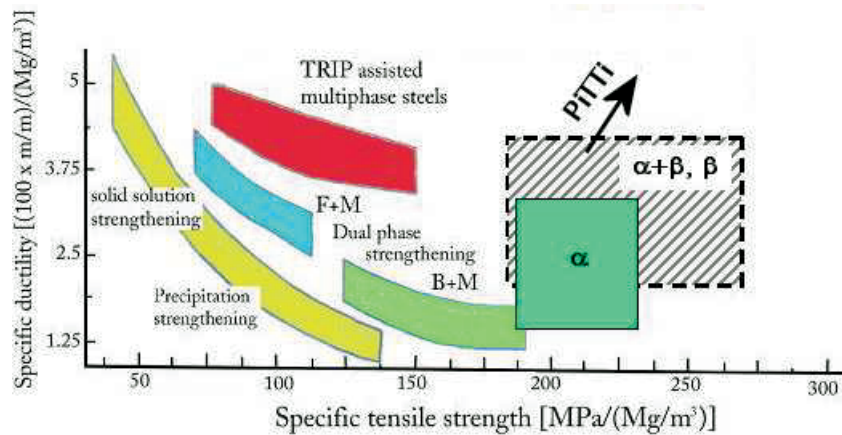


Figure 1.3: Schematic representation of the expected specific strength-ductility improvements for Ti alloys in comparison to steel grades.

due to PiTTi have been reported yet. The schematic representation of the targeted specific property improvements through PiTTi of existing metastable β or near β Ti alloys is also indicated in Fig. 1.3.

1.4 Scope and outline of the thesis

Stimulated by the possibility of enhancing the much demanded strength-ductility relation in titanium through the PiTTi effect, this thesis aims at identifying and quantifying the main factors that effectively control and promote the martensitic transformation in metastable β alloys. Considering the critical role of the athermal M_s temperature on PiTTi effect, a thermodynamic model for predicting the M_s temperature as function of binary solute concentration will be developed. Further, an equation for estimating the M_s temperature for generic multicomponent β alloys will be proposed. A novel alloy design methodology following the developed M_s equation along with β stability requirements will be presented. Such approach will be applied to design new grades of metastable β Ti alloys meeting the desired criteria for M_s , at or around room temperature with adequate β metastability. The prototype alloy compositions will be fabricated and experimentally characterized for validating the alloy design methodology.

Chapter 2 is focused on experimental investigations on existing commercial β – *Cez* and *Ti* – 1023 alloy systems in order to study their PiTTi behaviour for various solution treatment conditions. The corresponding microstructural features have been analyzed and linked to their influence on the SIM formation upon compression testing. The origin of the improved mechanical properties due to SIM has been studied with various characterization techniques.

Having observed the potential for tuning of the PiTTi effect in *Ti* – 1023, a comprehensive analysis of the fundamentals behind the PiTTi existence by reporting the various defining factors that could control/promote the SIM formation in *Ti* – 1023 is given in *Chapter 3*.

Considering the importance of the M_s temperature, *Chapter 4* presents a thermodynamic based model, following Ghosh-Olson’s approach for M_s in ferrous alloys, to predict the athermal M_s temperature for binary Ti systems. The binary predictions are validated with experimental M_s values. A further extension of the developed model is achieved by proposing a simple M_s equation for multicomponent Ti systems based on additivity rules, which is validated by correlating it to the so called Molybdenum equivalence values.

A novel alloy design methodology has been presented in *Chapter 5*, following the developed M_s equation from *Chapter 4* coupled with β stability estimations through the well established Molybdenum equivalence (Mo eq.) equation, resulting in proposing two new grades of potential PiTTi alloys. The fabrication of the prototype alloy compositions and their experimental characterization for the PiTTi properties is presented.

Chapter 6 further validates the predictions of the simple M_s equation by comparing them to the values predicted by an established neural network for M_s predictions for multicomponent Ti alloys. The mismatch between both model predictions in the composition domain has been analysed in terms of determining the effect of ternary solute interactions on the M_s , and some guidelines for a future extension of the thermodynamics based M_s model.

The main outcome of this thesis is finally presented as summary.

Chapter 2

Experimental verification of PiTTi effect in β – *Cez* and *Ti* – 1023 alloys

Deformation induced transformations are a widely observed phenomenon in several metallic systems. β titanium alloys, not being an exception, in principle has the ability to undergo such transformations. Related studies have shown that some near β and β metastable titanium alloys can undergo deformation induced martensitic or SIM transformation into α' (hcp structure) and/or α'' (Orthorhombic structure) [36, 44, 48, 50, 78, 84, 86] phases. Such formation of martensite upon loading depends on the microstructural state of the alloy, and in particular the austenite (β) phase stability [28, 43, 75, 84]. This mechanism, along with slip and twinning [87, 88, 89, 90], could result in improved strength-ductility properties. In analogy to ferrous alloys (multiphase steels)[91, 92], the ability of high temperature β phase to martensitically deform at room temperature can be controlled via well designed solution treatments [32, 48, 75]. Of prime importance is understanding the effects of the local alloying elements concentration variation and the deformation state, which results from various thermo-mechanical treatments [29, 93, 94]. These factors determine the ability to undergo SIM deformation at room temperature, which is the deformation mechanism behind the PiTTi effect.

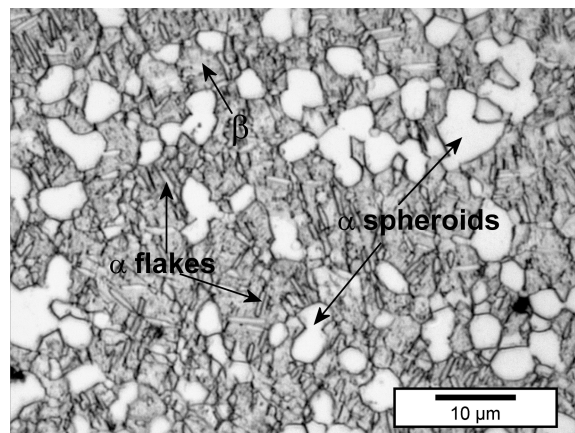
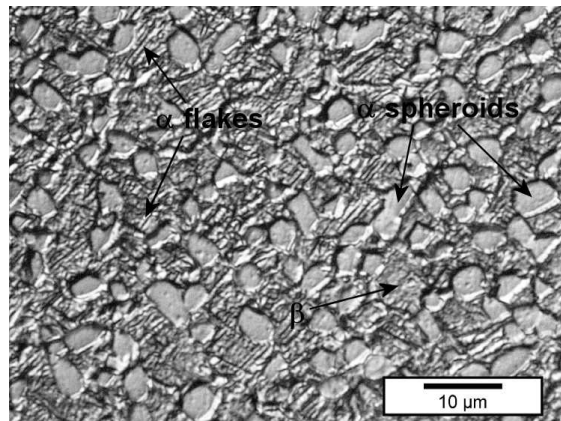
Generally, β metastable alloys show good response to solution treatments, and their microstructures can be modified reasonably well. This should permit the tuning of microstructural parameters in order to achieve an optimized PiTTi effect, improving mechanical properties [29, 75]. This chapter deals with studying the occurrence of stress-induced martensite in two commercial β alloys. Various solution treatments resulting in distinctive microstructural features have been considered to study their influence on PiTTi behaviour, which is evaluated using compression testing, and further analysed with different experimental physical characterization techniques.

2.1 Materials

The Ti alloys that are of interest for the deformation induced transformation studies are from the β alloy family as they can retain metastable β phase at room temperature upon quenching. The present study considers two commercially important alloy systems. One is Ti-5Al-4Zr-4Mo-2Cr-2Sn-1Fe (wt.%) alloy (further referred to as β -Cez), which was obtained from Cezus company, France. The β -transus temperature of this alloy is 878 ± 5 °C [75, 84]. The other alloy is the near β -metastable Ti-10V-2Fe-3Al (wt.%) - henceforth referred to as *Ti*-1023, which was obtained from TIMET, Germany. The β -transus temperature of this alloy is 795 ± 5 °C [28, 29]. The chemical analysis as provided with both the alloys is listed in Table 2.1. Both alloys display a bimodal $\alpha+\beta$ microstructure in the as-received condition, Figs. 2.1a and 2.1b, respectively. For *Ti*-1023, the as-received pancake structure had been obtained under unspecified conditions at the production site by i) forging the ingot at β -transus + 30 °C temperature, and then at 750 °C, where the bi-modal distribution was formed; this was followed with ii) a heat treatment at 760 °C for 1 h, water quenched and then aged at 525 °C for 8 h and air cooled. For the β -Cez alloy no information about the manufacturing route has been obtained.

Table 2.1: Chemical composition (in wt.%) of the considered β alloys.

Alloys	Al	V	Fe	Cr	Mo	Zr	Sn	O	N	C	Ti
β -Cez	4.9	-	0.93	2	3.99	4.37	2	0.099	0.005	0.006	bal.
Ti-1023	3	9.8	1.9	-	-	-	-	0.11	0.01	0.007	bal.

(a) Bi-modal distribution of α and β phases in β -Cez(b) Bi-modal distribution of α and β phases in Ti-1023Figure 2.1: As-received microstructures of considered β alloys.

2.2 Experimental Procedure

Machining and polishing

The as-received material was shaped into cylindrical samples of 4 mm diameter and 7 mm length using electrical discharge machining (EDM). The EDM affected sample surface layer was removed prior to further experimentation. Microstructural observations of all samples were made after the following steps.

i) Electropolishing: In order to avoid any transformation of metastable β phase to martensite during mechanical polishing, electropolishing was used. A solution of 36 ml perchloric acid, 390 ml methanol, 350 ml ethylene glycol and 24 ml water has been used to erode the sample surface at 45 V for 30 s using a Struers electropol setup. The solution bath is maintained at 5 °C.

ii) Etching: Standard Kroll's reagent (3 ml HF + 6 ml HNO₃ + 100 ml water) etchant for β Ti alloys has been used for revealing the various phases. Typical etching time was 10 - 20 s.

Solution treatments

The cylindrical samples of both alloys were solution treated at several temperatures and times in the β and/or $\alpha+\beta$ domains using a Bähr 805 horizontal dilatometer at a vacuum level of 10^{-5} mbar approximately, and helium (He) gas quenched at a high rate to room temperature. Heating to the solutionizing temperature, and cooling to the $\alpha + \beta$ temperatures from β regime was done at a rate of 10 °C/s. A thermocouple was spot welded to the sample longitudinal surface to record its temperature.

Compression

Stress-induced martensite formation ability of the alloys after subjecting them to various solution treatments has been assessed by compression testing in a Gleeble® 1500 thermo-mechanical machine. Per condition 3 samples were deformed at room

temperature to different strain levels ranging from 5 to 40 % at a strain rate of $10^{-3} s^{-1}$. In order to avoid friction between the anvils and the sample surface, a lubricant (Lubriplate - white grease) was used.

Microscopic analysis

The observation of various phases, their morphology and distribution along with other features of the polished and etched samples was carried out using a Leica DM LM microscope with a Leica DC300 camera. The longitudinal cross-section of the sample was observed. High resolution microscopic analysis was performed using scanning electron microscopy JEOL JXA 8900R coupled with an energy dispersive spectrometer (EDS).

Structural analysis

The identification of the various phases in the samples subjected to different conditions was carried out using X-ray diffraction (XRD) with Co K_{α} radiation at room temperature. XRD data were taken from the longitudinal cross section of the samples in the 2θ range from 30 to 130 degrees.

Nano indentation

Nano indentation using a CSM Instruments nano hardness tester was performed to measure the mechanical properties of the individual phases. A Berkovich diamond indenter applying a maximum load capacity of 10 *mN* at a loading/unloading rate of 20 *mN/min* was used for the indentation studies. A 10 *s* hold time after reaching the maximum load was maintained. Matrices of indents of various dimensions were made in the cross-sectional surface of cylindrical samples, which were mounted in a cold setting resin.

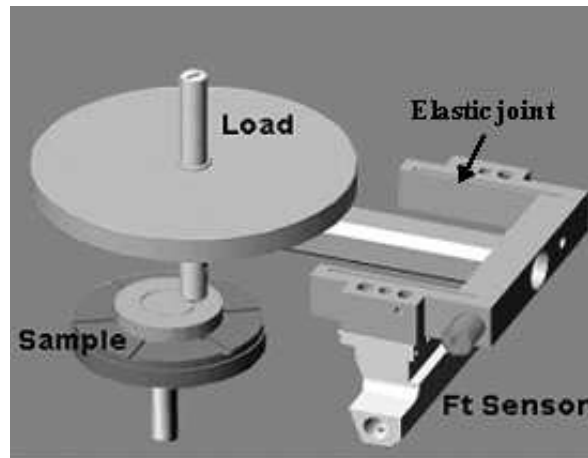


Figure 2.2: Schematic diagram of the Pin-on-disc Tribometer.

Wear test

Experiments to evaluate the friction and wear behaviour were performed on a pin-on-disc tribometer in contact with AISI 52100 hardened steel. The ball on disc geometry has been chosen to avoid misalignment problems. The schematic pin-on-disc setup used for the experiments is shown in Figure 2.2.

The sample disc is mounted on a holder driven by a motor. The motor is computer controlled, and by using built-in software one can determine the sliding velocity and the distance or the number of revolutions applied to the test. A ball shape counter body is mounted in a ball holder that is attached to a very stiff arm in normal direction which is held by two elastic joints flexible in lateral direction. The frictional force is obtained from the displacement experienced at the end of the elastic joint (Fig. 2.2). The normal load is applied by placing a corresponding mass on top of the pin holder. In order to obtain constant test conditions the tribometer was placed in a controlled environment with the temperature set at 23 °C and the relative humidity at 40 %. The sample discs were polished to a root mean square (RMS) value of less than 0.1 μm . Commercially available 10 and 20 mm steel balls (AISI 52100) were used as counterface. Both discs and balls were cleaned ultrasonically in isopropanol for 10 min and then rinsed with water and dried at 110 °C for 20 h prior to use. Per condition 3 samples were tested. Each test was carried

out for 1 km sliding distance. To study the wear behaviour, the same tests were done for both dry and lubricated conditions, where Vitrea 9 as lubricant was used in all lubricated tests. The wear volumes of the disc and the balls were measured using optical and interference microscopy.

2.3 Solution treatment schemes

The solution treatment is categorized into three domains: above β , below β and $\beta+(\alpha+\beta)$, depending on the chosen temperature (Fig. 2.3). Generally, the above β treatment is considered as the one dealing with various temperatures and/or times within the homogeneous β regime, *i.e.* above the β transus temperature. The highest β temperature was chosen so as to avoid significant grain growth. The below β treatment considers various temperatures and/or times in the $\alpha + \beta$ regime, *i.e.* below the β transus temperature, in order to cover the entire $\alpha + \beta$ domain. The $\beta+(\alpha+\beta)$ treatment considers various temperatures and/or times from both the homogeneous β , and the $\alpha + \beta$ regime. Homogenization at above β is followed with a controlled cooling to $\alpha + \beta$ regime, where annealing at the desired temperature is performed. The temperatures were chosen such that proper solute redistribution in a modest annealing time (60 min) could be achieved. The schematic diagram shows the different regimes of the solution treatments mentioned above (Fig. 2.3). At the β and $\alpha + \beta$ temperatures, several holding times were considered in order to study the alloy kinetics. It is to be noted that the estimated β transus temperature for $\beta - \text{Cez}$ and $Ti - 1023$ is $878 \pm 5^\circ\text{C}$ and $795 \pm 5^\circ\text{C}$, respectively. The various solution treatment temperatures, times considered within each regime are tabulated for the $\beta - \text{Cez}$ (Table 2.2) and $Ti - 1023$ (Table 2.3) alloys, respectively. The solution treatments and the β transus determination were performed using dilatometer.

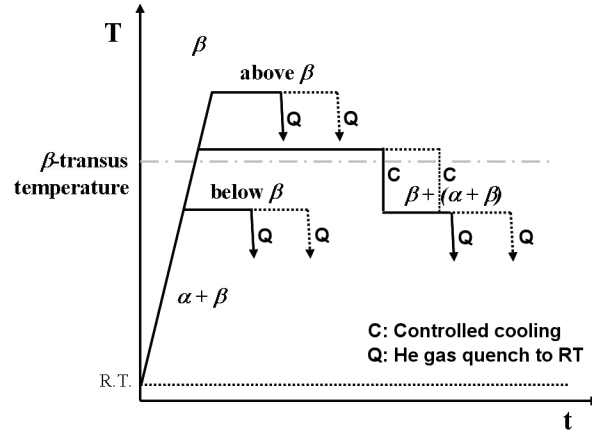


Figure 2.3: The schematic solution treatment diagram at various phase regimes.

Table 2.2: Solution treatment temperature and time considered for $\beta - \text{Cez}$.

Temperature domain	Solution treatment schemes		Cooling mode
	Temperature ($^{\circ}\text{C}$)	Soaking time (<i>min</i>)	
β	920	15, 60 and 1440	He gas quench
	1020	15	He gas quench
	1120	15	He gas quench
$\alpha + \beta$	850	180	He gas quench
	820	15	He gas quench
	750	180	He gas quench
	720	15	He gas quench
$\beta + (\alpha + \beta)$	920	60	Controlled Cooling
	850	7.5, 15 and 60	He gas quench
	920	60	Controlled Cooling
	750	7.5, 15 and 60	He gas quench
	920	60	Controlled Cooling
	650	7.5 and 15	He gas quench

Table 2.3: Solution treatment temperature and time performed for *Ti – 1023*.

Temperature domain	Solution treatment schemes		Cooling mode
	Temperature ($^{\circ}C$)	Soaking time (<i>min</i>)	Helium (He) gas quench
β	900	15, 60, 120 and overnight	He gas quench
	1000	15	He gas quench
	1100	15 and 60	He gas quench
	820	15	He gas quench
$\alpha + \beta$	700	15	He gas quench
	900	60	Controlled Cooling
$\beta + (\alpha + \beta)$	750	60	He gas quench
	900	60	Controlled Cooling
	650	60	He gas quench
	900	15 and 60	Controlled Cooling
	700	15 and 60	He gas quench
	900	15	Controlled Cooling
	650	15 and 60	He gas quench
	900	15	Controlled Cooling
	750	15 and 60	He gas quench

2.4 Characterization of the alloys

2.4.1 $\beta - \text{Cez}$

The influence of various solution treatments (Table 2.2) on the microstructure kinetics of metastable β alloy for potential PiTTi effect has been studied. The various microstructural features related to PiTTi properties are categorically analysed after selecting solution treatment temperatures in the β , $\alpha + \beta$ and $\beta + (\alpha + \beta)$ phase fields.

2.4.1.1 Microstructure formation

β phase field The above β -transus experiments were conducted at several temperatures ranging from 920 to 1120 °C for various timings from 15 min to 24 h (Table 2.2). The as-quenched microstructure of the alloys shows coarse retained β grains at room temperature [75], without any visible transformations (Fig. 2.4). This alloy seems to have enough β stability in order to retain it down to room temperature. Samples treated at different temperatures and times within the β regime show a uniform β phase with a more or less constant grain size of 300 - 450 μm (Figure 2.4).

$(\alpha + \beta)$ phase field A bi-modal mixture of α and β phase microstructures was observed for the below β -transus treatments (Table 2.2). α appears in different morphologies as i) globules and ii) laths, embedded within a β matrix [75]. With an increase in temperature or time, within the $\alpha + \beta$ domain, α laths dissolve leaving only globular α microstructures and retained β domains (Figures 2.5a and 2.5b). For temperatures far below β transus, in the $\alpha + \beta$ regime, with a longer holding times, a lower volume fraction of retained β is observed (Figures 2.5c and 2.5d), mainly because of the increased equilibrium α phase fraction.

$\beta + (\alpha + \beta)$ phase field This treatment involves β homogenization followed by cooling to $\alpha + \beta$ field before quenching to room temperature. The microstructures after these treatments (Table 2.2) exhibit different features (Figure 2.6). Intermediate annealing at $\alpha + \beta$ resulted in a more promising microstructure. Predominantly

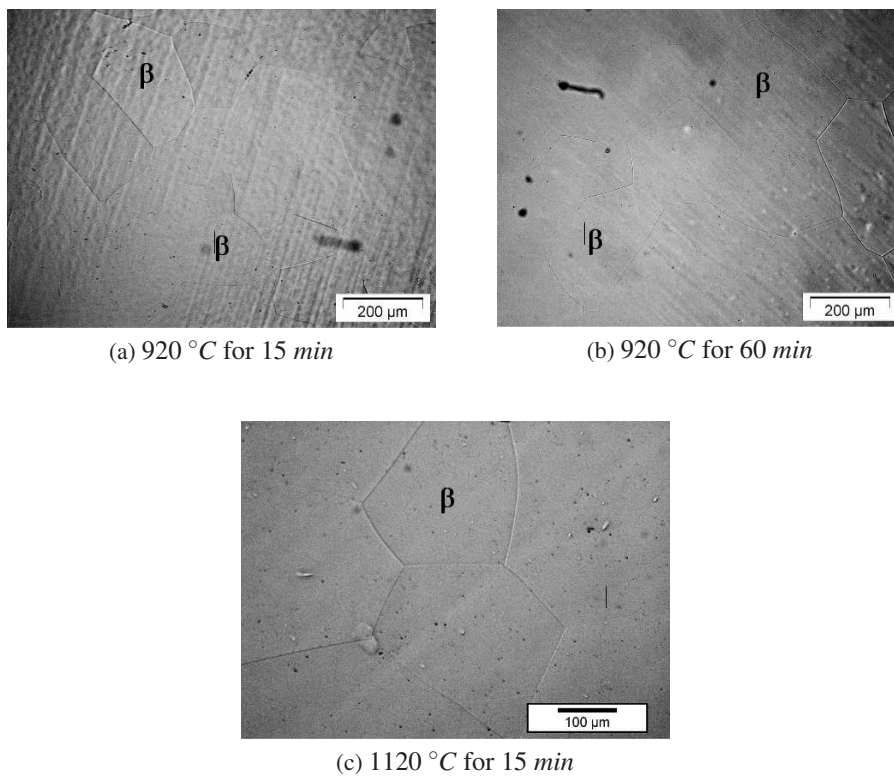


Figure 2.4: Microstructure kinetics of the above β solution treatments of β – Cez.

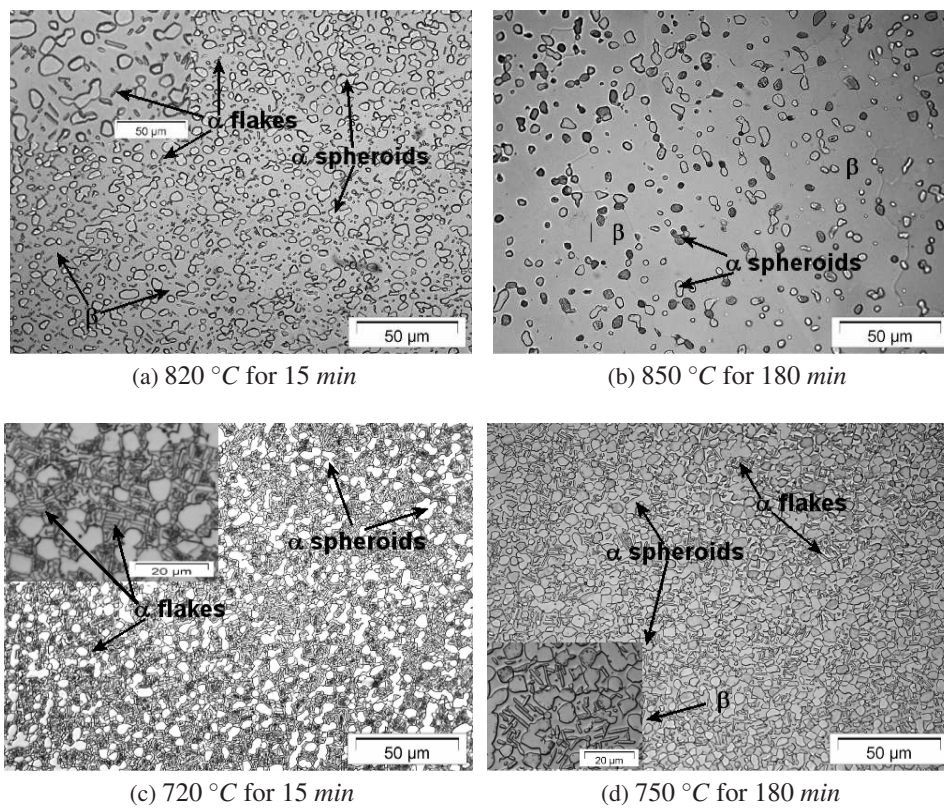


Figure 2.5: Microstructure kinetics of the below β heat treatments of β -CeZ; The insets show the magnified view of the features.

Table 2.4: Selected solution treatments of β - Cez for PiTTi analysis.

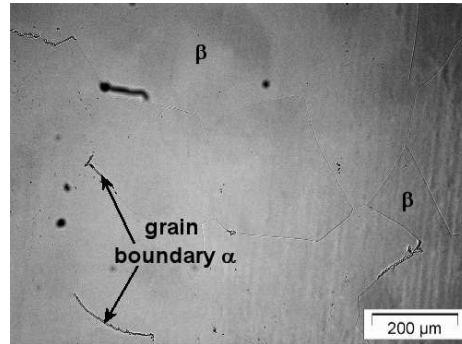
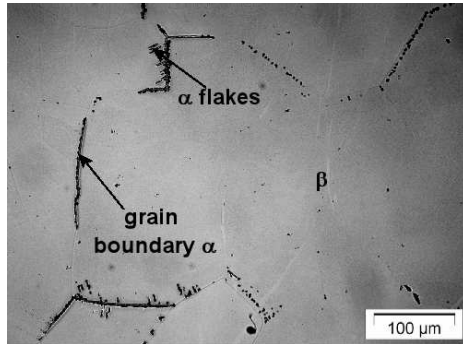
Solution treatment condition	Temperature regime	Further reference name
920 °C - 60 min	above β	Cez1
850 °C - 180 min	below β	Cez2
920 °C - 60 min/750 °C - 15 min	$\beta + (\alpha + \beta)$	Cez3

large retained prior β grains along with smaller α grains possessing different morphologies (laths and Widmanstätten) have been observed, Fig. 2.6 [83]. α Widmanstätten is observed at the prior β grain boundaries. Increasing temperature and/or time within the β regime results in larger prior β grains. Within such β grains, depending on the chosen temperature and/or time in the $\alpha + \beta$ regime, both α morphologies form. The upper $\alpha + \beta$ temperatures *i.e.* just below β transus, result in more untransformed metastable β domains (Figure 2.6a and Figure 2.6b) upon quenching as compared to the lower $\alpha + \beta$ temperatures far below β transus (Figs.2.6c, 2.6d and 2.6e).

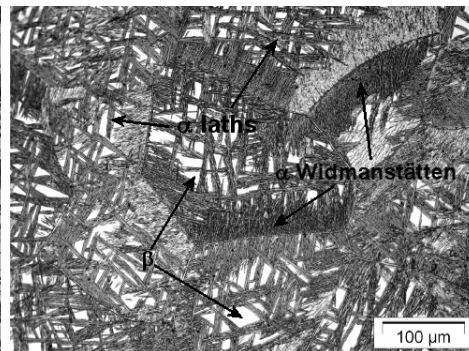
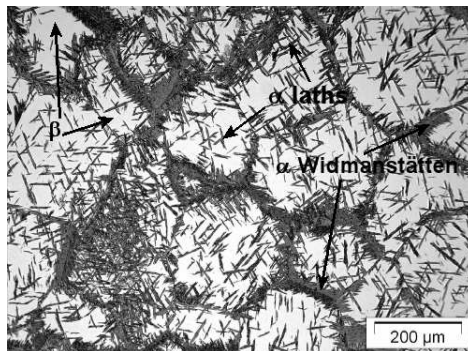
Based on the above detailed microstructural analysis of the various solution treatments a representative condition corresponding to each regime has been considered. The solution treatment conditions that have been considered for further analysis on PiTTi occurrence are given in Table 2.4. X-ray analysis of the selected treatments confirm the presence of α and β phases, Fig. 2.7.

2.4.1.2 Evaluation of mechanical properties

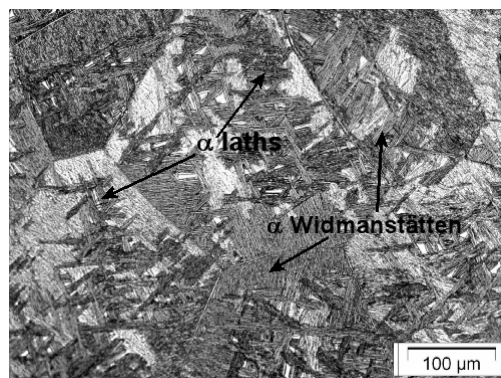
Stress - Strain curve The selected solution treated microstructures (Table 2.4), representing each phase regime, were compression tested in a Gleeble[®]1500 machine to evaluate their SIM formation capability. The samples Cez1, Cez2 and Cez3 were tested. Corresponding stress-strain curves are shown in Figure 2.8. There is no clear indication of martensite formation, generally reflected by the double-yield point like behaviour in stress-strain curves upon loading. Moreover, the different solution treatments with variations in microstructural features do not result in significant changes in their mechanical properties. Thus based on the



(a) 920 °C for 60 min and 850 °C for 15 min (b) 920 °C for 60 min and 850 °C for 60 min

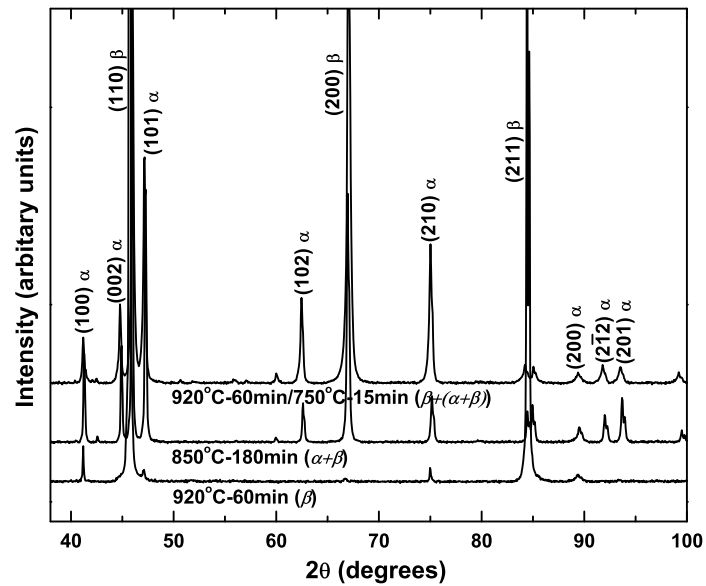
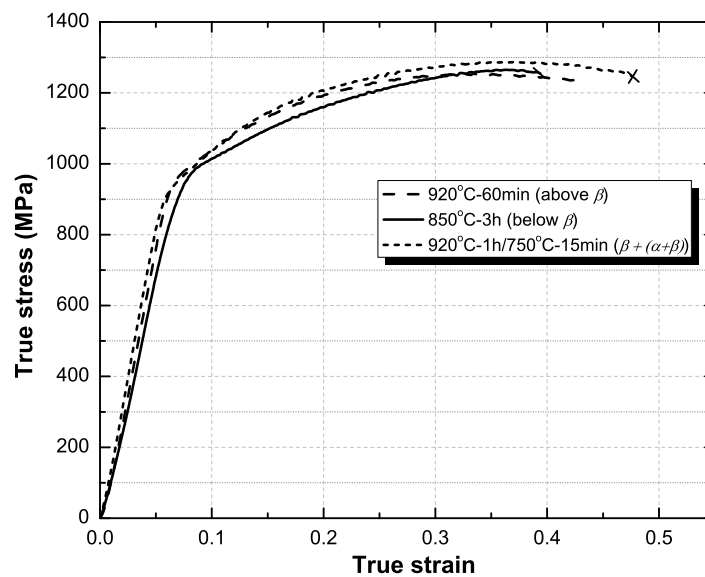


(c) 920 °C for 60 min and 750 °C for 7.5 min (d) 920 °C for 60 min and 750 °C for 15 min



(e) 920 °C for 60 min and 750 °C for 60 min

Figure 2.6: Microstructure kinetics of $\beta + (\alpha + \beta)$ solution treated $\beta - \text{Ce}_z$ alloy.

Figure 2.7: X-ray analysis after the selected treatments on β – Cez.Figure 2.8: Compressive stress-strain curves after various solution treatments of β – Cez alloy.

stress-strain response the $\beta - \text{CeZ}$ alloy does not seem to exhibit any PiTTi effect. Moreover, the different solution treated microstructures do not show any noticeable change in mechanical properties.

2.4.2 $Ti - 1023$

A detailed study to determine the influence of various solution treatments (Table 2.3) on the microstructure kinetics has been carried out. Similar to $\beta - \text{CeZ}$, the various microstructural features related to PiTTi properties are categorically analysed corresponding to each phase regime. The solution treatment temperatures were chosen within the β , $\alpha + \beta$ and $\beta + (\alpha + \beta)$ phase regimes.

2.4.2.1 Microstructure kinetics

β phase field The above β -transus treatments were conducted at various temperatures ranging from 800 to 1100 °C (Table 2.3), for different times ranging from 15 min to a few hours. Predominantly retained metastable β phase along with athermal martensite are the typical quenched microstructural features at room temperature of the above β treated samples (Figure 2.9). Similar results were reported by Duerig *et al.* [29]. Temperature variations within the β regime led to microstructures differing in grain size and the volume fraction of the athermal martensite. In general, higher temperatures or longer times were found to result in larger β grain size with a lower volume fraction of athermal martensite (Fig. 2.9c). Their presence is restricted to the neighbourhood of grain boundaries.

$\alpha + \beta$ phase field The below β -transus treatment of the as-received material was performed at 700 °C for 15 min. This treatment resulted in a bi-modal microstructure with a mixture of α and β phases. α appears in different morphology: i) in globular form and ii) as laths embedded in a β matrix. The microstructure of the alloy is shown in Figure 2.10. Further, with increasing temperature or time within the $\alpha + \beta$ domain, the α laths dissolve, resulting in only globular α with a lower volume fraction and more retained β domains [48].

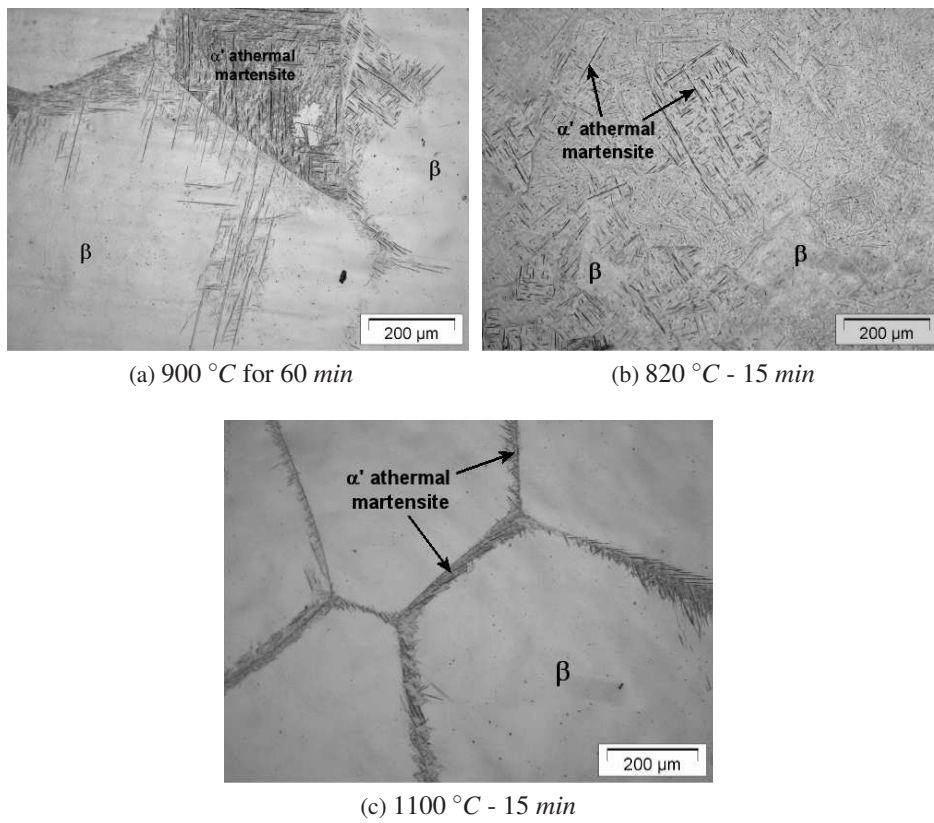


Figure 2.9: Microstructure kinetics of the above β solution treated $Ti - 1023$ sample.

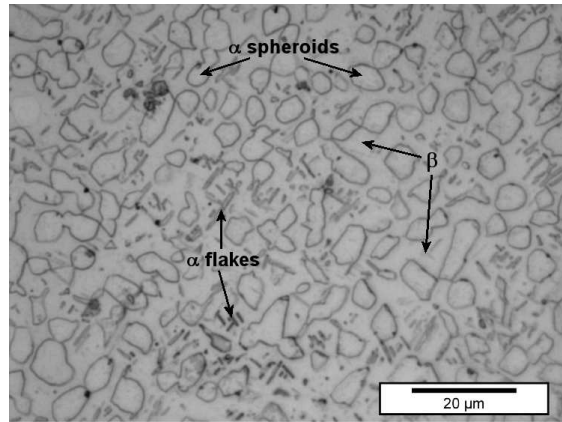
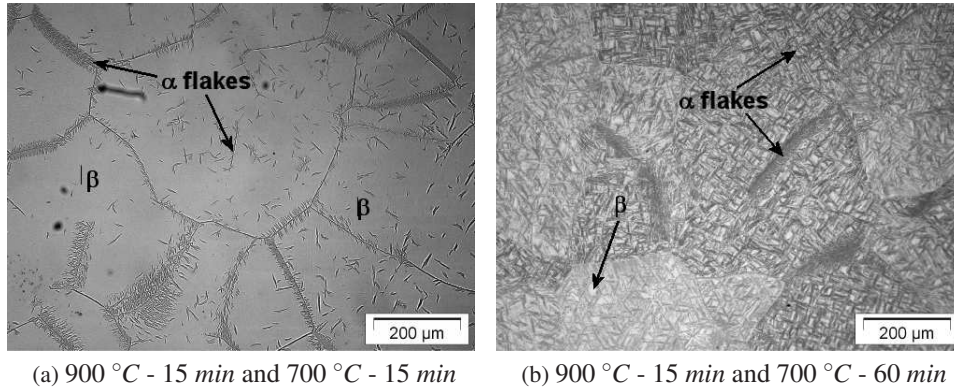


Figure 2.10: Microstructure of the 700 °C for 15 min ($\alpha+\beta$) solution treated Ti – 1023 sample.

$\beta+(\alpha+\beta)$ phase field Table 2.3 lists the heat treatment temperatures and times explored in this domain. The quenched samples show predominantly the α phase possessing different morphologies: laths inside the grains and Widmanstätten near prior β grain boundaries [95]. Higher temperatures or longer times within the β field resulted in larger prior β grains. Within the β grains, depending on the temperature and time in the $\alpha+\beta$ regime, α of both morphologies fill the grains. For instance, at the 700 °C $\alpha+\beta$ temperature (just below β transus temperature) shorter soaking time resulted in more untransformed metastable β domains (Figure 2.11a) upon quenching as compared to the longer time at the same temperature, Fig. 2.11b. Hardly any metastable β phase remain for the long time soaked $\alpha+\beta$ temperature.

The microstructural response to the different solution treatment schemes is an aid to tailor its plastic deformation capability. From microstructural analysis of the various solution treatment conditions, a representative condition corresponding to each regime is considered and tabulated below for further characterization towards observing optimum PiTTi properties. X-ray analysis of the selected heat treatments show the presence of β , α and martensite (α' , α'') phases as shown in Figure 2.12 and the corresponding crystal parameters are listed in Table 2.5.

Figure 2.11: Microstructure kinetics of $\beta + (\alpha + \beta)$ solution treated *Ti* – 1023 alloy.Table 2.5: Lattice parameters of selected solution treated *Ti* – 1023 samples.

		Lattice parameters (Å)		
		900 °C - 60 min	700 °C - 15 min	900 °C - 15 min/ 700 °C - 15 min
β	<i>a</i>	3.2433	3.2339	3.2355
α	<i>a</i>		2.933	2.9396
	<i>c</i>		4.6764	4.6582
α'	<i>a</i>	2.9190		2.9532
	<i>c</i>	4.6770		4.4887
α''	<i>a</i>	3.02		2.9992
	<i>b</i>	4.985		4.9222
	<i>c</i>	4.356		4.3598

Table 2.6: Selected solution treatments for PiTTi analysis in *Ti* – 1023.

Solution treatment condition	Temperature regime	Further reference name
900 °C - 60 min	above β	Sample A
700 °C - 15 min	below β	Sample B
900 °C - 15 min/700 °C - 15 min	$\beta + (\alpha + \beta)$	Sample C

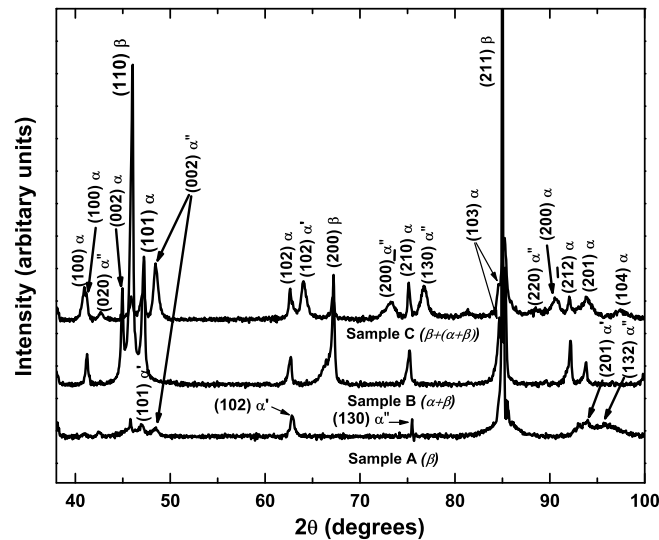


Figure 2.12: X-ray analysis showing the presence of desired phases in the selected heat treatments.

2.4.2.2 Evaluation of mechanical properties

Stress-Strain curve The selected microstructures (Table 2.6), representing each phase regime, were compression tested to evaluate their deformation induced martensite formation ability. Samples A) 900 °C - 60 min (above β), B) 700 °C - 15 min ($\alpha + \beta$) and C) 900 °C - 15 min/700 °C - 15 min ($\beta + (\alpha + \beta)$) were compression tested in a Gleeble[®]1500. Each sample was compressed to various strain levels ranging from ~5 to ~40 %. Figure 2.13 shows selected stress-strain curves for the as-received condition and samples A, B and C. Sample A was stopped before failure at ~35 % strain, samples B and C failed by macroscopic shearing. Samples A and C, which involve β homogenization, show a double yield point-like behaviour that is absent in sample B. Such a double yield phenomenon is ascribed to martensite formation producing the PiTTi effect [28, 48]. Further, samples A and C show an increase in strength by a noticeable amount (~20%), while still retaining a reasonable compressive failure strain (Table 2.7). Contrary to samples A and C, the multiphase microstructures of the as-received sample and sample B do not show the double yield behaviour [28], ruling out the work hardening change to

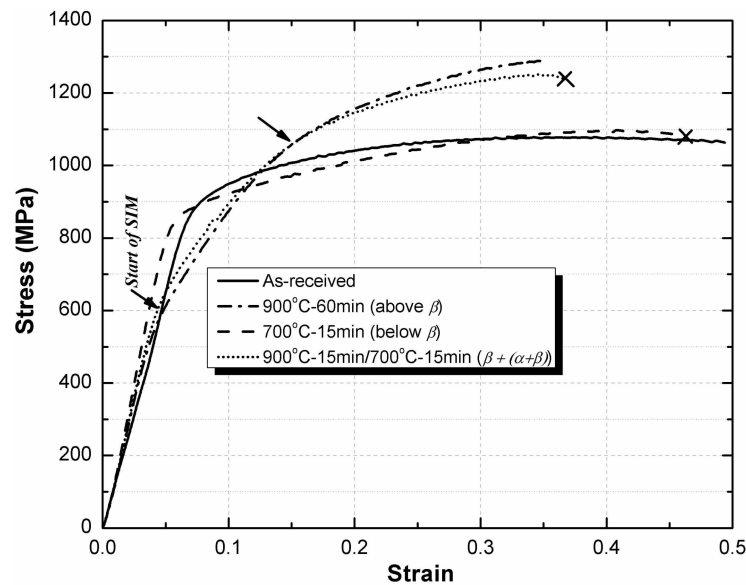


Figure 2.13: Compressive stress-strain curve of *Ti* – 1023 alloy.

be due to transformation plasticity. However, this particular treatment has shown large failure strain, although lower strength than the heat treatments leading to a PiTTi effect (Table 2.7).

The formation of SIM seems to be intrinsically related to the metastability of the β grains [28, 48, 75]. The results show that PiTTi effect stems from a number of microstructural factors derived from prior solution treatments. β undergoes SIM formation as confirmed by the double yield point, which is accompanied by an increase in alloy strength of approximately 20 % (Fig. 2.13). The nature of the SIM formed is α'' orthorhombic [28, 29]. The strength increase may be due to the work hardening of the SIM, which displays a change in the strain hardening exponent. Figure 2.13 demonstrates that SIM is also formed in a $\beta + (\alpha + \beta)$ microstructure (Sample C), displaying similar double yield behaviour and peak strength. The solute concentration in the β phase seems to be consistent with that required to form SIM. $\beta + (\alpha + \beta)$ microstructures display a larger degree of complexity. Higher $(\alpha + \beta)$ temperatures (700°C) combine β , martensite, Widmanstätten α and α flakes; the volume fraction of α increases by reducing the $(\alpha + \beta)$ temperature, increasing the concentration of β stabilisers, and reducing the likelihood of SIM

Table 2.7: Mechanical properties of *Ti* – 1023.

Condition	Martensite formation stress (σ_m) MPa	Yield stress MPa	Ultimate strength MPa	Strain to failure %
as-received	-	~920	~1060	49 (no failure)
Sample A	~550	~1100	~1300	35 (no failure)
Sample B	-	~860	~1100	47
Sample C	~670	~1125	~1250	37

formation. Moreover, the presence of α flakes in the samples aged at 700 °C may be an aid for SIM formation by increasing the volume fraction of its nucleation sites. The absence of SIM in Sample B is consistent with the single yield point in Figure 2.13 for such $\alpha + \beta$ microstructure, which is very similar to that of the as-received condition. Moreover, the large volume fraction of α stabilises the β grains, precluding the formation of SIM. In the compressed microstructures it becomes interesting to note that the obtained SIM displays a very different appearance than the athermal martensite; this α'' nucleates at the grain interfaces and an autocatalytic effect does not seem to apply. In the samples that underwent compression, the grains appear to be fully covered by martensite, suggesting that deformation provides the additional energy fostering the autocatalytic effect. Moreover, the structure of the martensite obtained by deformation is predominantly α'' orthorhombic, unlike the athermally obtained hexagonal martensite.

Strain hardening exponent The strain hardening exponent values of the different phases are derived from the stress-strain data. The well known flow stress equation $\sigma = K\varepsilon^n$, where K is the strength coefficient and n is the strain hardening exponent, is imposed to estimate the effective strain hardening exponent [61, 96]. The slope change at different stages of the stress-strain curve signifies a particular

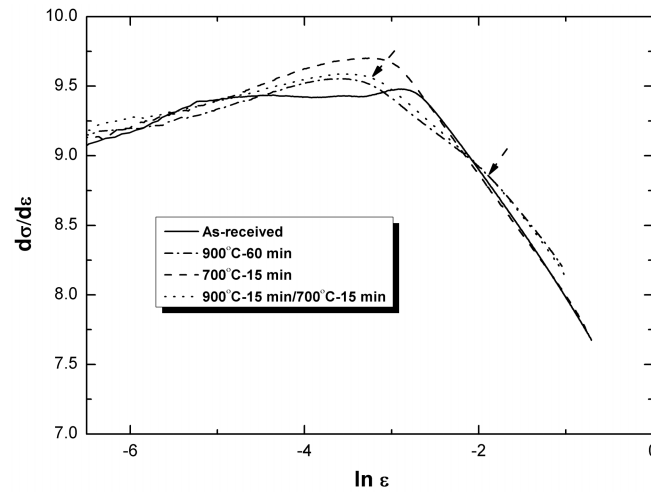
Figure 2.14: Strain hardening plot of the compression tested $Ti-1023$ samples.

Table 2.8: Strain hardening values signifying the transformation.

Sample condition	n (transformation)	K (transformation)
As-received	-	-
Sample A	0.52 ± 0.01	2865 ± 12
Sample B	-	-
Sample C	0.47 ± 0.03	2696 ± 238

deformation mode change, which is quantitatively measured for the corresponding strain hardening values. The solution treatments resulting in the PiTTi effect show a distinct change in the strain hardening exponent in between the two yield points of their stress-strain curve as highlighted in Figure 2.14. However, the non-PiTTi effect solution treatments do not result in such distinct behaviour during the plastic flow. Table 2.8 shows the strain hardening exponent and related parameter values for the PiTTi exhibiting solution treatments.

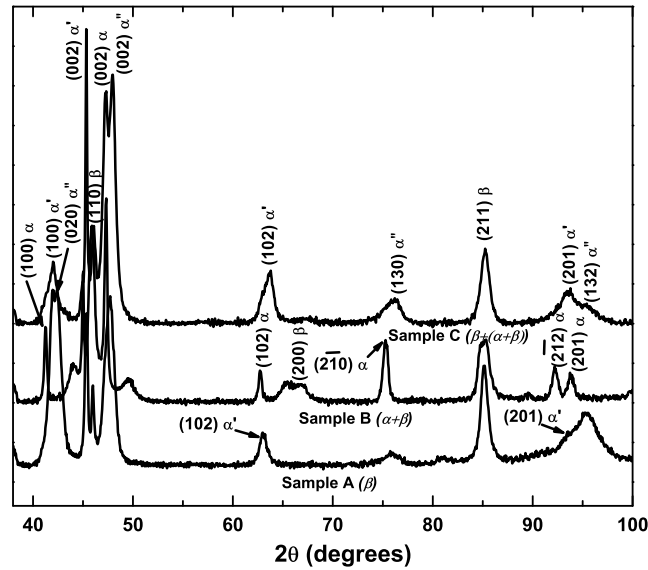


Figure 2.15: X-ray analysis of the compressed samples of selected treatments.

2.4.2.3 X-ray structural analysis

A detailed X-ray diffraction analysis to identify and confirm the various phases present in the microstructures of the compressed samples A, B and C has been carried out. Figure 2.15 shows the corresponding diffractograms. The peaks indicate that the phases present in these samples are α , martensite (α' , α'') and β ; their respective lattice parameters are given in Table 2.9. Moreover, the compressed samples show clear formation of SIM (α'' - orthorhombic and α' - hexagonal). α'' martensite peaks were observed only for the treatments involving above β temperatures. Similar observations were made by Duerig *et al.* [29] for above β heat treatments.

Ti – 1023 show a good response to solution treatment resulting in tuned microstructural parameters exhibiting an optimized PiTTi effect. PiTTi existence is reflected via a double-yield point like behaviour as seen unequivocally in the stress-strain curves for *Ti – 1023*, Fig. 2.13. Such behaviour results in a significant improvement in the compressive strength values along with reasonable strain to failure for *Ti – 1023*. Hence, *Ti – 1023* has been chosen for further studies to de-

Table 2.9: Lattice parameters values of different phases after compression.

		Lattice parameters (\AA)		
		900 °C - 60 min	700 °C - 15 min	900 °C - 15 min/ 700 °C - 15 min
β	<i>a</i>	3.2378	3.2439	3.231
α	<i>a</i>		2.933	2.929
	<i>c</i>		4.6723	4.457
α'	<i>a</i>	2.885		2.881
	<i>c</i>	4.64		4.643
α''	<i>a</i>	3.02		2.97
	<i>b</i>	4.95		4.983
	<i>c</i>	4.422		4.398

termine the defining factors that influence and promote PiTTi effect. Henceforth, all the characterization studies has been restricted to *Ti* – 1023 alloy unless otherwise mentioned specifically.

2.5 Further characterization of properties in *Ti* – 1023

The influence of plasticity induced martensite formation on surface mechanical properties has been measured. Additionally, the properties of individual phase are also measured.

2.5.1 Nano indentation

In order to identify the mechanical behaviour of individual phases and their contribution towards the overall mechanical characteristics [66], nano-indentation studies on the selected solution treated (Table 2.6) and compressed samples were carried out. Matrices of indents were made in the cross-section surface of the cylindrical samples, which were mounted on resin. A Berkovich indenter with a maximum

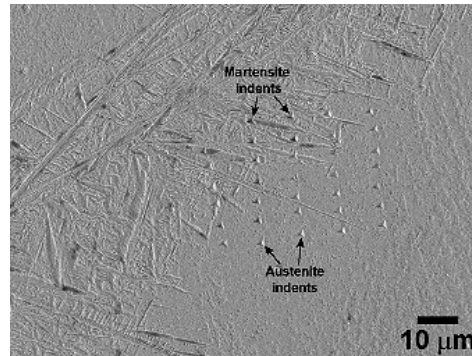


Figure 2.16: SEM image showing the matrices of indents highlighting their locations in austenite and martensite phases.

load of 10 *mN* at a rate of 20 *mN/min* has been employed. Indentation characteristics of the various phases (β (austenite), α (spheroid, flake morphologies) and α' , α'' (martensite)) present at different sample conditions have been measured. Figure 2.16 shows a representative SEM image of the austenite and martensite indent locations in the solution treated condition of Sample A.

Figures 2.17a, 2.17b, 2.17c and 2.17d show the indentation behaviour of the austenite, martensite and α (spheroids, flakes) phases, respectively. The indentation at different locations within the austenite phase exhibit more or less reproducible behaviour. The indentations at different locations within martensite phase show a distributed behaviour, where some indentation curves show low penetration depth as compared to other ones. This could arise from the existence of two kinds of martensite showing dissimilar characteristics. The indentation at α spheroids and α flakes show a distribution in their response, the penetration depth within the α spheroid indents and α flake indents at different locations show a large deviation. This behaviour could be related to the possible segregation among the phase microstructural features in the solution treated conditions. The indents on the austenite and the α flake show a noticeable slope change in their initial part (at ~ 0.5 *mN*) of the loading curve. While it seems attractive to attribute this to the locally induced martensite formation, no traces of such transformations were found for indents in the austenite phase. Furthermore, the behaviour was also found for indents in non-transforming α flakes and martensite phases. No proper explanation

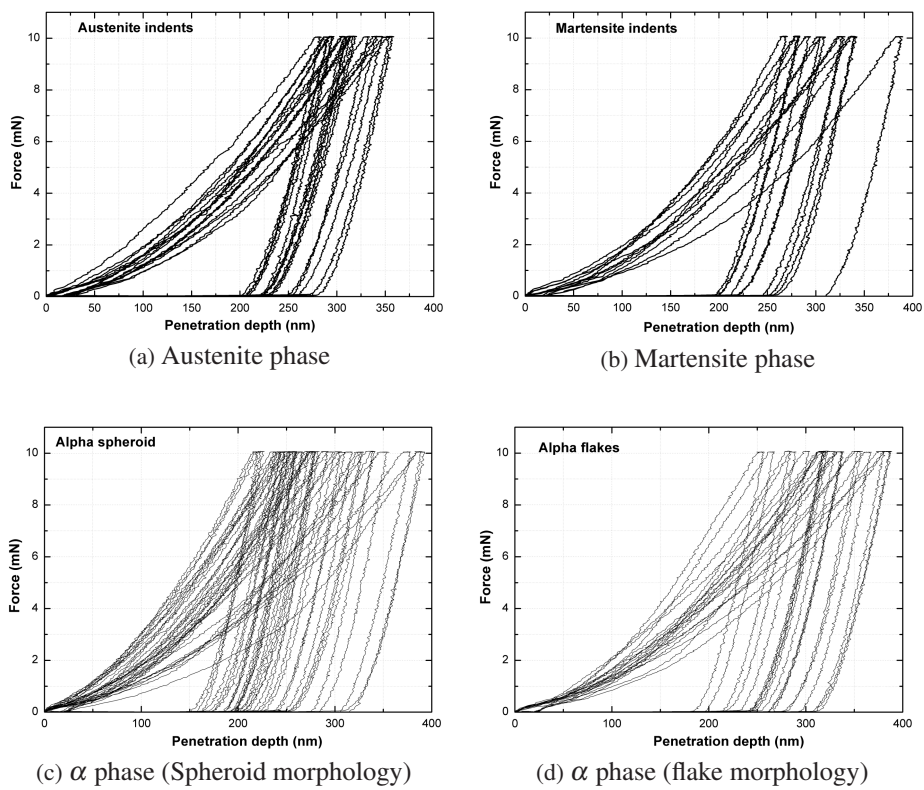


Figure 2.17: Indentation behaviour of various microstructural phases of *Ti* – 1023 samples subjected to different conditions.

Table 2.10: Hardness values of the various phases after different sample conditions of *Ti* – 1023.

Phase	Modulus (EIT), <i>GPa</i>	Hardness, <i>GPa</i>	H_v
Austenite	129 ± 12	5.0 ± 0.93	463 ± 86
Martensite	129 ± 30	6.2 ± 2.3	578 ± 209
α spheroids	173 ± 50	7.1 ± 2.6	654 ± 243
α flakes	131 ± 18	4.98 ± 0.98	461 ± 91

for the observation could be found. Table 2.10 summarizes the hardness values of the various phases present for the different conditions considered.

2.5.2 Tribological properties

In order to study the influence of PiTTi effect on tribological properties of *Ti* – 1023 two sample conditions i) as-received, showing no martensite formation and ii) 900 °C for 60 *min* solution treated, showing a clear PiTTi effect, have been considered. The friction coefficient of the samples, which were made as discs, sliding against a steel ball under different conditions has been measured. A normal load of 10 *N* (mean pressure 770 *MPa*) and 5 *N* (380 *MPa*) were applied to investigate the behavior of material under different contact pressures. The load values were chosen from the stress-strain curves corresponding to the non-martensite and martensite formation regions. Table 2.11 shows the corresponding friction coefficient values. The reported coefficient of friction is an average of the steady state regime values in the friction-time curve. The PiTTi effect does not show any noticeable improvements in the friction coefficients of *Ti* – 1023.

In addition to friction, the wear rates for the two sample conditions have been measured as well. Wear rate is defined as the volume of material removed (mm^3) divided by the product of the normal load (*N*) and the sliding distance (*m*) given as

$$k = \frac{\text{volume loss}}{\text{normal load} \times \text{sliding distance}} \frac{mm^3}{Nm}$$

Table 2.11: Friction coefficient measurements at different condition.

		Lubricated	Unlubricated
As-received	F = 5 N	0.46	0.68
	F = 10 N	0.45	0.57
900 °C - 60 min	F = 5 N	0.68	0.65
	F = 10 N	0.61	0.55

Table 2.12: Wear coefficient of ball for different test condition [mm^3/Nm].

		Lubricated	Unlubricated
<i>k</i> ball against	F = 5 N	1.9×10^{-4}	3.2×10^{-4}
as-received alloy disc	F = 10 N	6.9×10^{-5}	1.9×10^{-4}
<i>k</i> ball against solution	F = 5 N	1.6×10^{-4}	3.5×10^{-4}
treated (900 °C - 60 min) disc	F = 10 N	4.8×10^{-5}	2.1×10^{-4}

Table 2.13: Wear coefficient of discs for different test condition [mm^3/Nm].

		Lubricated	Unlubricated
<i>k</i> as-received alloy disc	F = 5 N	8.65×10^{-4}	1.08×10^{-3}
	F = 10 N	1.61×10^{-3}	2.15×10^{-3}
<i>k</i> solution	F = 5 N	8.12×10^{-4}	1.6×10^{-3}
	F = 10 N	1.27×10^{-3}	3.16×10^{-3}

The wear rate (k) values for the ball and the sample discs are tabulated in Table 2.12 and Table 2.13 respectively. The influence of plasticity induced martensite formation on wear properties is negligible as wear rates were comparable to those of the as-received condition.

2.6 Conclusions

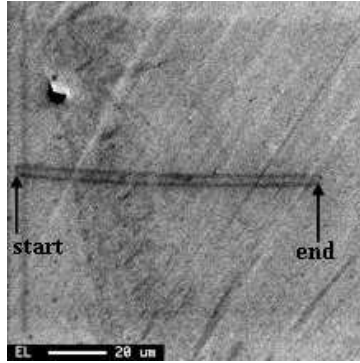
Detailed characterization of two commercial metastable β alloys for possible plasticity induced martensite transformation has been presented. The microstructural features of the considered β alloys have been modified via various solution treatment conditions. The near β type $Ti - 1023$ distinctly indicates the occurrence of plasticity induced martensitic formation for the treatments involving β homogenization. Such formation of martensite is reflected by a double yield point like behaviour in the compressive stress-strain curves. This behaviour resulted in an increase of the alloy compressive strength by $\sim 20\%$ as compared to the as-received alloy which does not show martensite formation. The solution treatment parameters promoting the capability to undergo such hardening via martensite formation upon loading have been identified. The following chapter will elaborate the various parameters that need to be taken into account in order to control or achieve optimum properties via plasticity induced martensite formation, PiTTi effect. Such studies have been performed using the $Ti - 1023$ alloy.

The $\beta - CeZ$ alloy did not show any distinct presence of PiTTi effect for the various solution treatment conditions considered. Moreover, the different microstructural features do not result in any noticeable variation or improvement in compressive properties.

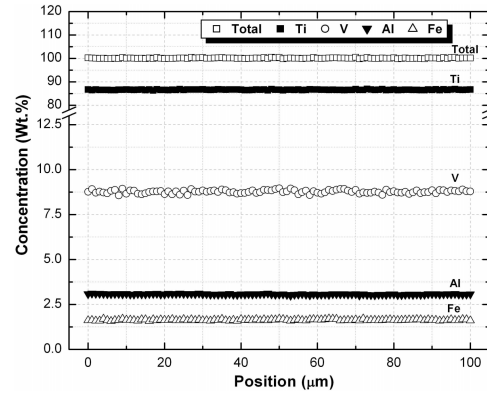
Chapter 3

Defining factors of PiTTi effect in β *Ti* – 1023 alloy

A fundamental understanding of the factors that cause martensitic phase transformation in β *Ti* – 1023 is necessary in order to achieve optimum mechanical performance. The ability of metastable β phase to transform to martensite depends on various parameters (solute concentration, deformation temperature, M_s , grain size and phase fraction) [28, 32, 33, 43, 75, 81, 85]. These parameters in turn depend on the thermo-mechanical treatment of the alloys, particularly the rate of cooling after solutionizing at elevated temperatures. Designing the desired microstructure exhibiting optimum strength-ductility properties, through PiTTi, requires understanding for the various solution treatment conditions [29, 75, 84]. The quenched structures of the β , $\alpha + \beta$ and $\beta + (\alpha + \beta)$ treatments show retained β that can transform to martensite on loading. However, the amount of martensite formation depends on the stability of the β phase, which is interrelated with the above parameters [28, 36, 44]. In this chapter a comprehensive study on the various factors (solute partitioning among the phases, β grain size, phase fraction, M_s and deformation temperature) potentially affecting the occurrence of SIM has been carried out for *Ti* – 1023 alloy.



(a) Microstructure of the probe measured region of Sample A



(b) Corresponding concentration variations as measured by EPMA

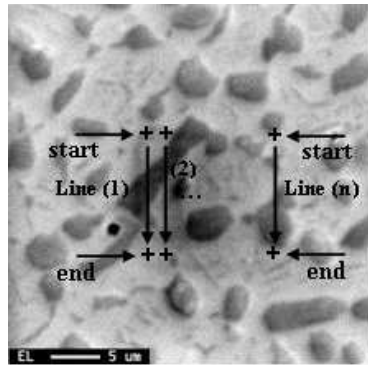
Figure 3.1: EPMA measurement of the solution treated Sample A.

3.1 Solute partitioning

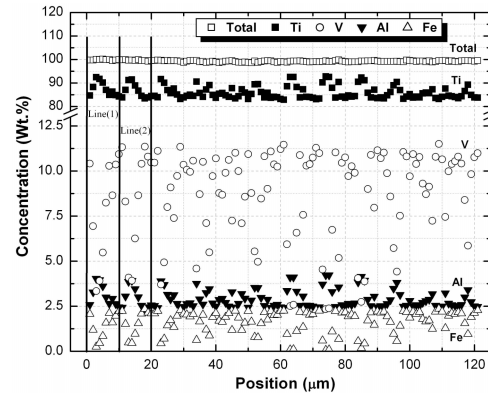
In order to determine the microstructural and solute partitioning conditions favouring the martensitic formation of β , local concentration variations have been measured using Electron probe micro analysis (EPMA). EPMA was performed in a JEOL JSM 6500F microscope to track the local concentration variations (accuracy $\pm 0.2\%$) of the major constitutive elements (V, Al, Fe and Ti) after various solution treatments. The concentration data were obtained using a 15 kV, 50 nA beam. A 1 μm probe size has been used with a resolution of $\pm 0.2\text{ wt.}\%$ for the measured concentration values.

The measurements were carried out on selected Samples A (900 °C - 60 min) and B (700 °C - 15 min) (Table 2.6 of Chapter 2), and 900 °C - 15 min/650 °C - 15 min corresponding to $\beta + (\alpha + \beta)$ treated sample (hereinafter referred to as Sample D) of $Ti - 1023$.

SEM microstructures of the different samples show the traces along which the probe measurements were carried out, Figures 3.1a, 3.2a and 3.3a; the start and end point of the line scan is highlighted in each figure. Figures 3.1b, 3.2b and 3.3b show the corresponding concentration variations of the major elements. In

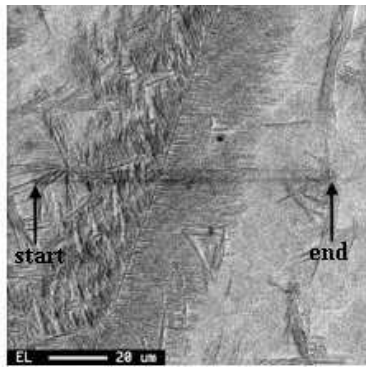


(a) Microstructure of the probe measured region of Sample B

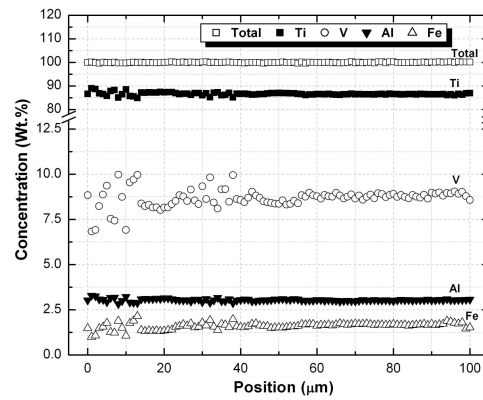


(b) Corresponding concentration variations as measured by EPMA

Figure 3.2: EPMA measurement of the solution treated Sample B.



(a) Microstructure of the probe measured region of Sample D



(b) Corresponding concentration variations as measured by EPMA

Figure 3.3: EPMA measurement of the solution treated Sample D.

Figure 3.2a the probe measurements were carried out as a series of parallel lines labelled as line 1, 2 till line n , and their respective concentration variations along the line are shown in Figure 3.2b, where the region corresponding to line 1 and line 2 is highlighted for illustration purpose. The EPMA results show clear evidence of partitioning or segregation of the major elements (V, Al, Fe and Ti) between the β and α phases within the microstructure for the $(\alpha + \beta)$ (Sample B) and $\beta + (\alpha + \beta)$ (Sample D) treatments, Figs. 3.2b and 3.3b. However, the above β treated sample (Sample A, Fig. 3.1b), where predominantly metastable β and athermal martensite near grain boundaries is present, does not show any evidence of solute fluctuations, as expected from the diffusionless nature of athermal transformation.

The concentration profiles shown in Figure 3.2b indicate strong concentration fluctuations between α and β phases of the bi-modal distributed two phase microstructure. Solute partitioning indicates that β is enriched with V and Fe, which are strong β stabilizing elements, while depleted in Al, which is an α stabilizing element that enriches the α phase. However, no athermal martensite was observed (Fig. 3.2a) after this treatment. Similar partitioning of the elements has been observed for $\beta + (\alpha + \beta)$ microstructure, mainly in the region near the start of the line scan, whose concentration profile is shown in Figure 3.3b. However, the redistribution of elements seems to be more prominent in the flake morphology than in the Widmanstätten morphology of α (Fig. 3.3a).

Such partitioning of the constitutive elements could locally change the M_s temperature of the transforming β phase. The effect of each of the solute element concentrations of Ti – 1023 on the M_s temperature, obtained from the respective binary systems [97, 98, 99], is given in Figure 3.4. A refined analysis of the effect of composition on M_s can be found in *Chapter 4*.

The graph shows that the concentration variations of Fe and V have a strong and moderate influence, respectively, on reducing the M_s temperature. Al has a contrasting effect of increasing it. The shift in M_s for Fe and V variation of 1 wt. % is about ~ 75 °C and ~ 50 °C, respectively.

Furthermore, the concentration values measured by EPMA have been compared to the equilibrium values of β phase calculated using the thermodynamics software Thermo-calc [100] with the TTTI3 Thermotech titanium database [101].

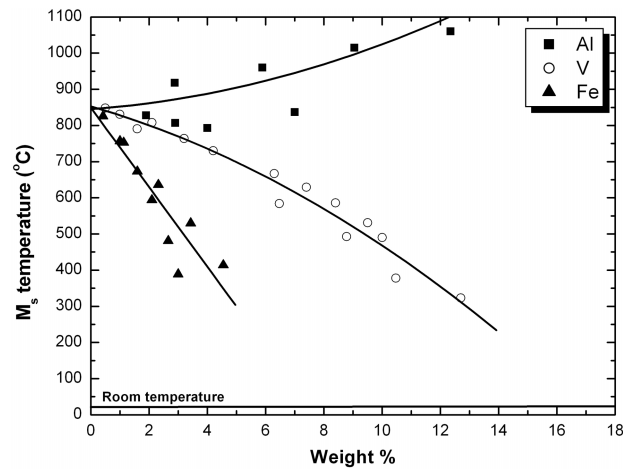


Figure 3.4: Variation of M_s temperature as function of binary element (Ti-V, Ti-Fe and Ti-Al) concentrations of Ti – 1023.

Figure 3.5 shows that the β concentration measured at different solution treatment temperatures is far from equilibrium values, especially for V, for low temperatures¹. The 900 °C for 60 min solution treated Sample A microstructure is closer to equilibrium as against the other two samples.

Hence, it may be postulated that at temperatures below β transus (*i.e.* in the range of 650-700 °C), α diffusionally forms, rejecting V and Fe while dissolving Al. For instance, given the large fraction of α at 700 °C temperature, the retained (small) β domains are enriched with β stabilizers (V) and eutectoid (Fe) elements; thereby increasing their stability such that martensite is not formed upon quenching. Thus, partitioning or solute re-distribution of elements within the microstructure affects the occurrence of PiTTi.

¹Although good care has been applied to the EPMA measurements and the conversion of intensities to concentrations, there is an unsolved inconsistency between the EPMA data (in particular for V) and the nominal concentration for the homogeneous microstructure of 900 °C for 60 min. We have not been able to resolve the discrepancy.

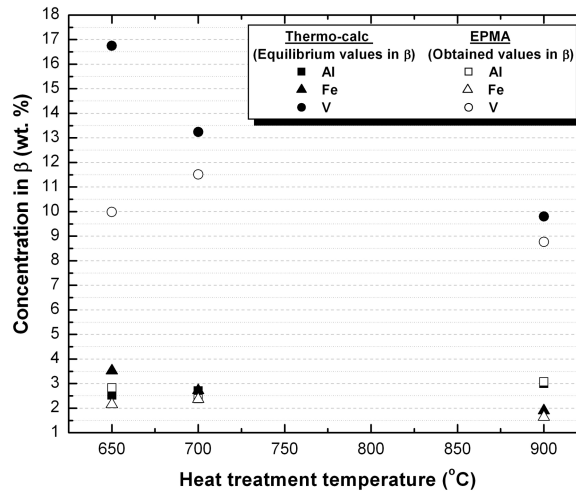


Figure 3.5: Comparison of the equilibrium and measured β concentration values

3.2 Microstructural features

The microstructure plays a key role in property control of any alloy, specifically in β titanium alloys, where the wide range of possible microstructures has a strong influence on their mechanical behaviour [32, 33, 43, 44]. In order to understand the effects of such microstructural features on PiTTi effect, the solution treated samples were subjected to a quantitative analysis of their prior β grain size and α phase fraction.

3.2.1 Grain size

The PiTTi capability after various solution treatments corresponding to different phase domains are analysed in terms of their as-quenched prior β grain size. The typical grain size of β after the various heat treatments within the β phase region is quite large, in the range of 300 to 600 μm (refer to Figure 2.9 of Chapter 2). This may become a major hurdle in achieving good ductility. Various attempts to reduce the average grain size of titanium alloys have been made. The addition of grain refining elements like B and N to various alloys has given successful results in reducing the average β grain size [23, 24, 25, 26]. However, only traces of such

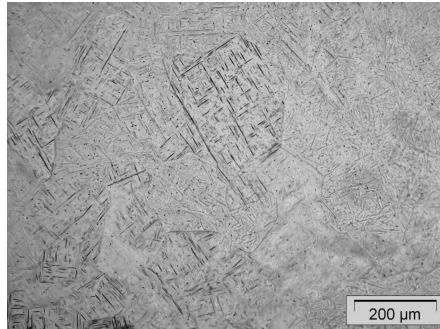


Figure 3.6: Microstructure of Sample E displaying reduced average grain size (100 to 200 μm).

grain refining elements can be added as higher amount will result in precipitation or intermetallic compounds formation leading to the deterioration of properties [102]. Hence, our primary approach is to reduce the grain size via solution treatment at temperatures around the β transus, thereby reducing the grain growth, and further study their influence on PiTTi properties. Such treatment was performed at 820 °C for 15 min (referred hereon as Sample E) that is slightly above the β transus (795.5 °C [Chapter 2]) of Ti – 1023. Representative microstructure of Sample E is shown in Figure 3.6 displaying an average grain size in the range of 100 to 200 μm .

The PiTTi properties of such microstructure is evaluated upon compression testing in a Gleeble[®]1500 machine. Figure 3.7 shows the corresponding stress-strain curve of Sample E along with Sample A, the treatment involving above β solutionizing temperature of large grain size as given in Chapter 2, and the as-received Ti – 1023. Sample E clearly shows the double yield point behaviour corresponding to SIM formation, and displays an increase in the strain to failure value while retaining almost the same strength level as other PiTTi exhibiting treatment. Evidently, the smaller prior β grain size (100 to 200 μm) achieved by tuning the solutionizing temperature has shown acceptable ductility within the PiTTi properties of Ti – 1023. The reduction in prior β grain size in the considered range did not alter the location of first and second yield point.

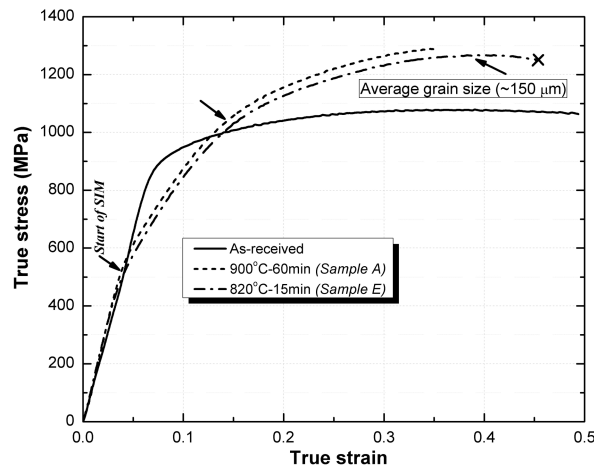


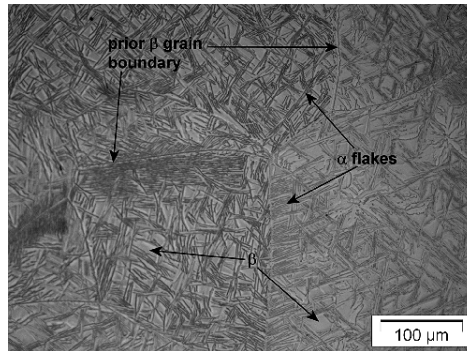
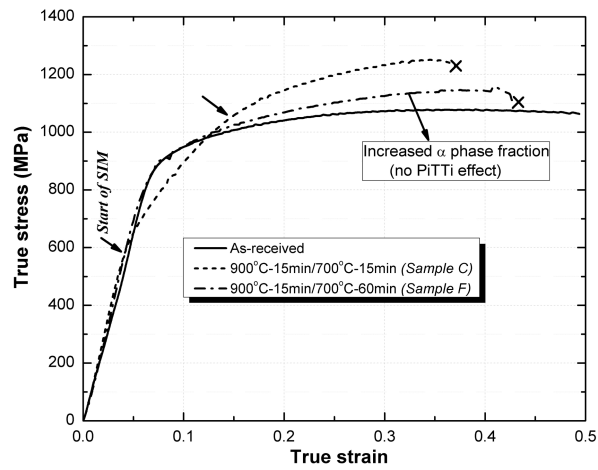
Figure 3.7: Stress-strain curves showing the effect of grain size reduction on PiTTi properties.

3.2.2 α phase fraction

Another indirect factor that may alter the PiTTi effect is the α phase fraction after various solution treatments. The solution treatments involving below β homogenization result in equilibrium α phase. However, the amount of α increases with decreasing $\alpha + \beta$ temperature, and increasing soaking time. Hence, a solution treatment that displayed PiTTi effect is repeated to observe the effect of increased α phase fraction. Such treatment is performed at 900 °C for 15 min followed by controlled cooling to 700 °C and soaking for 60 min (referred hereon as Sample F), whose respective microstructure is shown in Figure 3.8.

Sample F visibly displays an increased α phase fraction, which appears as needles within the prior β grains in Figure 3.8, and as feathers at their grain boundaries, in order to enrich them with β stabilising elements. Moreover, the morphology of α varies depending on the solution treatment scheme.

The observed microstructure has been subjected to compression testing in a Gleeble® 1500 machine for evaluating their PiTTi properties. Figure 3.9 shows the respective stress-strain curve of Sample F along with the behaviour of another similar treatment but with a lower α phase fraction. From Figure 3.9 we could infer that an increase in α fraction *i.e.* an increase in the stability of β , reduces the

Figure 3.8: Microstructure of Sample F displaying increased α phase fractionFigure 3.9: Stress-strain curves showing the effect of α phase fraction on PiTTi effect

likelihood of martensite formation upon loading and thus eventually the plausible improvement in mechanical properties. Other than the homogenized β microstructure, a reasonable amount of α along with β phase also results in PiTTi effect. However, the amount of α should be tunable by proper selection of heat treatment temperature and time in the $\alpha + \beta$ domain. Compared to previously reported results for similar treatments, namely $900\text{ }^{\circ}\text{C} - 15\text{ min}/700\text{ }^{\circ}\text{C} - 15\text{ min}$ (Figure 2.11a of *Chapter 2*), the increase in $\alpha + \beta$ soaking time and decrease in $\alpha + \beta$ heat treatment temperature increases the fraction of α phase, thereby solute enriching the β phase, which makes it too stable to undergo deformation induced martensite transformation.

3.3 Deformation temperature

Our studies, as presented in *Chapter 2*, have shown that the PiTTi effect exists at room temperature, and can be tailored to achieve improvements in β *Ti* – 1023 alloy mechanical properties [*Chapter 2*]. However, little information is available on the temperature dependence of deformation induced martensite for Ti alloys. The current work describes such a study to systematically explore the deformation temperature dependence of PiTTi properties in β *Ti* – 1023 alloy.

3.3.1 Experimental procedure

The β *Ti* – 1023 alloy details are the same as explained in *Chapter 2*. Of the many solution treatments performed [Table 2.6 of *Chapter 2*], the one at $900\text{ }^{\circ}\text{C}$ for 60 min was chosen as it displays a homogeneous microstructure with more metastable β domains without partitioning of the solute elements. The solution treatment was performed on a *Bähr* 805 horizontal dilatometer at a vacuum level of 10^{-5} mbar , and quenched to room temperature by helium gas flow. After subjecting to above treatment, the samples were compressed at various temperatures ranging from $\sim 33\text{ }^{\circ}\text{C}$ to $400\text{ }^{\circ}\text{C}$ at regular intervals (33, 93, 163, 183, 213, 233, 293, 350, 375 and $400\text{ }^{\circ}\text{C}$). The compression tests were carried out with a load cell capacity of 20 kN in the dilatometer. The deformation temperature has been maintained within an

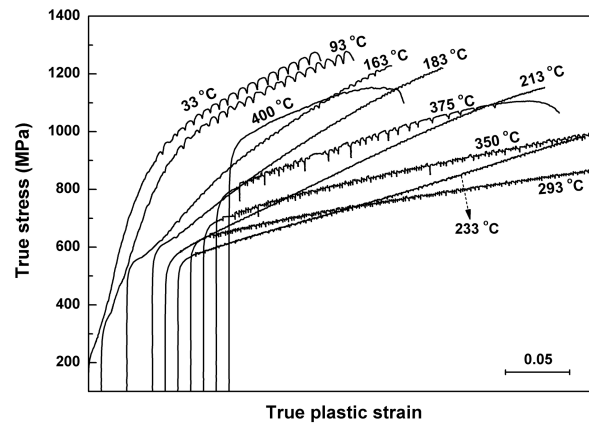


Figure 3.10: Compressive stress-strain curves of *Ti* – 1023 alloy at various deformation temperatures.

accuracy of ± 5 °C by attaching a thermocouple to the sample. All the compressed samples were characterized subsequently using X-ray diffraction (XRD) with $\text{Co K}\alpha$ radiation at room temperature.

3.3.2 Compression testing results

Compressive stress-strain curves obtained at various deformation temperatures ranging from ~ 33 °C to 400 °C are given in Figure 3.10. The low temperature stress-strain curves distinctly show the double-yield points, which correspond to martensite formation stress (or so called triggering stress [29]) and slip stress (due to plastic deformation), respectively. It is evident that the double-yield behaviour, a phenomenon associated to martensite formation showing SIM effect, disappears as the deformation temperature is increased; specifically after 213 °C only a single yield point corresponding to slip deformation is observed.

3.3.3 Discussion

Further elucidation of the temperature dependence of the two stress levels (the martensite formation stress - first yield point; the slip deformation stress - second yield point) is given in Figure 3.11.

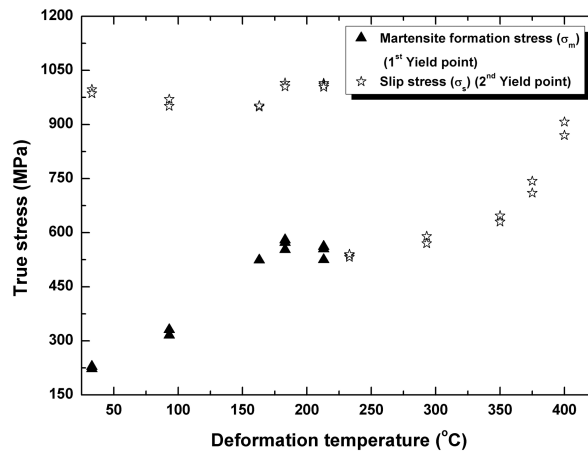


Figure 3.11: The critical stress values of the double-yield phenomenon as function of deformation temperature.

The two critical stress values from the stress-strain curves have been determined by the method of tangents intersection. It is obvious that the separation between two yield points decreases with an increase in the deformation temperature till 213 °C, Fig. 3.11. Such observation quantitatively reflects the amount of SIM formation. Overall, the deformation temperature seems to have a noticeable effect on the martensite formation stress or the so-called triggering stress. However, the triggering stress seems to remain constant after 163 °C deformation temperature, and eventually disappears at 233 °C. The slip deformation stress falls sharply after 213 °C to levels comparable to the martensite formation stress but shows a steady increase with further deformation temperatures. Contrastly, the prior β fraction increases with deformation temperature and becomes stable, losing metastability, resulting in simple plastic yielding.

It is interesting to assess whether the temperature at which the double yield disappears can be related to the athermal M_s temperature of the alloy. According to our thermodynamic model (to be explained in *Chapter 4*), the M_s temperature of Ti- X (where $X = \text{Fe, Mn, Cr, Mo, Ni, Cu, V, Nb, Zr}$ and Al) can be expressed as function of the alloy concentration. Using this equation, the M_s temperature for nominal composition of Ti – 1023 alloy is predicted as ~ 240 °C. This temperature coincides reasonably well with the temperature (~ 213 °C) above which the double

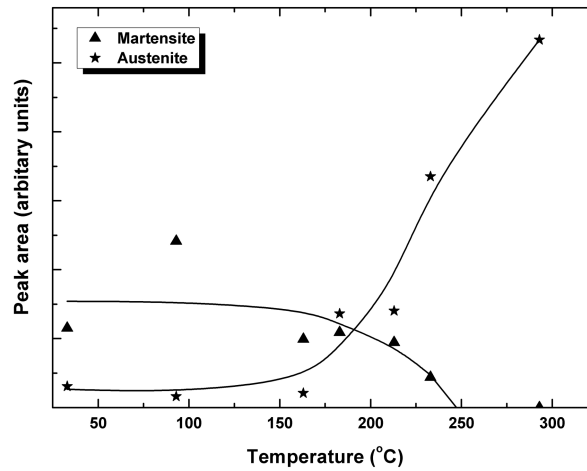


Figure 3.12: A quantitative measure of martensite and austenite peak areas in deformed samples as function of deformation temperature. Above ~ 233 °C (from Figure 3.11) temperature no martensite was found.

yield effect due to SIM formation disappears (Figures 3.10 and 3.11).

The temperature dependence of the SIM effect has been further quantified with the aid of X-ray diffraction. An analysis on the diffractograms of the various temperature compressed samples confirmed the disappearance of post deformation martensite peaks with increasing deformation temperature. Measurement of the austenite and martensite peak areas identified from the diffractograms of the various temperature compressed samples has been performed using MDI Jade 5.0 software [103]. A plot showing the measured martensite and austenite peak areas as function of deformation temperature reflects the trend of martensite disappearance, where a negligible or no martensite presence, after the 233 °C deformation temperature, is observed (Fig. 3.12). Attention was focused on the low angle diffraction peaks that exhibited clear transformation trends. Moreover, the diffractograms also show a concurrent increase in the formation of β phase in agreement with the disappearance of martensite as function of deformation temperature. Further, at higher deformation temperatures *i.e.* above 300 °C, the equilibrium α phase formation is observed.

3.4 Conclusions

Various factors that control and/or promote the stress induced martensite formation have been identified for *Ti* – 1023 alloy. The solute partitioning of the elements among the α and β phase is quite evident and alters the M_s temperature locally for various solution treatment conditions. It may be postulated that solution treatments: i) involving above β transus temperatures result in a partially transformed and compositionally homogenized microstructure; and ii) involving below β transus temperatures (*i.e.* below 795 °C), result in diffusional formation of α , which rejects V and Fe while absorbs Al. Given the large fraction of α formation at low temperatures, the retained small β domains are enriched with β stabilizers (V) and eutectoid (Fe) elements; increasing their stability such that martensite is not formed upon quenching.

A modest effect of prior β grain size and α phase fractions on the occurrence of PiTTi and its eventual improvement in mechanical properties is observed. The reduction of grain size down to the range of 100 to 200 μm by selection of lower solution treatment temperatures and shorter times at just above β transus (820 °C for 15 *min*) resulted in a moderate improvement of alloy ductility while retaining the same strength level as obtained through PiTTi effect. However, the smaller grain size did not affect the two critical stress levels in SIM formation. Similarly, increasing the α phase fraction by a solution treatment involving longer soaking time at below β phase regime (900 °C for 15 *min* followed by 700 °C for 60 *min*) precludes the martensite formation and thereby the improvement in PiTTi properties.

Another factor that determines the SIM formation capability is the deformation temperature. The temperature dependence of the strength improvements stemming from PiTTi effect is evident. However, the PiTTi formation capability, upon compression, disappears with an increase in deformation temperature, as demonstrated from X-ray measurements. The temperature at which the effect disappears is identified as 233 °C, which is comparable to the predicted M_s value of 240 °C for *Ti* – 1023 using the developed M_s prediction model.

It can be inferred that the PiTTi effect is controlled by the microstructural state

involving i) solute partitioning and ii) phase fractions, along with iii) deformation temperature, all interlinked with β phase stability and its ability to transform into martensite (i.e. M_s temperature). The M_s temperature's strong dependence on the concentration of alloying elements is explained in the next chapter.

Chapter 4

Thermodynamics based prediction of the martensite formation temperature in β Ti alloys

The formation of martensite in titanium alloys is of great importance for tailoring their mechanical properties. Its importance has long been recognized for steels, and recently demonstrated for titanium alloys [[29, 75], *Chapter 2*]. A key parameter in indicating the tendency to a martensitic transformation is the martensite start temperature, M_s . Several approaches have been proposed in the steel literature for computing the compositional dependence of the M_s . These include linear combinations of the weighted contributions of each component [104], as well as non-linear relations and unspecified interaction terms using artificial neural networks [105, 106, 107]. The input for such models comes from extensive data sets available in steel literature. Other approaches are based on thermodynamics and enjoy some physical foundation [108]. In contrast to the steel literature, the prediction of M_s temperature in titanium alloys has not been extensively explored. Although, enough experimental evidence is available on the martensitic transformation of metastable β alloys, only few attempts have been made to model such transforma-

tion. Malinov and co-workers have modelled the time-temperature-transformation kinetics along with the M_s temperature for titanium alloys using artificial neural networks [109, 110]. In addition, for titanium alloys, the Mo equivalence has been employed as a rough approximation for determining the likelihood for metastable transformations, specifically the ω transformation [2, 27, 111]. Inspired by the Ghosh–Olson approach to model the M_s in ferrous alloys, this chapter aims at providing a thermodynamic model that describes the compositional dependence of M_s temperature in β titanium alloys.

4.1 Need for thermodynamic based models

The application of thermodynamics to the understanding of the martensitic transformation has been relatively successful in capturing multicomponent effects in ferrous systems. The martensitic transformation happening at high cooling rates from the high temperature regime can be regarded as a form of spontaneous plastic deformation driven by chemical forces [112, 113]. This approach to the understanding of martensitic transformations can provide insight into the mechanism of transformation, serving as a generalization technique to predict M_s temperature among various alloying systems. The development of a thermodynamic framework to describe the nucleation of martensite laid the foundations for the thermodynamic models predicting the M_s temperature as a function of composition. Studies on the implementation of a thermodynamic model by Bhadeshia [114, 115] in plain carbon steels have estimated the driving force for martensite formation at M_s . This resulted in describing the driving force to form martensite (ΔG_c) as a function of carbon content. This function has been applied to predict the M_s temperature in steels with good agreement. In order to obtain a model of wider applicability, Olson and Cohen considered the heterogeneous martensite nucleation as a faulting mechanism. In this model, martensite transformation occurs when embryos of martensite, which are defects bounded by interfacial dislocations, can grow against the lattice friction experienced by these dislocations [112, 113]. This results from grouping existing dislocations present in the high-temperature phase. Such clustering onto neighbouring planes leads to stacking faults of a certain energy which

favour the formation of martensite nuclei [112]. In analogy to the classical nucleation theory, stacking faults are regarded as second-phase embryos, which display volume and surface energy contributions. Relative to the original perfect lattice, the free energy contribution per unit mole caused by forming such embryos has a chemical component (ΔG_{chem}) term, which stems from the chemical thermodynamic differences between parent and product phases, a strain energy (E^{str}) term due to the accompanying lattice distortion by the embryo, and a true surface energy (σ) term due to the formation of new particle/matrix interface. The fault energy of such a nucleus per unit area along the fault plane can be expressed as [112]:

$$\gamma = n\rho_A(\Delta G^{chem} + E^{str}) + 2\sigma(n) \quad (4.1)$$

where n is the number of fault planes and ρ_A is the density of atoms in a close-packed plane in moles per unit area. Ghosh and Olson proposed a method to describe the composition dependency of the critical driving force [108, 116, 117, 118] including interstitial and substitutional solutes. This proposed theory leads to the modelling of martensitic transformations based on thermodynamic principles. A detailed description of the martensite nucleation mechanism can be found elsewhere [112, 119, 120].

4.2 Ghosh-Olson model

The Olson and Cohen's thermodynamics-based heterogeneous martensite nucleation theory was employed by Ghosh and Olson [108] to develop a model that computes the critical driving force for athermal martensitic nucleation in multi-component solid solution strengthened steels excluding any effect the grain size may have. The critical driving force from equation 4.2 is modelled as the sum of the strain energy, a defect-size dependent interfacial energy and a composition-dependent interfacial frictional work contribution:

$$\Delta g_{ch} + g^{el} + 2\sigma/nd = -(w_{\mu} + w_{th}) \quad (4.2)$$

where Δg_{ch} is the Gibbs energy difference between the phases per unit volume, g^{el} is the strain energy per unit volume, σ is the semi-coherent interfacial energy, n is the number of fault planes comprising the nucleus thickness, d is the spacing between them, w_μ and w_{th} are the athermal (composition-dependent) and the thermal (composition- and temperature-dependent) components of the interfacial work, respectively.

In describing the nucleation of athermal martensite, expressions for the composition dependence of the athermal frictional work, and expressions for the motion of martensitic interfaces have been proposed by Ghosh and Olson [108]. They incorporated the solid solution hardening theory in describing the kinetics of barrierless heterogeneous nucleation. A fixed defect potency displaying weak composition dependence is assumed, along with a temperature-independent shear modulus. This allows equation 4.3 to be expressed in molar quantities, represented in upper case, to obtain the critical driving force for martensite nucleation for multicomponent single-phase systems in general as:

$$-\Delta G_{crit} = K_1 + W_\mu(K_\mu^i, X_i^t) \quad (4.3)$$

where K_1 is a constant which covers the work due to the transformation strain, W_μ is a function describing the molar interfacial work, K_μ^i is the athermal strength of solute i , X_i is the concentration of solute i expressed in atom fraction and t is a solute-dependent exponent. In describing the martensitic transformation in ferrous alloys, Ghosh and Olson found $t = 1/2$ to provide the best fit to experimental results. Although the choice for such exponent was claimed to be rooted in solid solution hardening theories [108], other choices for t could have been made. Gypen and Deruyttere [121] have reviewed several possible values for t , while Friederichs and Haasen [122] have postulated $t = 3/2$. There is no physical objection to choosing other values for t for other base materials where different hardening mechanisms may prevail.

4.3 Martensite formation in Ti alloys

In analogy to the thermodynamic modelling of face-centered cubic (FCC) to body-centered cubic (BCC) martensitic transformations in steels, an idealized BCC to hexagonal close-packed (HCP) scenario is defined for computing the transformation energetics in β titanium alloys [113, 123]. In such alloys, the high temperature austenite (β) phase is of BCC structure and transforms into α phase of HCP structure in equilibrium conditions. However, the β phase also undergoes transformation to phases like ω (HCP), martensite (α' (HCP) and α'' (Orthorhombic)) in non-equilibrium conditions. Solution treated β alloys undergo transformation to athermal martensite, which is defined by M_s temperature, upon quenching [2, 29].

The binary alloy systems of titanium that undergo such transformation are gathered. Such alloying elements can be classified into α and β stabilizers and neutral elements, in which the β stabilizing elements can be further categorized into β isomorphous (Mo, V, Nb, Zr) and β eutectoid elements (Fe and Cr). The β eutectoid elements have a strong effect on decreasing the M_s temperature in binary Ti systems, while the β isomorphous elements have a more moderate influence; α stabilizers (e.g. Al) have the effect of increasing the M_s temperature, and neutral elements (e.g. Sn) display a negligible influence. Unlike Fe-based systems, there is relatively limited data available from the literature on M_s temperature as a function of composition for Ti binary alloy systems. The reliability of the gathered data for various systems involving ($X = \text{Fe, Mn, Mo, V, Nb}$ and Al) has been assessed by comparing them with the T_0 temperature (the temperature at which the driving force $-\Delta G = 0$), calculated using the thermodynamic software (Thermo-calc) [100] considering the TTTI3 Thermochem titanium database [101], Fig. 4.1.

Since the M_s temperature is sensitive to various factors, the processing conditions and the amount of interstitials, mainly the oxygen and nitrogen content within acceptable levels has also been analysed before choosing the corresponding data for our studies. In this analysis the effect of grain size is not considered and all the experimental data were taken from materials reported to have a large grain size. The considered data is utilized to develop the model for M_s temperature prediction in β Ti alloys. The following algorithm explains the model development for binary systems, Fig. 4.2.

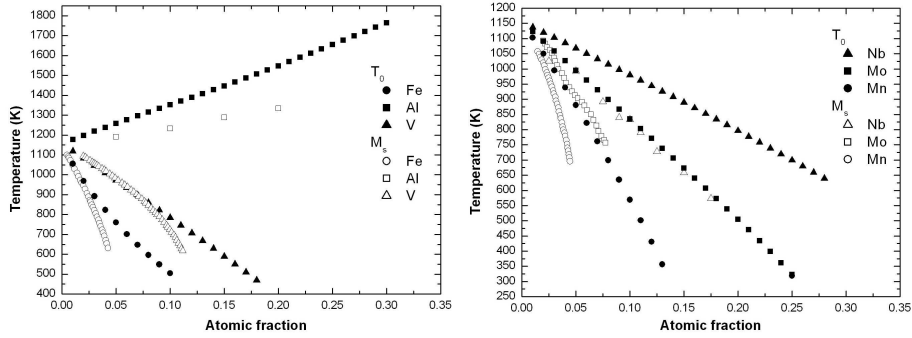


Figure 4.1: Reliability check on gathered M_s vs. X_i data by comparison with corresponding T_0 temperatures.

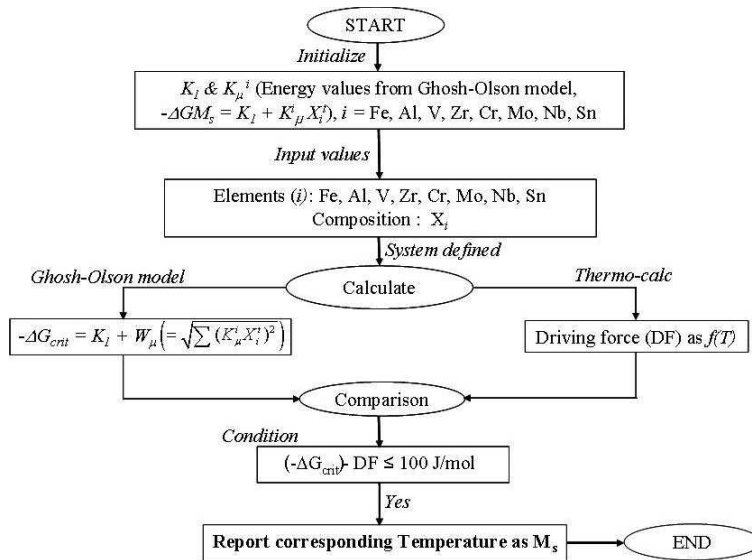


Figure 4.2: Algorithm of the martensite model for β titanium alloys.

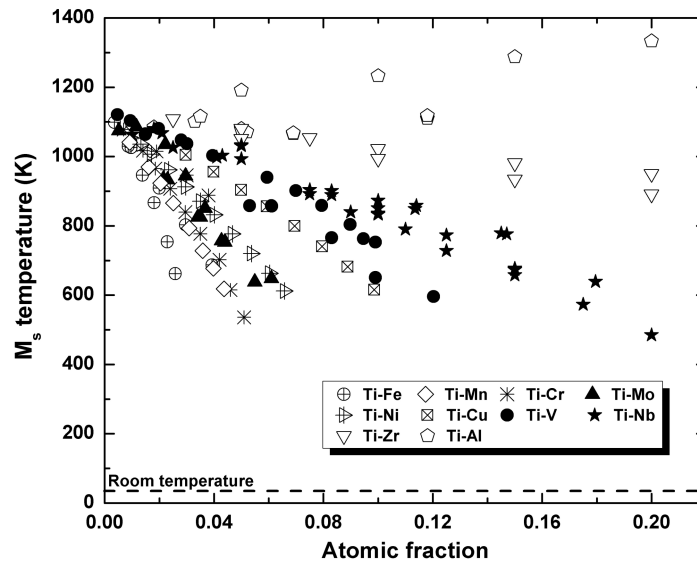


Figure 4.3: Concentration dependence of M_s for Ti-X ($X = \text{Fe, Mn, Cr, Mo, Ni, Cu, V, Nb, Zr}$ and Al) binary systems [97, 98, 99, 124, 125].

4.4 Application of modified Ghosh-Olson model

4.4.1 β Ti-binary systems

Reported data on the athermal martensitic transformation in binary systems [97, 98, 99, 124, 125] have been employed to calculate the critical driving force for martensite nucleation at the M_s temperature as function of X_i . Figure 4.3 shows the reported M_s temperature for Ti-X binary systems (where $X = \text{Fe, Mn, Cr, Mo, Ni, Cu, V, Nb, Zr}$ and Al). Other elements like O and Sn displayed a lot of scatter in the reported data, not representing their exact trend, and are thus not considered for our model.

Equation 4.4 can be used to determine the M_s temperature for binary systems. Employing thermodynamic software (Thermo-calc) [100] and TTTI3 Thermotech titanium database [101], it is possible to obtain the driving force ($-\Delta G$) at the reported M_s temperatures (Fig. 4.4) for the $\beta \rightarrow \text{martensite}$ transition. The driving force for the martensite transformation is obtained by fixing the product phase (HCP) to be dormant, and of same composition as the β phase, due to the diffu-

sionless nature of the martensite transformation. Such driving force must equal the critical driving force for martensite nucleation (equation 4.4), which for binary alloys of Ti is approximated by the expression:

$$-\Delta G_{M_s} = K_1 + K_\mu^i X_i^t \quad (4.4)$$

where $i = \text{Fe, Mn, Cr, Mo, Ni, Cu, V, Nb, Zr and Al}$, t is the solute dependent exponent. The calculated driving force at the reported M_s temperatures is plotted as a function of the binary element concentrations, Figure 4.4. The variation of the driving force is traced by fitting with equation 4.5. The K_1 , K_μ^i and t values are derived by several iterations for all the considered binary elements. The K_1 , which is the fault energy that arise from the base system, is supposed to be a constant. Hence K_1 is fixed at $0.150 \text{ kJ mol}^{-1}$ (mean of all derived K_1 values) and t is fixed at 1.5. Thus the $-\Delta G_{M_s}$ vs. X_i is fitted with the following equation

$$-\Delta G_{M_s} = 150 + K_\mu^i X_i^{1.5} \quad (4.5)$$

resulting in the best fit for all considered elements as shown in Figure 4.4, where the lines represent the variation of equation 4.5 resulting in different solute strength (K_μ^i) constants as listed in Table 4.1.

It is interesting to note that the solute-dependent exponent (t) employed in this work is 1.5, while Ghosh and Olson [108] obtained the best agreement with experimental data using 0.5. The value of $t = 1.5$ agrees well with that postulated by Friedrichs and Haasen [122] for the BCC to HCP transformations.

The solute strength values are employed in equation 4.5 and the $-\Delta G_{M_s}$ for the reported compositions of binary alloys are estimated and compared to the driving force calculated using Thermo-calc for same compositions. The corresponding temperature where the two driving force values are nearly the same is considered as the M_s temperature of the given alloy composition.

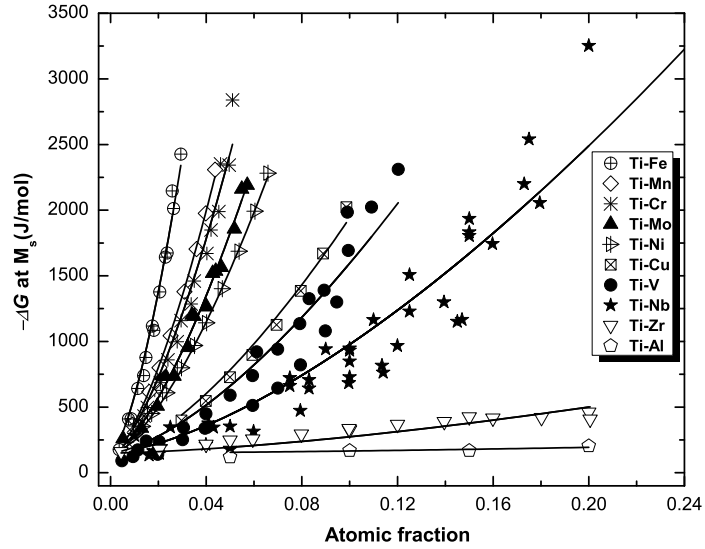


Figure 4.4: Concentration dependence of $-\Delta G$ at M_s for Ti-X ($X = \text{Fe, Mn, Cr, Mo, Ni, Cu, V, Nb, Zr}$ and Al) binary systems.

Table 4.1: The athermal solute strength values of different solutes in Ti-X systems.

Titanium binary (X) elements	K_μ (kJ/mol)
Fe	440 ± 20
Mn	231 ± 2
Cr	216 ± 6
Mo	157 ± 3
Ni	125 ± 1
Cu	57 ± 1
V	45 ± 3
Nb	27 ± 1
Zr	4.0 ± 0.5
Al	0.5 ± 0.2

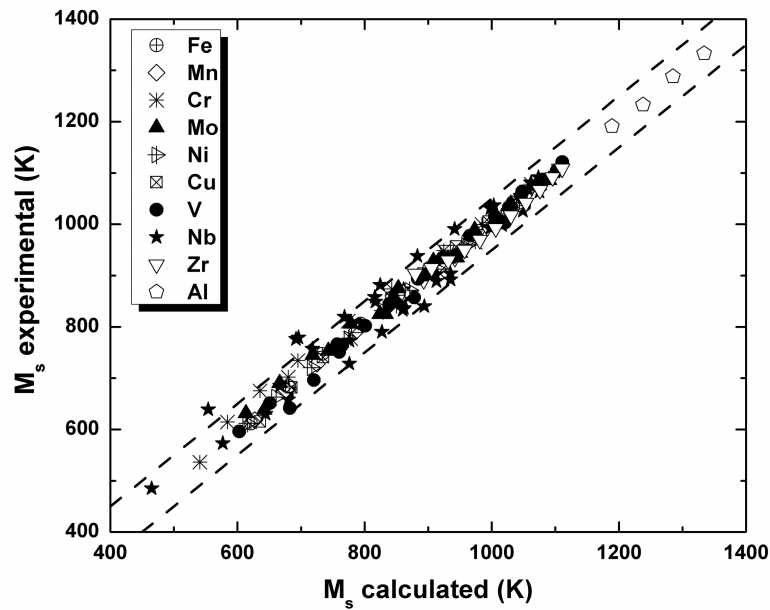


Figure 4.5: Comparison of calculated and experimental M_s values of Ti-X ($X = \text{Fe, Mn, Cr, Mo, Ni, Cu, V, Nb, Zr}$ and Al) binary systems.

4.4.2 Validation of M_s predictions

The model was applied to the reported values of various Ti-X systems ($X = \text{Fe, Mn, Cr, Mo, Ni, Cu, V, Nb, Zr}$ and Al) from the literature (Fig. 4.3) [97, 98, 99, 124, 125]. The predicted values of M_s from the model for various existing composition of binary alloys from literature have been validated as shown in the Figure 4.5. The agreement of the predictions are well within $\pm 50 K$ of the reported experimental values, *i.e.* within the experimental scatter band as shown in Figure 4.5.

4.5 Extension to β Ti multicomponent systems

The binary M_s predictions for Ti alloys following Ghosh-Olson's approach are quite good. Extending the predictions to multicomponent systems is necessary to capture existing engineering alloys. Moreover, our aim to control the PiTTi properties via tailoring M_s generally involves multicomponent systems.

4.5.1 Development of M_s equation

The M_s predictions for the various binary systems considered follow a relatively smooth trend. Such trend can be best approximated by an equation of the type

$$M_s = M_s^0 + C_i X_i^t \quad (4.6)$$

where $i = \text{Fe, Mn, Cr, Mo, Ni, Cu, V, Nb, Zr}$ and Al and C_i is a constant reflecting the solute effect on M_s . t is the solute dependent exponent. M_s^0 is the M_s temperature of the pure Ti, which is the β -transus temperature (882.8 °C or 1156 K). The resultant approximations of equation 4.6 for all the elements, except Mn, Ni and Cu, are given in Figure 4.6.

It is interesting to note that the best approximation is obtained when the solute dependent exponent (t) is 1.5 (similar to the one observed for $-\Delta G_{M_s}$ vs. X fit). Moreover, the M_s^0 approximately converge to comparable values for $X_i \rightarrow 0$ of all the binary approximations. The mean of all M_s^0 values (*i.e.* 1092 K) is more or less the same as the β -transus. Ignoring strong interactions between elements and grain size dependence, an approximation for M_s is postulated, in analogy to Andrew's equation for steels [104], by assuming that the contributions from the i components obey additivity:

$$M_s = 1092 - 108701X_{Fe}^{1.5} - 49994X_{Mn}^{1.5} - 47973X_{Cr}^{1.5} - 33776X_{Mo}^{1.5} - 27403X_{Ni}^{1.5} \\ - 13865X_{Cu}^{1.5} - 12615X_V^{1.5} - 6832X_{Nb}^{1.5} - 2018X_{Zr}^{1.5} + 1829X_{Al}^{1.5} \quad (4.7)$$

where the concentrations X_i are atom fractions and M_s is in K in equation 4.7.

Similar equation for the elemental concentrations expressed in wt.% (equation 4.8) is given below

$$M_s = 1095 - 86Fe_{wt.\%}^{1.5} - 43Cr_{wt.\%}^{1.5} - 41Mn_{wt.\%}^{1.5} - 21Ni_{wt.\%}^{1.5} - 13Mo_{wt.\%}^{1.5} \\ - 12V_{wt.\%}^{1.5} - 10Cu_{wt.\%}^{1.5} - 3Nb_{wt.\%}^{1.5} - 1Zr_{wt.\%}^{1.5} + 4Al_{wt.\%}^{1.5} \quad (4.8)$$

The proposed equation has to be validated for its effective use. However, due to lack of succinct and reliable experimental data on multicomponent Ti systems in the literature a direct validation could not be achieved. Nevertheless, a novel

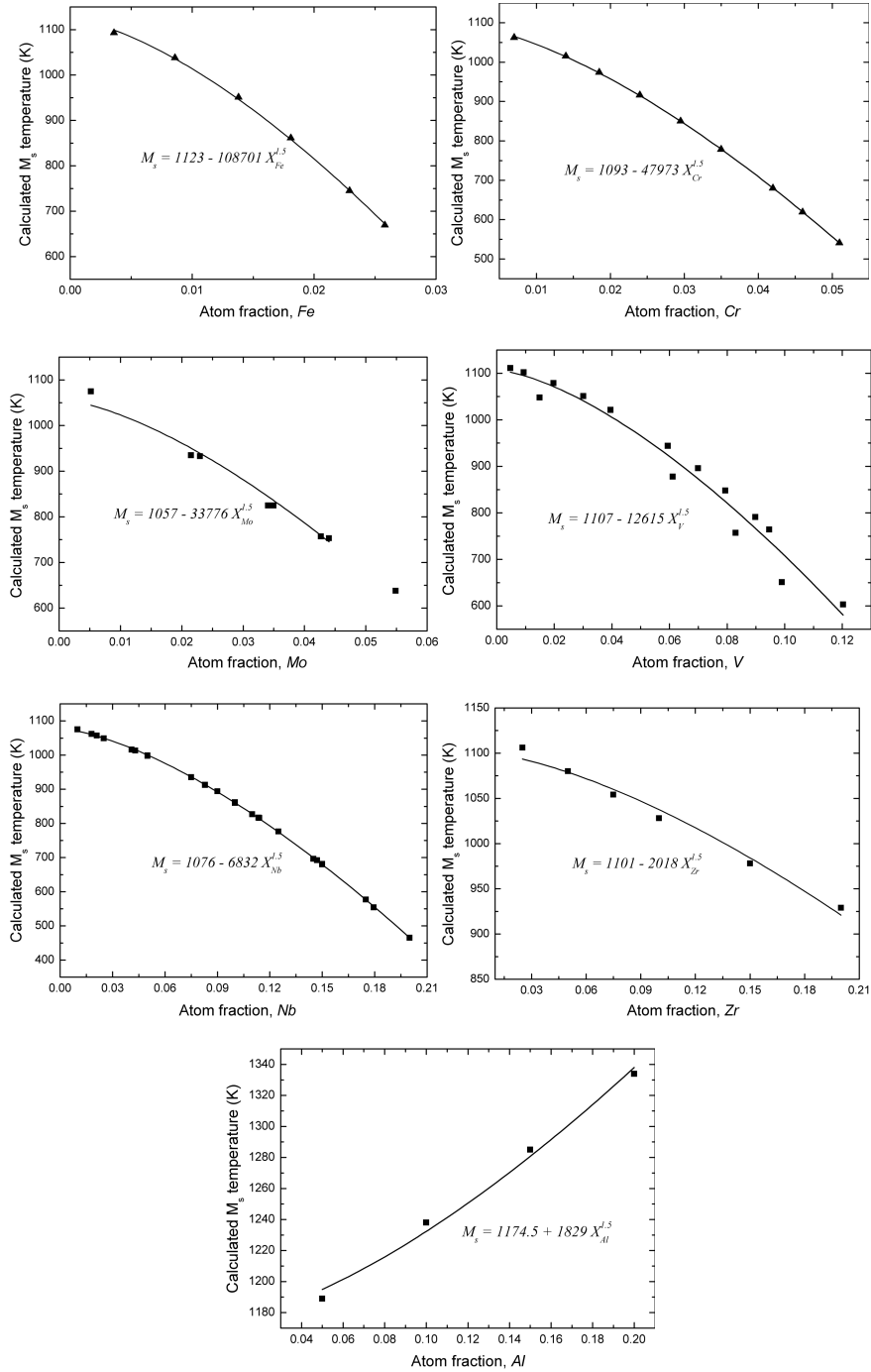


Figure 4.6: Approximations for the predicted M_s values of Ti-X binary systems to obtain the coefficients for various solutes.

approach or attempt to validate it by comparing to already established equation, which is the Molybdenum equivalence (Mo Eq.) criterion, for Ti alloys has been made.

4.5.2 Validation of M_s equation

In order to effectively compare the above equation with the Mo Eq., it may be linearised and expressed in terms of the elemental concentrations both in atom fraction (equation 4.9) and wt.% (equation 4.10) as follows:

$$M_s = 1156 - 17480X_{Fe} - 12186X_{Mn} - 11299X_{Cr} - 9463X_{Mo} - 8096X_{Ni} - 5250X_{Cu} - 4354X_V - 3160X_{Nb} - 1200X_{Zr} + 865X_{Al} \quad (4.9)$$

and

$$M_s = 1156 - 150Fe_{wt.\%} - 107Mn_{wt.\%} - 96Cr_{wt.\%} - 67Ni_{wt.\%} - 49Mo_{wt.\%} - 41Cu_{wt.\%} - 37V_{wt.\%} - 17Nb_{wt.\%} - 7Zr_{wt.\%} + 15Al_{wt.\%} \quad (4.10)$$

The results of the linearized equation to predict the M_s temperature (equation 4.10) can be compared to the results of the Mo Eq. criterion (equation 4.11) as given below [2, 27, 126]:

$$Mo_{Eq.} = 1.00Mo + 0.28Nb + 0.22Ta + 0.67V + 1.6Cr + 2.9Fe - 1.00Al \quad (4.11)$$

Mo Eq. (equation 4.11) is a measure of β (meta-)stability in β Ti alloys that can be expressed as the sum of the weighted averages of the alloying elements in wt.%. It is a well established parameter that provides the stability degree of β for further transformations. Thus, the Mo Eq. of various commercial alloy systems from equation 4.11 are compared with the M_s temperature value predicted using the equation 4.10, developed for the multicomponent alloy systems, Fig. 4.7.

A desirable and interesting linear relationship between both criteria is found. Moreover, it is noted that M_s values reaching room temperature are achieved by alloys displaying a Mo Eq. approaching the experimentally observed range of 9.5–11.5 [2]. It is interesting to note that the alloy Ti–10V–2Fe–3Al has a predicted

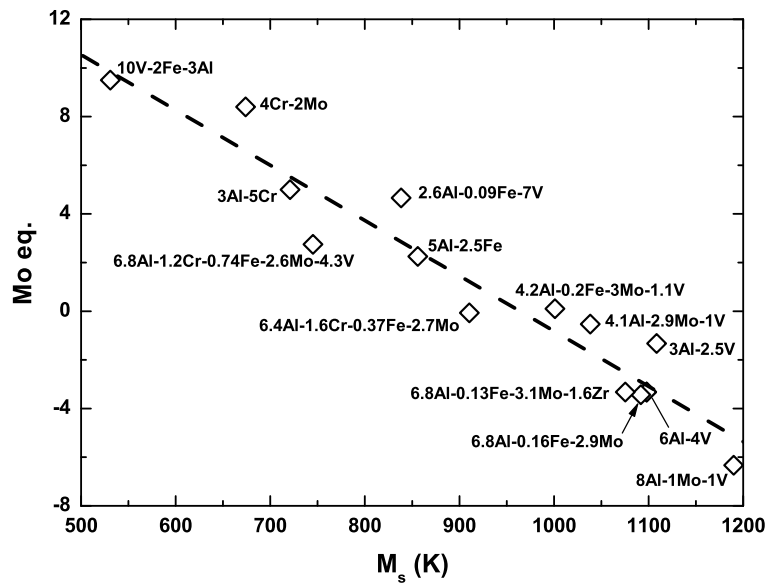


Figure 4.7: Comparison of calculated M_s values and the Mo equivalence criterion for various Ti alloys.

M_s temperature reasonably above the room temperature, which is confirmed by its tendency to form stress-induced martensite at room temperature in the fully solution treated condition.

4.6 Application of M_s model for $Ti - 1023$ experimental conditions

The model developed for estimating the M_s temperature (equation 4.8) for β multicomponent systems has been applied to $Ti - 1023$ alloy. The solution treatment conditions performed on $Ti - 1023$ alloy as explained in *Chapter 2*, and repeated in Table 4.2 have been considered in this study. These are the treatments for which the PiTTi effect was evaluated by compression testing.

A noticeable variation of the local concentration due to solute partitioning among β and α phases was observed for certain solution treated samples, as detailed in *Section 3.1 of Chapter 3*. The model M_s equation has been applied to the

Table 4.2: Considered solution treatment conditions of $Ti - 1023$ for the model.

Temperature regime	Solution treatment condition
above β	900 °C - 60 min
	820 °C - 15 min
below β	700 °C - 15 min
$\beta + (\alpha + \beta)$	900 °C - 15 min/700 °C - 15 min
	900 °C - 15 min/650 °C - 15 min

experimentally measured local β concentration values of the $Ti - 1023$ samples using Electron Probe Micro Analysis (EPMA) in order to predict their possibility of martensite formation. The samples were subjected to different solution treatments and the corresponding EPMA measured values are given in Table 4.3¹. The M_s temperature obtained using the model equation is also reported. The measured concentration values are the non-equilibrium ones for the soaking time considered. In general, the predictions reflect the trend observed for the solution treatments involving above β solutionizing step. The measured values for 900 °C - 60 min seem to nearly reach the equilibrium as seen from the comparison of Table 4.3 and Table 4.4. The M_s predictions reflect the trend of athermal martensite formation for this condition. However, the 700 °C - 15 min below β treatment, does not show a martensite formation as against the model predictions. The small β domains in this condition hinder martensite formation as they require high stress levels, which could be beyond the slip deformation levels [28, 75, 76, 85].

The equilibrium β concentration values at the different heat treatment temperatures are obtained from Thermo-calc [100] using the Thermotech TTTI3 titanium database [101]. It is to be pointed out that Thermo-calc gives only the equilibrium values for defined conditions and hence the soaking time of the heat treatment temperatures are not relevant for the calculations. Table 4.4 shows the equilibrium β concentration values for the considered temperatures. The corresponding

¹Although good care has been applied to the EPMA measurements and the conversion of intensities to concentrations, there is an unsolved inconsistency between the EPMA data (in particular for V) and the nominal concentration for the homogeneous microstructure of 900 °C for 60 min. We have not been able to resolve the discrepancy.

Table 4.3: Measured EPMA concentration values of β phase at different solution treated temperatures.

Solution treatment conditions	EPMA concentration values in β phase, wt.%	M_s temperature $^{\circ}\text{C}$	PiTTi effect observed
900 $^{\circ}\text{C}$ - 60 min	Ti-8.96V-1.7Fe-3.06Al	331	Yes
700 $^{\circ}\text{C}$ - 15 min	Ti-11.5V-2.36Fe-2.41Al	57	No
900 $^{\circ}\text{C}$ - 15 min /650 $^{\circ}\text{C}$ - 15 min	Ti-9.98V-1.89Fe-2.83Al	239	Yes

Table 4.4: Calculated equilibrium concentration values of β phase at different solution treated temperatures.

Solution treatment temperatures	Equilibrium concentration values in β phase, wt.%	M_s temperature $^{\circ}\text{C}$	PiTTi effect observed
900 $^{\circ}\text{C}$	Ti-9.8V-1.9Fe-3Al	249	Yes
820 $^{\circ}\text{C}$	Ti-9.82V-1.91Fe-3Al	246	Yes
700 $^{\circ}\text{C}$	Ti-14V-2.93Fe-2.73Al	-220	No
900 $^{\circ}\text{C}$ /650 $^{\circ}\text{C}$	Ti-17.5V-3.7Fe-2.58Al	<-273	No

M_s temperature estimated from the M_s equation (equation 4.8) is also reported. At equilibrium concentration levels, in the $\alpha + \beta$ regime, the β is significantly enriched to an extent that it does not show martensite formation at room temperature. The experimental results support the calculations for the corresponding solution treatments, whereas for 700 °C - 15 min no athermal or stress-induced martensite formation was observed.

Apart from the β grain size consideration, the M_s equation reflects a reasonable trend of the martensite formation for the Ti – 1023 alloy system.

4.7 Conclusions

A thermodynamic approach to predict the martensite start temperature for β Ti alloys is presented. Following Olson and Cohen's theory on martensite nucleation and Ghosh-Olson's approach, a model representing the compositional dependence of the critical energy for martensite formation for Ti alloys involving BCC to HCP lattice transformation energetics has been developed. The model successfully reflects the energy contribution of each element towards the martensite formation. It was found that the solute-dependent exponent for Ti-binary systems is 1.5. The model has been successfully applied to binary systems of Ti with Fe, Mn, Cr, Mo, Cu, Ni, V, Nb, Zr and Al, and reproduced the reported M_s data with an accuracy of ± 50 K.

Extending the binary M_s predictions to multicomponent Ti systems, a first order approximation has been postulated assuming non-linear dependence with solute concentrations. The equation ignores the interaction between solute elements and β grain size dependence. An approximately linear relation has been observed between the postulated M_s equation and the already established and frequently employed Mo equivalence criterion for β Ti alloys, effectively validating the proposed equation for Ti-multicomponent systems.

The application of the developed thermodynamic based M_s model equation predicts reasonably well the trends in martensite formation for Ti – 1023 alloy. The above β (900°C - 60 min) solution treated condition showed athermal martensite formation in accord to the M_s prediction value. However, for the below β

conditions the equation predicts martensite formation against observations mainly due to neglecting the grain size effect, which is critical for smaller β domains.

Chapter 5

Design and characterization of the newly developed Ti alloys

The significance of the martensite formation and its contribution to improve the mechanical properties of β titanium alloys in general [36, 44, 48, 78, 84], and of *Ti* – 1023 alloy in particular [Chapter 2], has been studied in this work. It resulted in a thermodynamics based model to predict the M_s temperature [Chapter 4]. The key requirement for optimizing the martensite formation is a sufficient but low β phase stability level, which can be estimated from the M_s temperature or the well established Mo eq. equation [2, 27]. Hence, from an alloy design perspective, the tendency for martensitic transformation can be expressed in terms of parameters like M_s temperature and β -phase stability (Mo eq. value). Controlling such parameters by linking them to the concentration of the alloying elements results in tailor-made alloy compositions to achieve the desired mechanical properties via martensite formation. This chapter deals with designing such new alloy compositions expected to display the PiTTi effect. The new alloy compositions have been fabricated as experimental casts. In addition to the alloys of a new composition, also the occurrence of PiTTi effect in an existing commercial alloy (β – 21S) has been considered. All three alloys have been characterized on their tendency to show the desired plasticity induced martensite formation.

5.1 Design of new alloy compositions

5.1.1 Design approach

Inspired by the property improvements achieved in *Ti*–1023 displaying the PiTTi effect, new alloy compositions having the potential to optimally exhibit such effect have been designed as follows. The main design criteria for the new alloy compositions are: 1) Obtaining an athermal M_s temperature at around room temperature ($-25\text{ }^\circ\text{C} \leq M_s \leq 25\text{ }^\circ\text{C}$) (using the M_s model, equation 4.8 of *Chapter 4*), which corresponds to a (meta-)stability of β , in the range $9.5\text{ wt.}\% \leq \text{Mo eq.} \leq 11.5\text{ wt.}\%$ (using the Mo eq., equation 4.11 of *Chapter 4*). 2) Designing an alloy and processing modification leading to a reduction in grain size without altering much their M_s or Mo eq. value. Using these considerations, two alloys have been designed i) a composition, based on *Ti*–1023 to realize the β grain size reduction on PiTTi effect by adding a grain refining element, Boron (B): Ti-10V-2Fe-3Al-XB. B has a strong influence on β grain size reduction in various β and $\alpha + \beta$ Ti alloys [23, 24, 25, 127, 128, 129, 130, 131]; ii) a composition, based on Ti-5Al-5V-5Mo-3Cr (a commercial replacement for the *Ti*–1023 alloys [132, 133]), with adjusted V (X_1), Mo (X_2) and Cr (X_3) levels to induce PiTTi effect: Ti-5Al- X_1 V – X_2 Mo – X_3 Cr. The approach followed to reach the final optimum composition for both the alloys is elucidated below.

5.1.2 Results and discussion

The Ti-10V-2Fe-3Al-XB alloy composition has been aimed to further improve the existing PiTTi properties of *Ti*–1023 by reducing its prior β grain size. To achieve this, traces of B additions have been considered. Since the influence of B on M_s temperature has not been quantified in our model due to lack of literature data, calculations were performed to study its effect (up to 0.15 wt.%) on the driving force for martensite formation ($-\Delta G$ at M_s) employing thermodynamic software (Thermo-calc) [100] and the TTTI3 Thermotech titanium database [101].

Figure 5.1 shows the variation of the driving force ($-\Delta G$ at M_s) as a function of B content and temperature. B additions up to 0.15 wt.% have a negligible effect

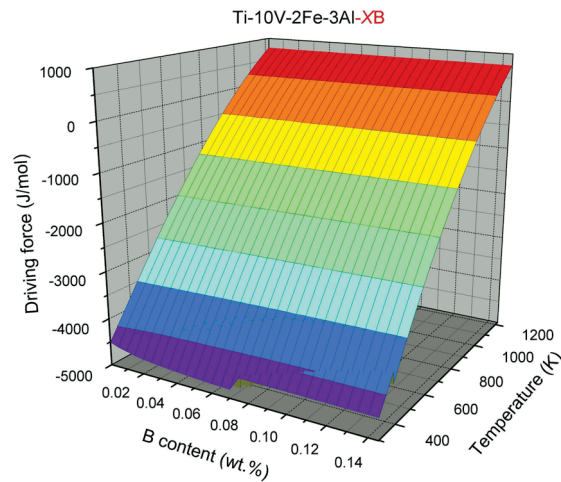


Figure 5.1: Driving force ($-\Delta G$ at M_s) variation as function of B content for different temperatures.

on the variation of $-\Delta G$ at M_s , and hence on the martensite formation ability. So, expected property improvements can very well be related to the alteration in the β grain size. Literature experimental studies report that B additions up to 0.1 wt.% reduce the grain size to a significant degree without deteriorating the mechanical properties [23, 128, 129, 130]. Since, from the design perspective, increasing the B content beyond 0.1 wt.% does not have a noticeable effect on $-\Delta G$ at M_s (Fig. 5.1), the final concentration of B has been limited to 0.1 wt.%, in accordance to studies involving other β Ti alloys [130, 131].

The other new composition (Ti-5Al- X_1 V- X_2 Mo- X_3 Cr) is a modification of the existing β alloy (Ti-5Al-5V-5Mo-3Cr), whose Mo eq. value is 8.2, and as such does not exhibit deformation induced martensitic formation [132, 133, 134, 135, 136]. Concentration variations of the dominant β stabilizers V, Mo and Cr in this alloy have been considered in order to reach a composition that satisfies our criteria to achieve martensitic transformation and the eventual PiTTi properties.

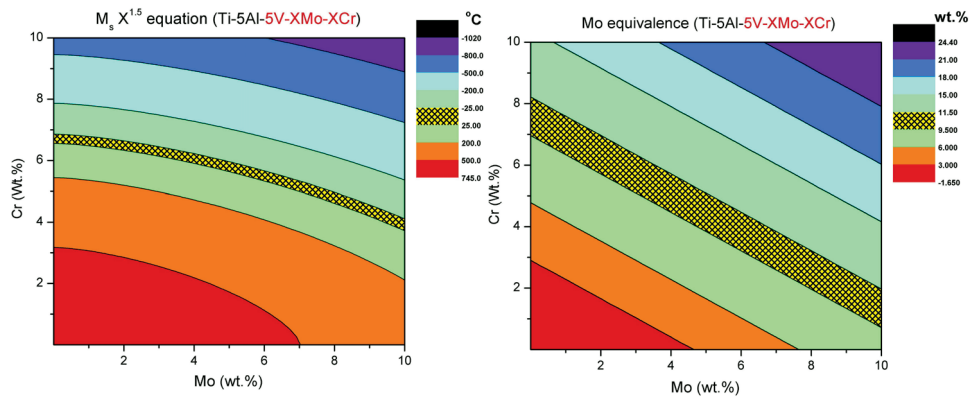
It follows from our model binary system calculations that Cr and Mo have a reasonably strong influence on M_s while V only has a moderate influence. Hence, the range of concentrations for Mo and Cr are limited within 0 to 10 wt.%. Additions beyond this would either make β highly stable (Mo eq.) or promote the

formation of undesirable precipitates: intermetallic compounds of Cr [102]. The window in which V has been varied is between 5 and 12.5 wt.%, as V has a positive influence on pushing the M_s down to the desired range. Furthermore, the Al content has been maintained to 5 wt.% in order not to deviate too far from the base commercial alloy.

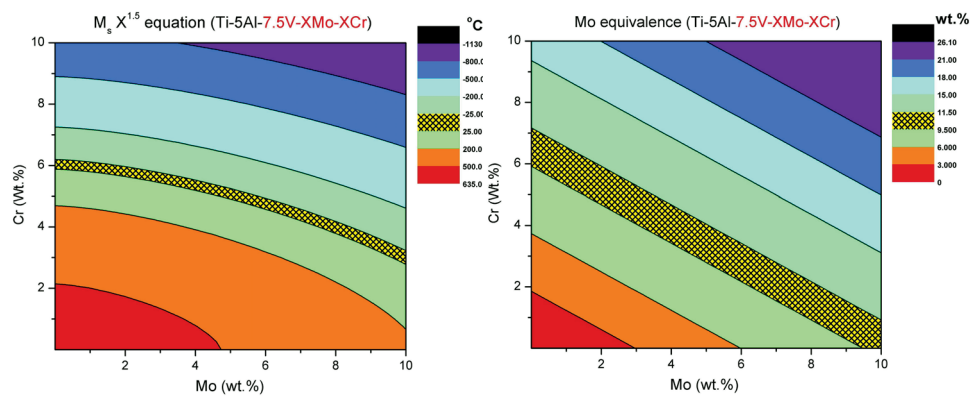
To simplify the computations, the V concentrations have been varied in steps as 5, 7.5, 10 and 12.5 wt.%, while varying the Mo and Cr in the considered range. Figures 5.2a to 5.2f and 5.3a, 5.3b show the computed M_s temperature and the Mo eq. for various V levels, from 5 to 12.5 wt.%. To illustrate our design approach, the results of the computations in which the V was fixed to 10 wt.%, while varying the Mo and Cr content as shown in Figures 5.3a and 5.3b has been considered. The figures show the M_s temperature (following equation 4.8 of Chapter 4) and the Mo eq. variation (following equation 4.11 of Chapter 4) as function of Mo and Cr content in the considered ranges. The hatched regions in Figures 5.3a and 5.3b correspond to the desired values of M_s : $-25\text{ }^\circ\text{C} \leq M_s \leq 25\text{ }^\circ\text{C}$ and Mo eq.: $9.5\text{ wt.}\% \leq \text{Mo eq.} \leq 11.5\text{ wt.}\%$, respectively for various combinations of Mo and Cr concentrations that potentially could lead to PiTTi effect. However, the final optimum composition is reached by selecting the overlapping region (as highlighted by the filled area within the hatched region in the Figures 5.3a and 5.3b) that satisfies both the criteria. The final new compositions stemming from our calculations after further analysis are given in Table 5.1, along with their estimated β transus from Thermo-calc and M_s temperatures from the M_s model.

The new alloy compositions are validated by observing their position in the standard plot of M_s vs. Mo eq., where they are alongside a number of commercial alloys. The Mo eq. and the M_s temperature values of the commercial alloys are estimated following our model equations (equation 4.8 and equation 4.11 of Chapter 4) that has been considered for the new alloys design, Fig. 5.4. An approximately linear correspondence between both equations has been observed.

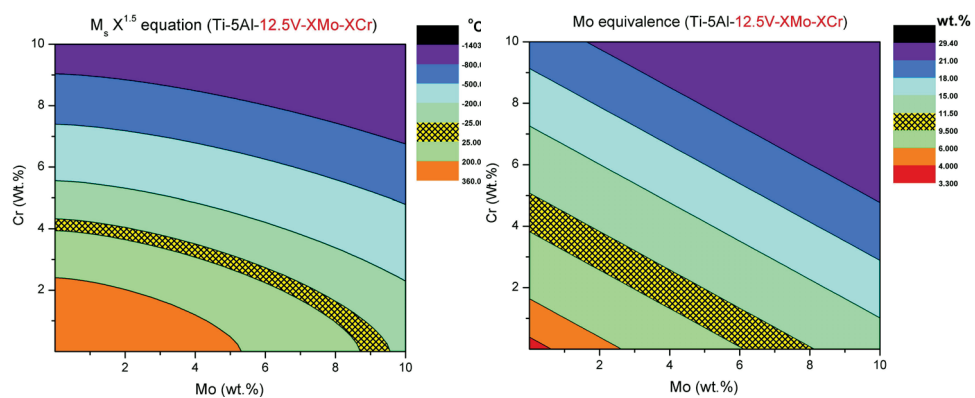
Moreover, it is to be noted that room temperature M_s values are in principle achieved by alloys displaying a Mo eq. approaching the experimentally observed range of 9.5 to 11.5 wt.% for most of the existing metastable alloys. The designed new alloys fit within this range as seen in Figure 5.4.



(a) The M_s temperature as function of Mo and (b) The Mo eq. as function of Mo and Cr for 5 wt.% V



(c) The M_s temperature as function of Mo and (d) The Mo eq. as function of Mo and Cr for 7.5 wt.% V



(e) The M_s temperature as function of Mo and (f) The Mo eq. as function of Mo and Cr for 12.5 wt.% V

Figure 5.2: Alloy design calculations (M_s and Mo eq.) as function of concentration of alloying elements (Mo, Cr and V); the hatched region highlights the desired values for PiTTi effect.

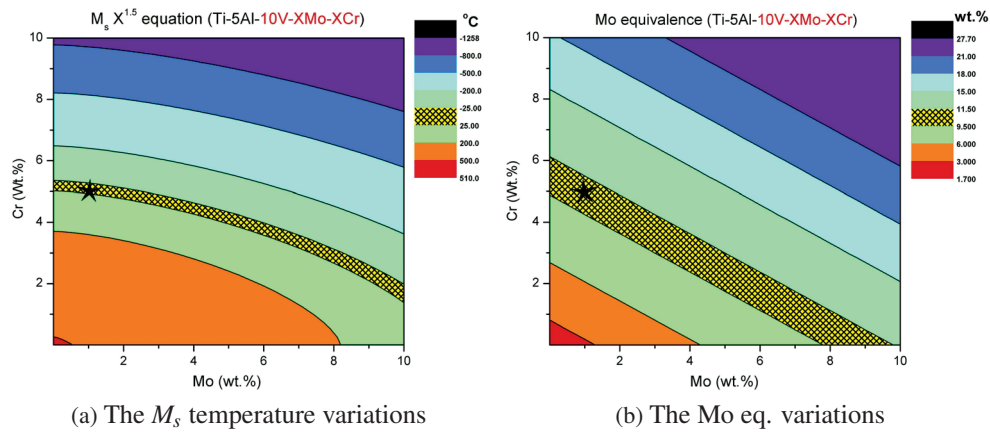


Figure 5.3: Alloy design calculations as function of concentration of alloying elements (Mo and Cr) for 10 wt.% V; the hatched region is the desired values; the highlighted concentration point is of alloy 2 that satisfies both criteria.

Table 5.1: The designed new alloy compositions.

	New alloy compositions (wt.%)	β -transus ($^{\circ}\text{C}$) (Thermo-calc)	M_s temperature ($^{\circ}\text{C}$)
Alloy 1	Ti-10V-2Fe-3Al-0.1B	~ 760	~ 240
Alloy 2	Ti-10V-5Al-5Cr-1Mo	~ 742	15

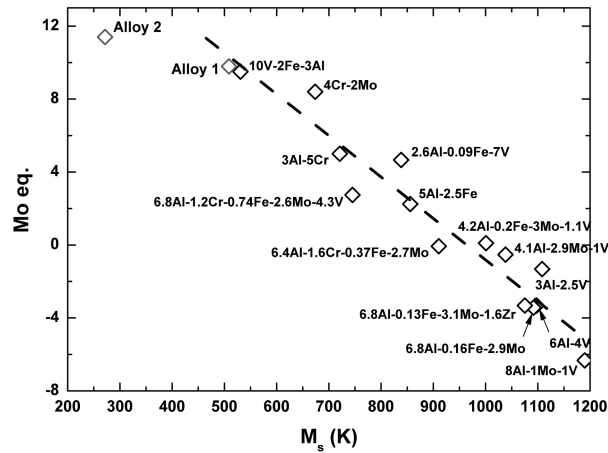


Figure 5.4: Validation of the designed new alloys composition with various existing β and $\alpha + \beta$ Ti alloys.

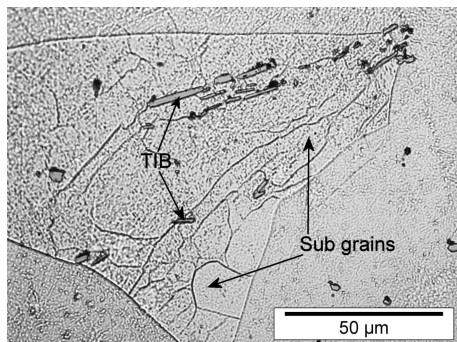
5.2 Alloy fabrication

The designed new compositions Alloy 1 and Alloy 2, further referred to as *Ti1023 – B* and *Ti10551* respectively, have been fabricated on a laboratory scale by a commercial alloy company, GfE Gesellschaft für Elektrometallurgie mbH, Nuremberg, Germany. Each alloy ingot weighing about 15 Kg approximately has been delivered in forged condition. The ingots were prepared by double vacuum arc reduction (VAR) melting and machined before hot forging below 1000 °C. A final heat treatment to the forged material below 1000 °C has been applied. After machining and surface finishing, the material has been delivered in rod form of dimensions D 90 mm x L 500 mm as shown in Figure 5.5. The achieved compositions provided by the manufacturer are tabulated in Table 5.2.

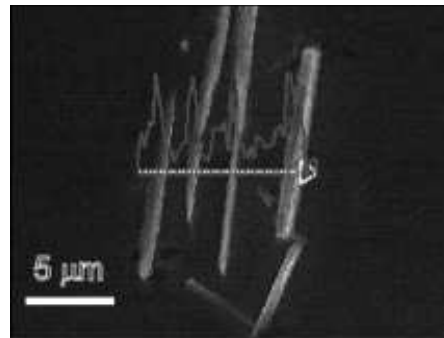
The β transus temperatures for the material in its as-received state have been measured using differential thermal analysis (DTA) and Dilatometer. The measured β transus values of *Ti1023 – B* and *Ti10551* are approximately 765 ± 5 °C and 794 ± 5 °C, respectively. These values correspond reasonably well with the predicted β transus values reported in Table 5.1. The as-received microstructure of the *Ti1023 – B* shows large β grains within which sub-grains are clearly visible, along with needle-like particles, Fig. 5.6a. The needles are identified as Boron



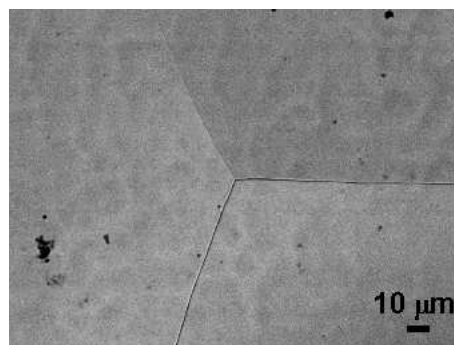
Figure 5.5: The as-received new alloys in rod form.



(a) Alloy 1 showing sub-grains and TiB needles



(b) EDS line scan analysis proving the boron enrichment (Grey lines) in the TiB needles



(c) Alloy 2 showing large β grains

Figure 5.6: The as-received microstructure of the designed new alloys.

Table 5.2: The achieved compositions (in wt.%) of the fabricated new alloys.

	V	Cr	Fe	Al	B	Mo	Cu	Si	O	H	N	C	Ti
Alloy 1	10.69	-	1.99	3.14	0.089	-	0.007	0.057	0.210	0.014	0.008	0.034	balance
Alloy 2	10.09	5.54	-	5.47	-	1.25	0.005	0.015	0.110	0.008	0.004	0.019	balance

rich Titanium boride (TiB) intermetallics by EDS line scan analysis (Fig. 5.6b). The intention of B addition to *Ti* – 1023 was to form small TiB needles that can control the prior β grain size by Zener pinning [137]. However, that has not been realized in the as-received condition of *Ti*1023 – B as the TiB needles are large and are located primarily in the grain interior and do not show any pinning effect on the grain boundary. The *Ti*10551 alloy shows very large prior β grains in the as-received condition (Fig. 5.6c). The Vicker's macro hardness values for *Ti*1023 – B and *Ti*10551 are $\sim 350 H_v$ and $\sim 270 H_v$, respectively. Overall, both alloys in their as-received condition have a homogeneous β structure with a large grain size.

5.3 Experimental details

The as-received alloys have been subjected to various experimental techniques to test them for the occurrence of PiTTi effect.

Machining and polishing

The ingot rod material has been parted into three parts: top, middle and bottom. In each of these sections, many cylindrical samples along the longitudinal and transverse directions have been prepared by electrical discharge machining (EDM). The cylindrical samples are of approximately 4 mm diameter and 7 mm length dimensions. Preliminary analysis on the samples from three parts does not show much variation in properties and hence further characterization has been limited to the samples machined along their longitudinal direction from the middle portion of the ingot rod. Smaller size samples have been cut using a slow speed ($< 500 rpm$) diamond saw (ISOMET 11-1180 Low speed saw, BUEHLER).

The polishing procedure and etchant solutions are the same as described in Chapter 2, except for the as-received and below β transus samples of *Ti*10551 (etchant: 5 ml HF + 10 ml HNO₃ + 35 ml water), and β – 21S samples (etchant: 40 ml glycerol + 15 ml HF + 20 ml HNO₃ + 5 ml water).

Table 5.3: Optimized solution treatments for PiTTi analysis in new alloys.

Solution treatment condition	Temperature regime	Further reference name
900 °C - 60 min	above β	ST-1
700 °C - 15 min	below β	ST-2
900 °C - 15 min/700 °C - 15 min	$\beta + (\alpha + \beta)$	ST-3

Solution treatments

The cylindrical samples have been solution treated in a *Bähr* 805 horizontal dilatometer at a vacuum level of 10^{-5} mbar approximately, and helium gas quenched to room temperature. A thermocouple has been spot welded to the sample surface to track the sample temperature.

The fabricated new alloys have been subjected to the previously optimized solution treatment schemes (*Section 2.4.2.1 of Chapter 2*) before evaluating their martensite formation capability. The solution treatment conditions, representing each of the different microstructure domains β , $\alpha + \beta$ and $\beta + (\alpha + \beta)$ are tabulated in Table 5.3.

Compression

Stress-induced martensite formation ability of both the new alloys in the as-received, and various solution treated conditions has been assessed by compression testing in a Gleeble[®] 1500 machine. The samples were deformed at a strain rate of 10^{-3} s⁻¹ at room temperature. In order to avoid friction between the anvils and the sample surface a lubricant (Lubriplate (white grease)) has been used.

Sub-ambient temperature compression testing has been carried out using an INSTRON machine of 250 kN load cell at a strain rate of 10^{-3} s⁻¹. The test temperature of -50 °C is maintained within a temperature chamber cooled using a Liquid N₂ atmosphere.

Microscopic analysis

The observation of various phases, their morphology and distribution along with other features of the polished and etched samples has been carried out using Leica DM/LM microscope with a Leica DC300 camera. The longitudinal cross-section surface of the sample has been observed. High resolution microscopy analysis has been performed using scanning electron microscopy JEOL JXA 8900R coupled with an energy dispersive spectrometer (EDS).

Structural analysis

The identification of the various phases in the samples subjected to different conditions has been carried out using X-ray diffraction (XRD) with Cu K_{α} radiation at room temperature. XRD data were taken from the longitudinal cross section of the samples over a 2θ range from 10 to 90 degrees. It is to be noted that instead of the usual Co the Cu radiation has been used here as it produced less background.

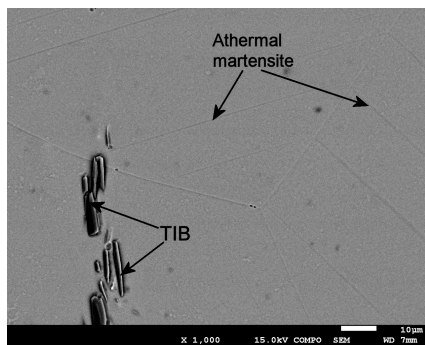
In the following sections the microstructure and properties of the three alloys considered in this chapter are reported.

5.4 Characterization of the new *Ti1023 – B* alloy

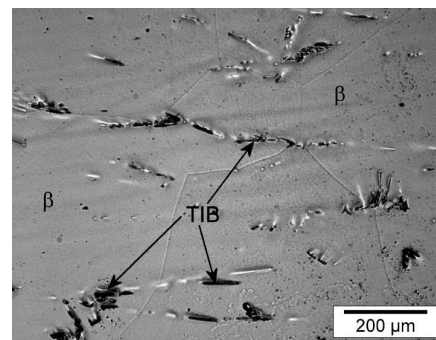
5.4.1 Results

5.4.1.1 Microstructure

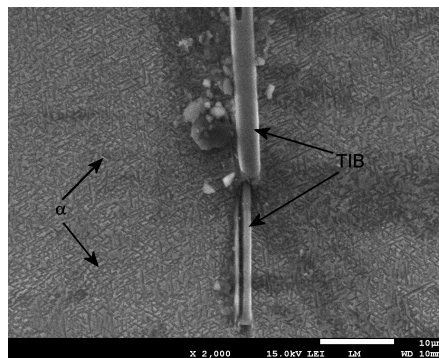
The heat treated samples have been analysed metallographically. The microstructures of *Ti1023 – B* show the formation of martensite, specifically for the above β treatments, along with the dispersed TiB needles as shown in Fig. 5.7a. In contrast, the $\beta + (\alpha + \beta)$ treatment, surprisingly, did not show the presence of equilibrium α phase. Only the appearance of large prior β grains with random distribution of TiB particles has been observed, Fig. 5.7b. The absence of α points at a slow nucleation kinetics, but there is no obvious reason for α nucleation to be hampered.



(a) The above β (ST-1) treated microstructure with β , athermal martensite and TiB



(b) The $\beta + (\alpha + \beta)$ (ST-3) treated microstructure with β and TiB particles, no equilibrium α is present



(c) The below β (ST-2) treated microstructure with equilibrium α and TiB particles

Figure 5.7: The solution treated microstructures of *Ti1023 – B*.

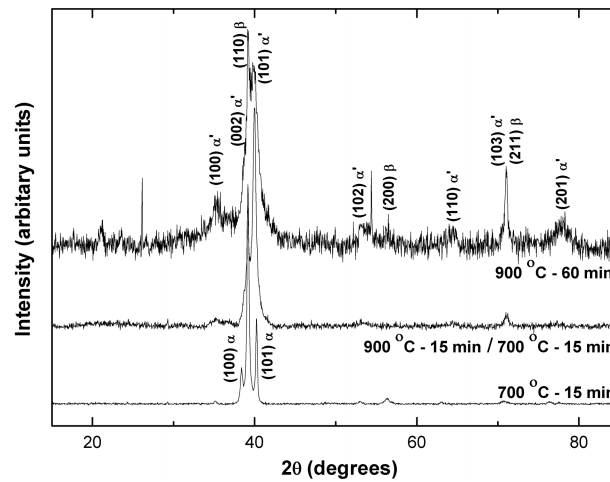


Figure 5.8: X-ray studies after various solution treatments of *Ti1023 – B*.

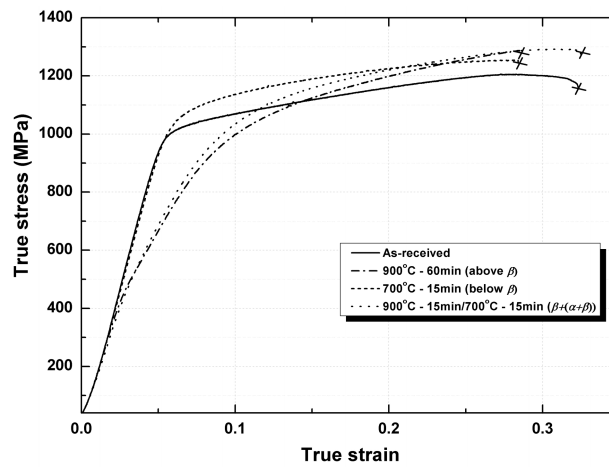
alloy did show athermal martensite formation upon quenching (refer Fig. 2.9 of Chapter 2). The below β treatment shows the equilibrium $\alpha + \beta$ microstructure, along with randomly distributed TiB particles, Fig. 5.7c. The X-ray results confirm the presence of different phases at various conditions. Though the TiB particles are present in all conditions they are not discernible in the XRD results, mainly due to their very small volume fraction, Fig 5.8. The crystal parameters including the phase fraction estimated from the X-ray peaks of the various treated *Ti1023 – B* alloy are tabulated in Table 5.4.

5.4.1.2 Mechanical property evaluation

The different *Ti1023 – B* samples have been subjected to compression testing in a Gleeble[®] 1500 machine for evaluating their martensite formation capability (PiTTi effect). Figure 5.9 shows the compressive stress-strain behaviour of the as-received material and the three different solution treated samples. The treatments that involve a β solutionizing step show the PiTTi effect. A clear signature of such effect is evident with the double-yield point behaviour of the stress-strain curves. The above β and $\beta + (\alpha + \beta)$ treatments clearly exhibit formation of martensite upon loading. However, the below β microstructure does not show the PiTTi effect.

Table 5.4: Lattice parameters of selected solution treated *Ti1023 – B* samples.

		Lattice parameters (Å)		
		900 °C - 60 min	700 °C - 15 min	900 °C - 15 min/ 700 °C - 15 min
β	a	3.25	3.255	3.256
α	a		2.952	
	c		4.687	
α'	a	2.9190		2.961
	c	4.6690		4.650
phase	α		0.371	
fraction	β	0.524	0.635	0.297
	α'	0.476		0.703

Figure 5.9: Compressive stress-strain behaviour of different solution treated samples of *Ti1023 – B*.

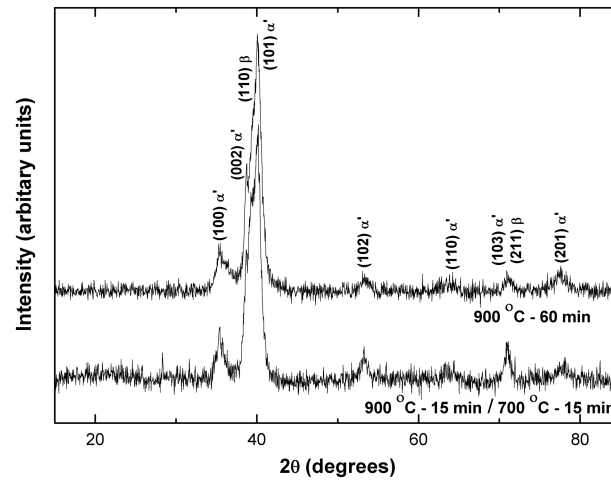


Figure 5.10: Diffractograms of *Ti1023 – B* compressed samples at different conditions.

5.4.2 Discussion

5.4.2.1 Structural analysis

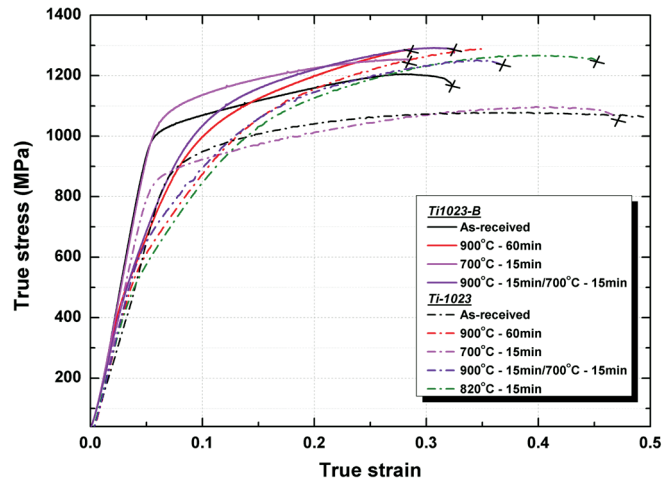
XRD has been used to confirm the occurrence of martensite formation in β solutionised samples after compressive loading. The diffractogram results are given in Figure 5.10. For both samples a substantial α' martensite signal is observed. The lattice parameters for the phases present after compression are listed in Table 5.5. There are some minor differences in lattice parameters between both samples in their initial and compressed state, but no significant trends have been identified. The volume fraction of α' martensite in the compressed ST-1 sample is considerably higher than that in the unstrained condition, in accordance with the distinguishable PiTTi effect, in the stress-strain curve. However, the increase in martensite fraction was considerably smaller for the $\beta + (\alpha + \beta)$ sample, although this showed a clear PiTTi effect as well.

5.4.2.2 Comparison with *Ti – 1023*

In Figure 5.11 the stress-strain curves of *Ti – 1023* and *Ti1023 – B* alloy for the three heat treatments performed is shown. The figure shows that the *B* containing

Table 5.5: Lattice parameters of compressed *Ti1023 – B* samples.

		Lattice parameters (Å)	
		900 °C - 60 min	900 °C - 15 min/ 700 °C - 15 min
β	a	3.238	3.25
	c	4.659	4.636
phase fraction	β	0.189	0.223
	α'	0.811	0.777

Figure 5.11: Comparison of the PiTTi properties of *Ti – 1023* and *Ti1023 – B* alloys.

alloy has a comparable yield point but a higher initial strain hardening coefficient, resulting in a lower strain to failure. To a first approximation the stress range over which the $\beta \rightarrow$ martensite transformation occurred remained more or less constant. Table 5.6 compares the mechanical properties of both the *Ti-1023* and *Ti1023-B* alloys. For the fabricated conditions used the TiB particles are too coarse and no grain refinement has been observed and the effect of grain size on the conditions for PiTTi transformation could not be established.

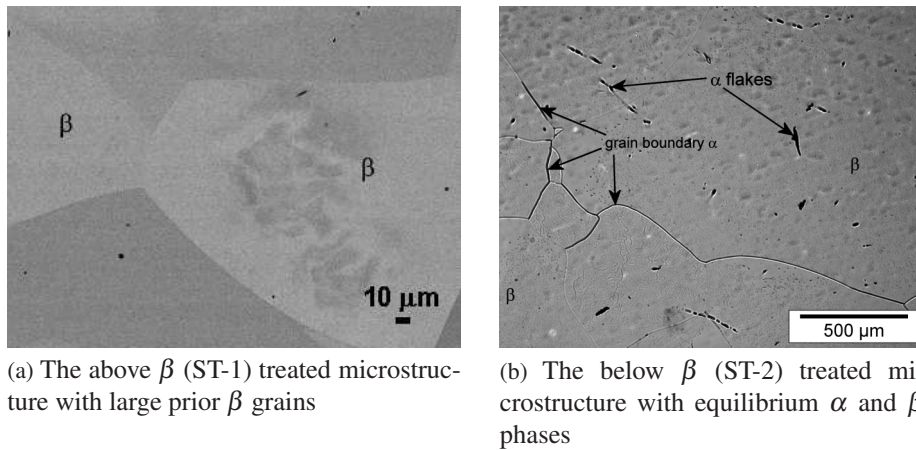
In order to realize the aspired grain refinement in *Ti1023-B*, a homogenization treatment at $\sim 1500^\circ\text{C}$ (*i.e.*, above the $\sim 1430^\circ\text{C}$ solvus temperature of TiB) for 2 h has been performed resulting in segregation of fine TiB needles along the grain boundaries. However, no pinning effect has been observed to achieve the reduction in grain size. Further experiments imposing cold rolling strains of up to 13 % followed by recrystallization treatment at above β transus still does not result in any reduction of the β grain size.

5.5 Characterization of *Ti10551 alloy*

5.5.1 Results

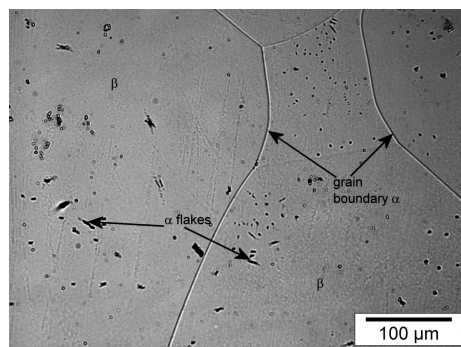
5.5.1.1 Microstructure

In the case of *Ti10551*, the different heat treatment conditions did not result in much different microstructures, as the resulting microstructure of all treatments shows a homogeneous β of large grain size with only a small α fraction. Figures 5.12a, 5.12b and 5.12c show the respective microstructure of the above β , $\alpha + \beta$ (below β) and $\beta + (\alpha + \beta)$ treatments. More importantly, the treatments involving below β temperatures did show the presence of more grain boundary α and few randomly distributed α flake regions. X-ray results confirm the presence of different phases. The predominant β peaks are quite evident for the different solution treatments, Fig 5.13. The crystal parameters including the phase fraction estimated from X-ray peaks are tabulated in Table 5.7.



(a) The above β (ST-1) treated microstructure with large prior β grains

(b) The below β (ST-2) treated microstructure with equilibrium α and β phases



(c) The $\beta + (\alpha + \beta)$ (ST-3) treated microstructure with β and small fraction of grain boundary α film, α flakes

Figure 5.12: The solution treated microstructures of *Ti*10551.

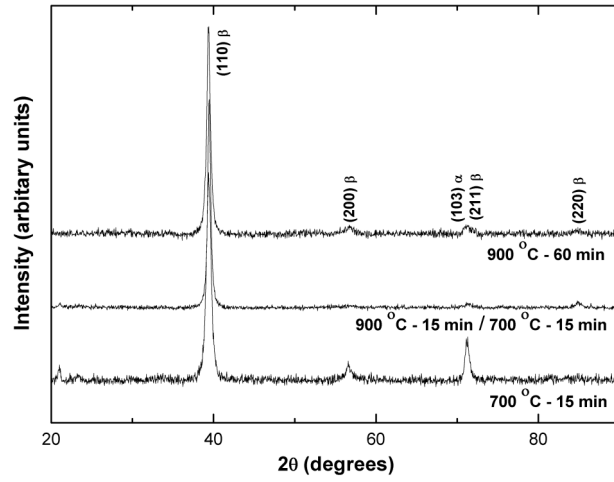


Figure 5.13: X-ray studies after various solution treatments.

Table 5.7: Lattice parameters of selected solution treated *Ti10551* samples.

		Lattice parameters (\AA)		
		900 °C - 60 min	700 °C - 15 min	900 °C - 15 min/ 700 °C - 15 min
β	a	3.237	3.243	3.233
	c		4.610	
α	a		2.648	
	c		4.610	
phase fraction	α		0.078	
	β	1.000	0.922	1.000

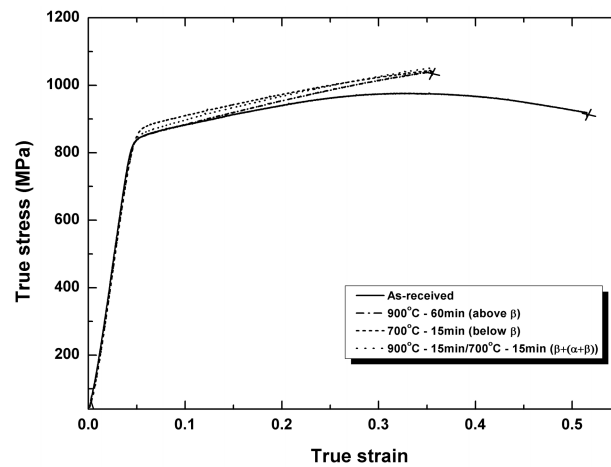


Figure 5.14: Compressive stress-strain behaviour of different solution treated samples of *Ti*10551.

5.5.1.2 Mechanical property evaluation

In *Ti*10551, the different solution treated microstructures were evaluated for their PiTTi characteristics. Figure 5.14 shows the respective compression stress-strain response of the as-received and the solution treated sample conditions. None of the solution treated samples show any existence of PiTTi effect *i.e.* no double-yield point behaviour is observed. The mechanical response of the samples subjected to the different conditions are all similar.

5.5.2 Discussion

5.5.2.1 Structural analysis

The compressed phase composition of *Ti*10551 alloy after subjecting it to various solution treatments has been identified as shown in Figure 5.15. The absence of a significant martensite peak formation even after compression is quite evident for all the conditions. The corresponding crystal parameters along with the phase fractions are tabulated in Table 5.8. As observed in the previous sections, all the solution treated samples have untransformed large stable β grains and thus show

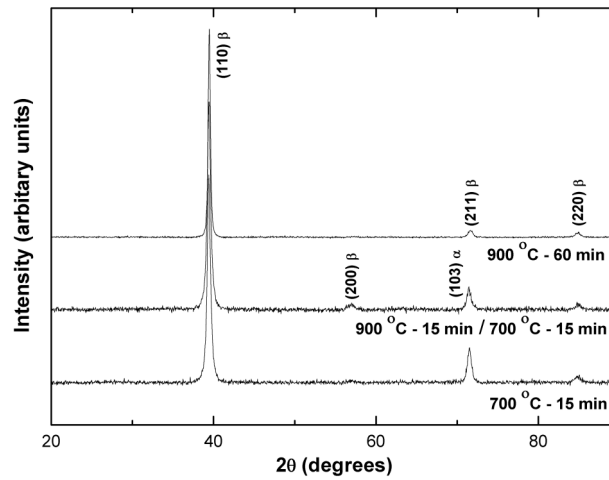


Figure 5.15: Diffractograms of *Ti10551* compressed samples at different conditions.

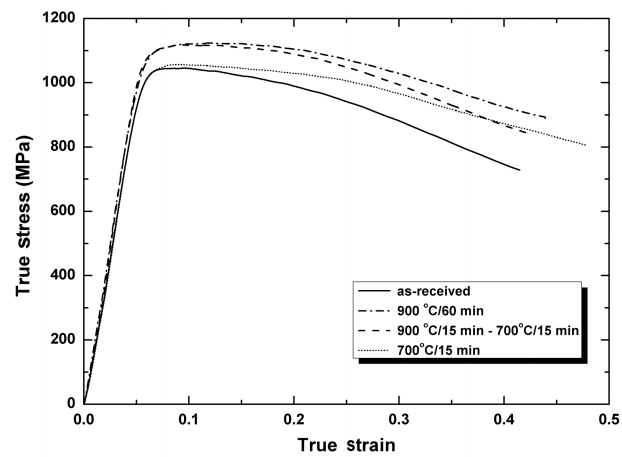
almost identical mechanical properties upon compression. The retained β grains seem to be very stable precluding any martensitic transformation upon quenching and loading at room temperature. Interestingly, the absence of a PiTTi effect at room temperature compression testing is in a way plausible, as the as-received *Ti10551* compositions, according to our model predictions, has an M_s temperature below room temperature.

5.5.2.2 Sub-ambient temperature compression testing

Since the compression curves at room temperature did not show any signs of martensite formation or martensite plasticity, deformation at lower temperature, well below the calculated M_s was performed. Compression experiments have been made at $-60\text{ }^\circ\text{C}$ (Fig. 5.16) for the three solution treated conditions of *Ti10551*. However, the sub-ambient temperature experiments do not show any evidence for the double-yield phenomenon attributed to the PiTTi effect. Instead, simple shear softening was observed.

Table 5.8: Lattice parameters of compressed *Ti*10551 samples.

		Lattice parameters (Å)		
		900 °C - 60 min	700 °C - 15 min	900 °C - 15 min/ 700 °C - 15 min
β	a	3.227	3.229	3.231
α	a		2.904	2.909
	c		4.642	4.648
phase fraction	α		0.078	0.048
	β	1.000	0.922	0.952

Figure 5.16: Sub-ambient (-60 °C) compression testing of *Ti*10551 alloy samples subjected to different conditions.

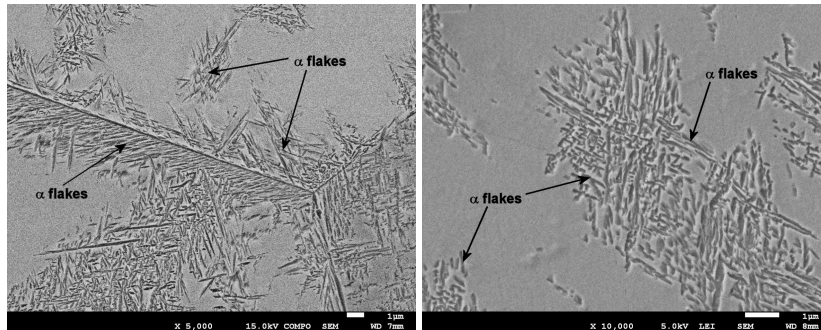
5.5.2.3 Optimization of Ti10551 microstructures

Since the previously followed solution treatments did not result in martensite formation, attempts to tune the experimental parameters (solution treatment temperature and time, β phase stability and microstructure) have been made. Various new solution treatments have been performed to alter the as-quenched microstructure, the β phase stability, and the solute partitioning in order to achieve the PiTTi effect in Ti10551 alloy. Microstructures obtained from new solution treatments, in which one was obtained from solutionizing at 850 °C for 30 min followed by aging at 550 °C for 2 h (Fig. 5.17a), and another treatment at 1100 °C for 60 min followed by cooling to 600 °C and aging for 60 min (Fig. 5.17b) are shown in Figure 5.17. The expected equilibrium α platelets have indeed been observed for these treatments in the $\alpha + \beta$ regime. Various other solution treatment schemes resulted in microstructural features of equilibrium α phase, and partly recrystallized β grains with sub-grain boundaries.

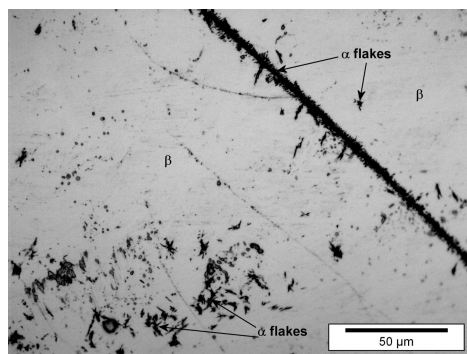
Further, the different solution treated microstructures were compression tested for studying their martensite formation capability, Fig. 5.18. The stress-strain curves do not show any double yield phenomenon, associated to the PiTTi effect in metastable β alloys. Though the presence of α , along with some unknown precipitates, is neither expected to, nor seen to induce the PiTTi effect, it however shows an improvement in the compressive strength properties as compared to the previously analysed microstructures (subsection 5.5.1.1). The increase in strength that is achieved by changing the microstructure shows promising prospects for the alloy.

The absence of the PiTTi effect for the developed new solution treated microstructures at lower $\alpha + \beta$ temperatures can be explained from quantitative EDS spot measurements on local β concentrations. Figures 5.19a and 5.19b show the respective β location of the EDS spot analysis for the two solution treated conditions.

The measured values of selected solution treatments have been applied to the developed M_s equation for β Ti alloys (equation 4.8 of Chapter 4). Table 5.9 shows the β concentration values of the main elements and their respective M_s temperatures for the two conditions.



(a) Presence of equilibrium α flakes in 850 °C for 30 min followed by 550 °C for 2 h solution treated microstructures



(b) Initial stages of equilibrium α flakes nucleation in 1100 °C for 60 min / 600 °C for 60 min microstructures

Figure 5.17: Modification of the Ti10551 microstructure by different solution treatments.

Table 5.9: EDS measured β concentration values for different conditions.

Temperature	Method	V	Cr	Mo	Al	Ti	M_s (°C)	Mo eq. (wt.%)
650	EDS	4.35	8.56	0.57	2.56	bal.	<-273	14.6
	Thermo-calc (equilibrium)	14.9	8.53	1.92	4.76	bal.	<-273	20.79
600	EDS	3.61	8.43	0.55	2.88	bal.	<-273	13.6
	Thermo-calc (equilibrium)	17.9	10.4	2.32	4.29	bal.	<-273	26.7

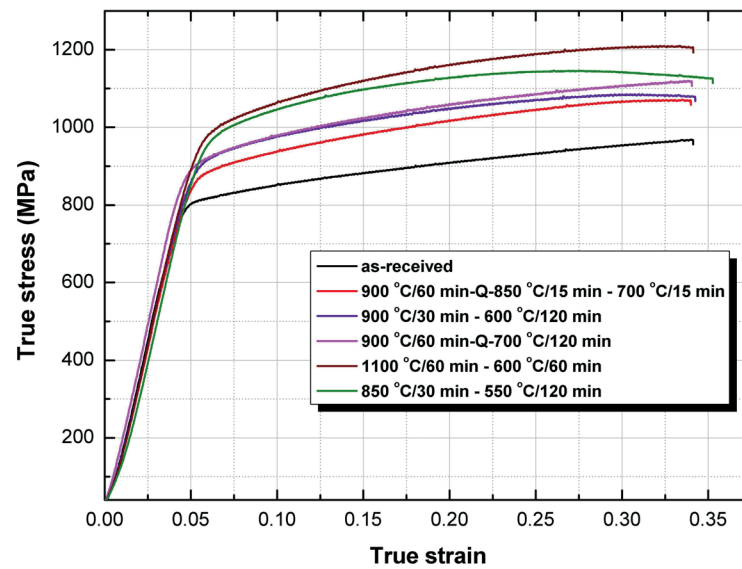
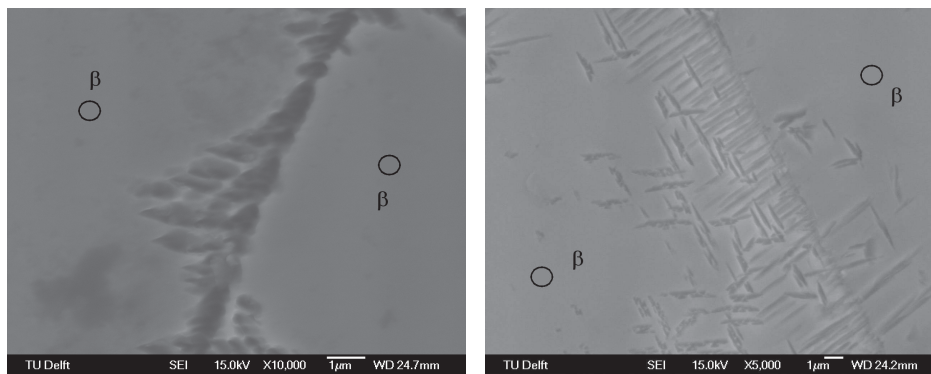


Figure 5.18: Compressive stress-strain curves of the various new solution treatments of Ti10551 alloy.



(a) 900 °C for 15 min / 650 °C for 120 min (b) 1100 °C for 60 min / 600 °C for 60 min

Figure 5.19: SEM showing EDS spot measurements (circled) at β phase.

The estimated M_s temperatures of the new treated microstructures are well below the room temperature, in fact even below 0 K. β is enriched with the β stabilizers and thus making it very stable precluding any transformation upon quenching or even after loading at ambient temperature. Since for these conditions, the amount of driving force needed to form the martensite by loading is very high as compared to the plastic deformation. Hence the Ti10551 alloy subjected to above conditions deform by slip rather than the martensite formation and thus do not show the PiTTi effect.

5.6 Characterization of Ti β – 21S commercial alloy

Since the Ti10551 alloy does not show a clear PiTTi existence as against the model predictions, efforts have been made to test the consistency of the model. Another commercial grade alloy (β – 21S) was considered for assessing its potential for martensite formation. The as-received β – 21S composition is Ti-14.1Mo-3.5Nb-3Al-0.14Si-0.32Fe [138, 139], whose reported β transus is 805 ± 5 °C [140]. The newly developed M_s equation and the established Mo eq. equation have been applied to the as-received β – 21S composition, resulting in respective values of ~ 120 °C and 13 wt.%. The alloy position in the proposed M_s temperature vs. Mo eq. plot (Fig. 5.20) show they fall well in the linear relation observed for the existing alloys. In terms of M_s temperature, their position is in between the two new alloys Ti1023 – B (Alloy 1) - one that shows PiTTi effect, and Ti10551 (Alloy 2) - one that does not show PiTTi effect. But the β stability level (*i.e.* the Mo eq. value) of β – 21S is moderately higher than the desired levels, and that of the new alloys, for athermal martensite transformation. Hence the alloy seems to be within the limits of the possibility of PiTTi effect for metastable β alloys. Studies has been performed on β – 21S to observe its potential for PiTTi effect by subjecting it to the selected solution treatment conditions (Table 5.3) considered for other experimental alloys in this chapter.

The as-received structure of the β – 21S alloy is shown in Figure 5.21. A bi-modal microstructure of needle like α phase along with β has been observed.

The as-received material has been subjected to selected solution treatments in

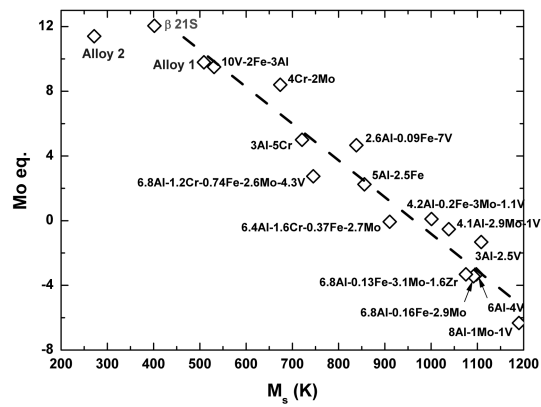


Figure 5.20: The prediction of martensite formation capability of $\beta - 21S$ alloy.

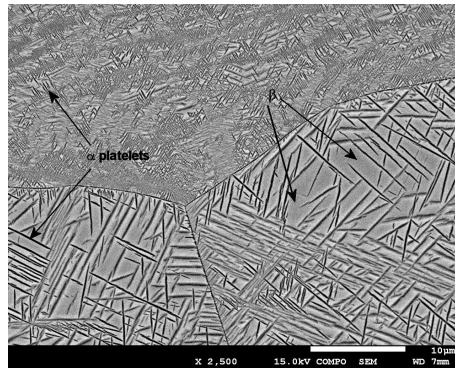
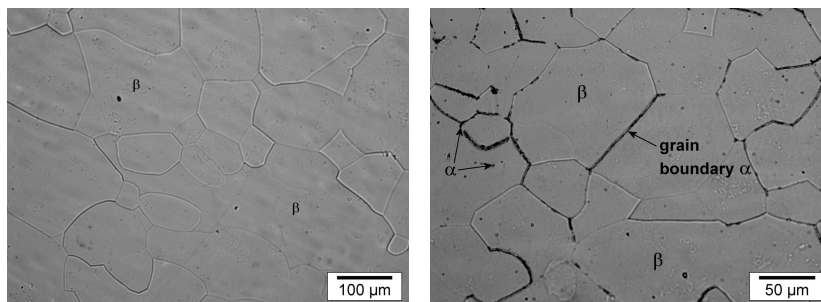


Figure 5.21: As-received microstructure of $\beta - 21S$.



(a) 900 °C for 60 min (ST-1)

(b) 900 °C for 15 min / 700 °C for 15 min (ST-3)

Figure 5.22: The solution treated microstructures of $\beta - 21S$ alloy.

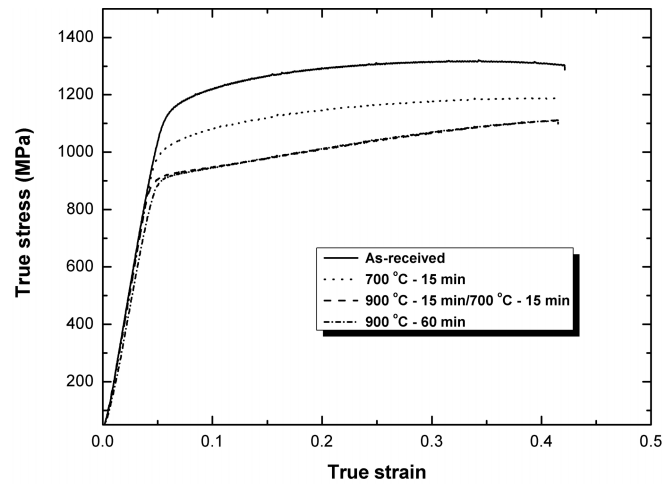


Figure 5.23: Compressive stress-strain curves of β – 21S after various conditions.

the β , $\alpha + \beta$ and $\beta + (\alpha + \beta)$ regime and quenched at high rate, similar to *Ti* – 1023 alloys, using He gas. The solution treated microstructures show that the β was stable enough to be retained to room temperature for both the ST-1 (Fig. 5.22a) and ST-3 treatments, where ST-3 treatment showed a predominant β phase along with the equilibrium α nucleating in the prior β grain boundaries due to the intermediate $\alpha + \beta$ annealing before quenching (Fig. 5.22b). The solution treated samples have been further compression tested in a Gleeble[®] 1500 machine to study their PiTTi capabilities. Similar to the previously observed PiTTi exhibiting alloys, the stress-strain curves of the treatments involving an above β solutionizing showed different characteristics than the other treatments, wherein here a small plateau after the first yield point, Figure 5.23 has been observed. The signature of PiTTi effect from our hitherto studies is a clear double-yield phenomenon, which is not the case here though. Still the occurrence of the same could not be ruled out due to the low first yield point and the strong slope change after that, in the stress-strain curves. Further, the stress-strain behaviour of the below β treated sample does not correspond to any martensite formation, and more or less show a similar characteristics as the as-received sample.

The corresponding compressed microstructures after ST-1 and ST-3 treatments are given in Figures 5.24a and 5.24b, respectively. Microstructural features of both

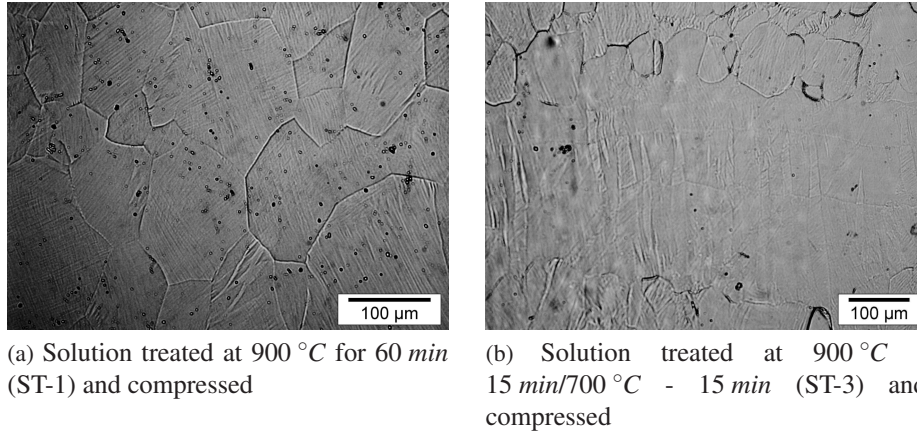


Figure 5.24: Compressed microstructures of $\beta - 21S$ alloy.

Table 5.10: The estimated M_s and Mo eq. value for the equilibrium β concentration values obtained from Thermo-calc for different conditions.

Temperature	Fe	Nb	Mo	Al	Ti	$M_s(^{\circ}C)$	Mo eq. (wt.%)
900 (ST-1)	0.32	3.5	14.1	3	bal.	120	13
900/700 (ST-3)	0.49	4.91	21.1	2.4	bal.	<-273	21.5

the compressed samples resemble that of the martensite, though that could not be confirmed from their respective X-ray diffractograms.

Further analysis has been made by estimating the M_s temperature for the equilibrium conditions of ST-1 and ST-3 treatments of $\beta - 21S$, (Table 5.10). The equilibrium β concentration values at the ST-1 and ST-3 treatment temperatures are obtained by calculations from thermodynamic software, Thermo-calc [100] using the Thermochem TTTI3 titanium database [101]. The estimated values show the possibility of martensite for ST-1 but not for ST-3 condition. However, it is to be pointed out that Thermo-calc gives only the equilibrium values for defined conditions and thus the soaking time of the solution treatment temperatures is not relevant for the calculations. Hence the estimated M_s and the Mo eq. values do not exactly reflect the experimental conditions, where the considered soaking time

could be far from attaining equilibrium.

Thus, the $\beta - 21S$ does not show clear evidence of martensite formation, which may be related mainly to the higher β stability levels of this alloy.

5.7 Discussion

The developed M_s vs. Mo eq. plot (Fig. 5.25) was used to define the compositional window for which a PiTTi effect is to be expected. The commercial composition of $Ti - 1023$, and the designed alloy $Ti1023 - B$ had an M_s temperature well above the room temperature and thus further solution treatments enriched the β stability within the limits of metastable β concentrations in the approximate region as highlighted in Figure 5.25, thereby inducing more SIM formation than athermal transformations resulting in improved mechanical properties due to PiTTi effect. In line with this, it will be interesting to make observations on PiTTi occurrence in $Ti-4Cr-2Mo$ alloy, which falls near to the PiTTi showing alloys ($Ti - 1023$ and $Ti1023 - B$, the shaded region in Fig. 5.25). Although the other alloys ($Ti-3Al-5Cr$ and $Ti-6.8Al-1.2Cr-0.74Fe-2.6Mo-4.3V$) have an M_s temperature comparable to the PiTTi alloys, they possess a low Mo eq. value, which reflects a less stable nature of the β phase. It is very likely that such β phase will undergo other favourable athermal transformations to ω and β' phases. On the other hand, if the β stability *i.e.* Mo eq. value, is too high as comparable to the stable β alloys range then even with a reasonably well above room temperature M_s temperature the possibility of martensite formation or tailoring the microstructure for optimum PiTTi effect is minimal as observed for the $\beta - 21S$ alloy, which did not show an explicit PiTTi behaviour for the experimented conditions. Hence it is critical to ensure an appropriate (meta-)stability level in order to observe optimum mechanical properties through PiTTi effect.

Furthermore, in retrospect it has been realized that a design criteria of room temperature M_s and Mo eq. of ~ 11.5 only applies to the fully austenitic state of the new $Ti10551$ alloy. Any heat treatment resulting in the formation of α would lead to the β fraction becoming too stable. The new alloy composition seems to have slow α kinetics as compared to other systems studied in this thesis. Even after

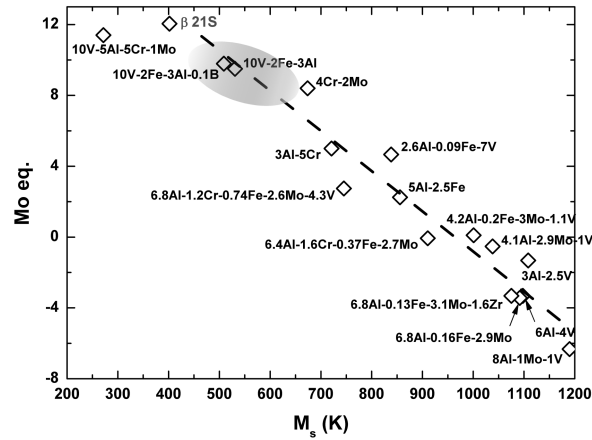


Figure 5.25: The M_s vs. Mo eq. plot highlighting the PiTTi showing region for metastable β alloys.

cooling to a temperature well below β trusus, α fraction was found to be lower than the expected equilibrium value.

In case of the *Ti1023 – B* alloy, though the designed composition had shown the PiTTi effect, the addition of B did not improve the PiTTi properties to higher levels than those observed for *Ti – 1023* alloy. This is mainly because the formation of TiB particles did not result in prior β grain refinement by Zener pinning, which contradicts the general observation of borides pinning the grain boundaries for many β or $\alpha + \beta$ alloys [23, 128, 129, 130]. Moreover, it is believed that the pinning of the TiB particles to β grains is mainly achieved in the fabrication stage of the alloy, which was not achieved with our as-received *Ti1023 – B* alloy and thus resulting in their comparable PiTTi properties, if not improved ones, with nominal *Ti – 1023*. Hence, as any other Ti alloy, the processing or fabrication route of the PiTTi alloy as well may play a critical role in achieving the final properties.

5.8 Conclusions

A novel alloy design approach has been proposed, wherein the key parameters like M_s temperature and Mo eq. are optimized to desired values for designing new alloy compositions. The designed and fabricated two new alloy compositions

are: 1) Ti-10V-2Fe-3Al-0.1B, for observing the influence of prior β grain size reduction on PiTTi properties; 2) Ti-10V-5Al-5Cr-1Mo, for achieving optimum PiTTi properties.

The *Ti1023 – B* alloy exhibit the PiTTi effect with reasonably good properties comparable to *Ti – 1023* alloy. The TiB particles in *Ti1023 – B* did not result in prior β grain size reduction due to the random distribution of TiB needles in as-received sample. Redistribution and segregation of those TiB particles along grain boundaries after homogenizing at 1500 °C for 2 h *i.e.* above the solvus of TiB has been achieved, however the grain refinement has not been realized.

Ti10551 alloy characterization studies do not exhibit the PiTTi effect for the considered solution treatments. The β fraction created was found to be highly stable precluding any transformation upon loading at room temperature. However, the alloy microstructure has been altered to exhibit improved mechanical properties. As a further validation to the developed model, the commercial $\beta – 21S$ alloy has been characterized for martensitic transformation. Though the stress-strain behaviour is different for above β involved treatments, it does not show clear evidence of the typical double yield phenomenon corresponding to the PiTTi effect.

Chapter 6

Comparison of thermodynamic and neural network model predictions for M_s in Ti alloys

Notwithstanding careful experimentation the new *Ti10551* alloy based on the design rules following the simple additive M_s equation did not show the intended PiTTi effect. This may be due to the M_s equation being simple as grain size effects and alloying element interactions were not taken into account. In this chapter, we explore the possibility of interactions between the alloying elements by comparing our M_s predictions ultimately based on data for binary Ti-*X* systems with a statistical model for M_s predictions in multicomponent alloys. As stated in *Chapter 4*, fundamental physical models are best validated for complete datasets with simple and pre-imposed cross correlations having minimal or no uncertainties. Hence such an approach has been good for modelling M_s in Ti-binary alloys. However, for more complex and sparsely populated datasets, non-linear statistical models using non-prescribed functional relationships, such as Artificial Neural Networks (ANNs), are more appropriate [106, 110, 141, 142, 143]. Even for a sparsely filled database the ANNs allows a crude approximation of interaction terms [143]. Such a test on elemental interactions could not be properly made using a physical model with pre-assumed functions for the interaction terms. The current chapter

deals with incorporating the gathered binary alloys M_s temperature vs composition database into the existing ANNs model and to make comparisons with the TD model predictions for both binary and multicomponent systems. Additionally, the updated ANN model has been used to identify any interactions among main solute elements that influence the M_s temperature.

6.1 Artificial neural network model

Artificial Neural Networks (ANNs) are a powerful statistical technique that has found wide application for property estimations within materials science [106, 109, 144, 145]. In general, ANNs follow the following steps: database collection; analysis and pre-processing of data; selection of architecture, non-linear functions, algorithms and network parameter for training the neural network; testing of trained network; application of the trained ANNs model [106, 110]. ANNs consist of simple synchronous processing elements, inspired by nervous systems found in biology [141, 143]. The basic unit in an ANNs is the so-called neuron. Neurons are connected to each other by links called as synapses; associated with each synapse there is a weight factor. The number of neurons in the input and output layers are determined by the desired number of input and output parameters. Usually neural networks (NNs) are trained to a particular set of inputs, in order to reproduce as closely as possible the training data. For reliable training and performance of any ANNs an appropriate and reliable database is necessary [145, 146, 147, 148].

For this study, the well established ANNs model for Ti alloys developed by Malinov and co-workers has been considered [109, 143]. The ANNs model has been developed for simulation of time-temperature-transformation (TTT) curve and M_s temperature estimation as function of composition for Ti alloys. The model has been designed following the standard back-propagation multilayer feedforward network and trained with reliable and extensive literature databases on transformation kinetics to perform complex functions. The general scheme of the model considered is shown in Fig. 6.1 as presented in [109]. The main input layer of the ANNs model is the chemical compositions of the alloys involving common elements (Al, Mo, Sn, Zr, Cr, Fe, V, Cu and O). The output layer is either the TTT

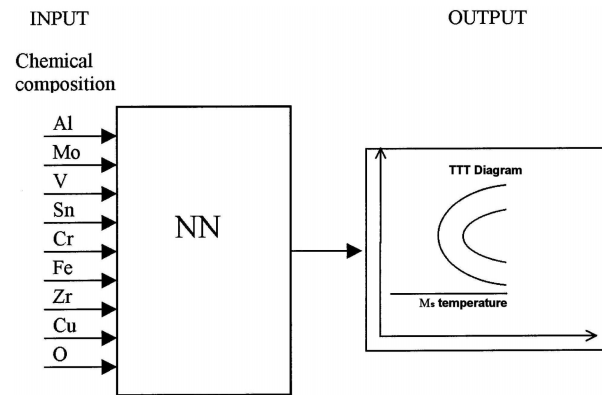


Figure 6.1: Schematic of the artificial neural network model for simulation of TTT diagrams and M_s temperature of Ti alloys [109].

Table 6.1: The compositional ranges of the new datasets.

Alloying elements	Fe	Cr	Mo	V	Nb	Zr	Al
Concentration range, wt. %	0-4.5	0-5.5	0-10.4	0-12.7	0-32.7	0-32.3	0-12.4

diagram or the M_s temperature.

As the ANNs model has a database predominantly derived from TTT diagrams, it has been decided to update and improve the existing ANNs model with the datasets collected for developing our thermodynamic model presented in *Chapter 4*. New input data consist of the composition and M_s temperatures of various Ti– X binary systems, where the alloying element X is of Fe, Cr, Mo, V, Nb, Zr and Al, obtained from literature (see *Chapter 4*) in the ranges as tabulated in Table 6.1. The updated database has then been used to retrain the ANNs using various transfer functions [143]. The new ANN based on binary and multicomponent alloys is then used to predict M_s values and to reconstruct approximate cross interaction relations between various elements.

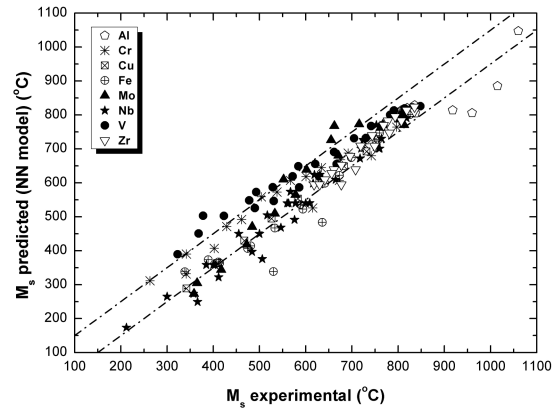


Figure 6.2: Performance of the ANNs model M_s predictions to that of M_s experimental values for Ti-binary systems.

6.2 Application of ANN model

6.2.1 ANN predictions and validation of M_s

The trained new ANN model has been applied to the Ti-binary systems that were obtained from the literature [97, 98, 99, 124, 125]. The binary elements considered are Fe, Cr, Mo, Cu, V, Nb, Zr and Al. The ANN model M_s predictions for binary alloys were compared with the literature values. Fig. 6.2 shows the ANN predictions vs. the experimental values of M_s . A good agreement is obtained except for a few results from specific author [98].

The M_s using the ANN model has been extended to the Ti-multicomponent systems involving any of the Fe, Cr, Mo, Cu, V, Nb, Zr and Al elements. A minimum amount of 0.1 wt.% oxygen and 0.15 wt.% Fe has been considered, irrespective of their presence in system constituents, for all the calculations. The predicted M_s values of the ANN calculations are compared with the experimental M_s values [97, 98, 99, 124, 125] in Fig. 6.3. The predictions for the multicomponent systems are within ± 50 °C of the reported experimental values *i.e.* within the scatter band given in Fig. 6.3.

The ANN model predictions for both the binary and multicomponent systems are quite good and hence can be considered as an appropriate benchmark for vali-

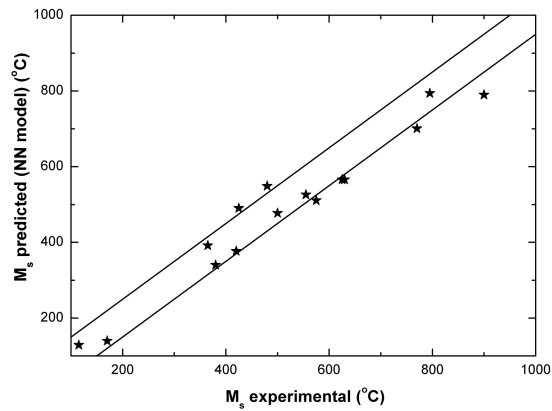


Figure 6.3: Performance of the ANNs model M_s predictions to that of M_s experimental values for Ti-multicomponent systems.

dating our thermodynamic based predictions.

6.3 Comparison between thermodynamic and neural network model predictions

The predictions of both models, the new ANN model presented in the above section and the Thermodynamic (TD) model presented in *Chapter 4* are now compared. Figure 6.4 shows the comparison for Ti-binary system data. The comparison shows slight deviations mainly in the predictions of Al, and few data points of Fe and Cr but, in general, all results fall within the limits of ± 50 °C scatter band also found for the comparison of both models to experimental data, Fig. 6.4. The Ti-Al systems show larger deviations due to the use of deviating data for Ti-Al [97, 98] in the training of the ANN model.

Similarly, the M_s results of both models have been compared for multicomponent alloys. The physical model for M_s is based on a simple linear additivity rule, excluding any element interaction term, similar to the Andrews model for the prediction of M_s in ferrous alloys [104]. Figure 6.5 shows the comparison of both models, in which the acceptable scatter band of ± 50 °C is highlighted. In general, the agreement between both the models is unsatisfactory. However, when com-

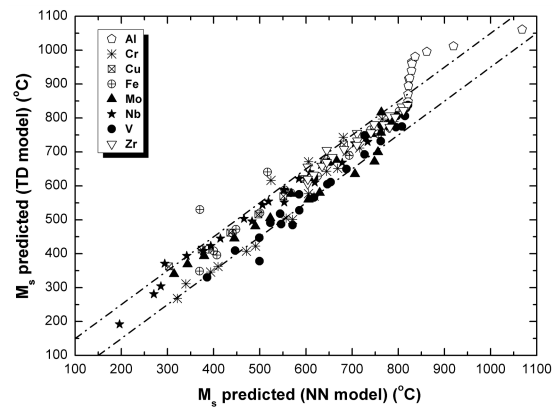


Figure 6.4: Comparison of TD and ANNs model M_s predictions for Ti-X binary systems.

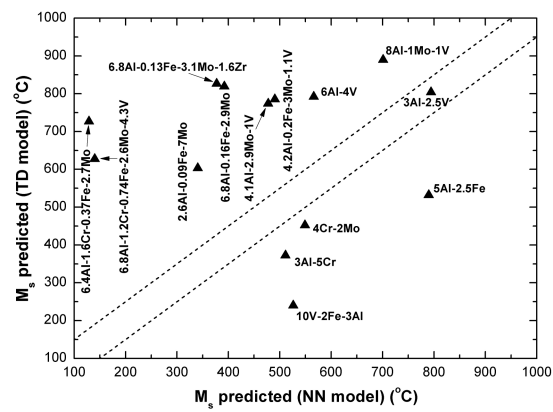


Figure 6.5: Comparison of TD and ANNs model M_s predictions for Ti-multicomponent systems.

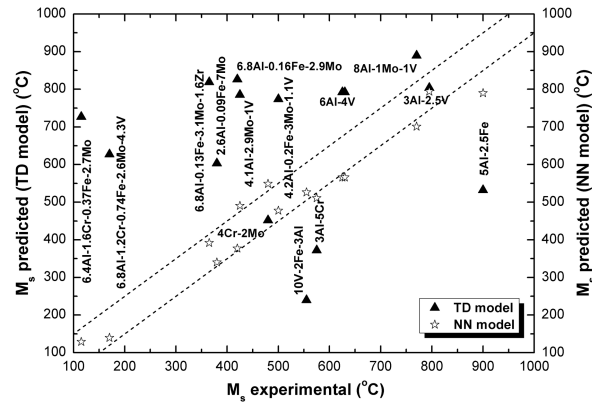


Figure 6.6: Comparison of TD and ANNs model M_s predictions with experimental values.

paring the M_s predictions from both models to experimental data (Figure 6.6), it is clear that the misfit is related to the modest performance of the thermodynamic model for M_s based on the additivity principle for individual alloying elements. Ignoring the factors related to interactions among solute elements on the M_s predictions, specifically for multicomponent systems, could play a decisive role in the accuracy of the TD model predictions.

6.4 Identification of solute interactions

One of the key factors that has not been considered in our TD model is the solute interaction contributions to the overall driving force for martensitic transformation ($-\Delta G$ at M_s), which may have a noticeable significance when dealing with multicomponent systems. Thus attempts have been made using the updated ANN model to determine if any interactions exist among the main solute elements. Such observation may lead to clarify the discrepancies in the TD M_s model predictions for multicomponent systems.

6.4.1 Method

The variation of M_s temperature as function of solute concentration for Ti- X binary systems involving the main solutes ($X = \text{Fe}, \text{Cr}, \text{Mo}, \text{V}$ and Al) has been

considered. For each binary systems, except Ti-Al, the solute concentration that result in a M_s temperature of approximately 500 ± 50 °C has been chosen as the base composition from which the interaction effects in ternary systems have been quantified. The initial binary M_s temperature of 500 ± 50 °C was chosen as it is in the middle of the validated M_s vs composition range. The Ti-Al system has not been considered mainly because Al has the tendency to increase the M_s temperature, and its interaction with other solutes would not, in general, decrease much the M_s as per our requirements. The calculations are performed in the updated ANN model by varying the ternary element concentrations and recording the respective variation in M_s temperature. For instance, in Ti-Fe system, it is assumed that 2 wt.% of Fe leads to a M_s temperature of ~ 500 °C, then in such system the addition of, for example, Mo at varying concentrations (*i.e.*, Ti-2Fe- X_{Mo}) would lead to identify the nature of Fe-Mo interaction by its influence on the resulting M_s temperature trend. It is made sure that the concentration variations of ternary element are limited within the existing range (refer to Table 6.1).

Generally, the interaction effect on M_s is classified in three categories: i) positive (+), meaning the slope of the M_s trend is stronger than expected, on the basis of simple superposition of the binary dependencies observed in TD model; ii) neutral (0), meaning the slope of the M_s trend is as expected; and iii) negative (-), meaning the slope of the M_s is opposite to the expected trend.

6.4.2 Results and discussion

The binary solute concentration (in wt.%) that results in a M_s temperature of $\sim 500 \pm 50$ °C was deduced from the Fig. 4.3 of Chapter 4, which correspond to Ti-10V, Ti-8Mo, Ti-4Cr and Ti-2Fe systems. In Figure 6.7, the M_s temperature is plotted as a function of the alloying element concentration for the base binary system (*i.e.*, to the left of the 0 wt.% point). The change of M_s with the concentration of the ternary alloying elements (Fe, Cr, Mo, V or Al) is plotted on the right hand side of the 0 wt.% point. Figure 6.7a shows the interaction trend for Ti-10V- X_i system, where $i = \text{Fe, Cr, Mo and Al}$. Similarly the interaction trend for Ti-8Mo- X_i , Ti-4Cr- X_i and Ti-2Fe- X_i systems are shown in Figures 6.7b, 6.7c and 6.7d, respectively. Corresponding Tables 6.2, 6.3, 6.4 and 6.5 show the slope of the M_s variation due to

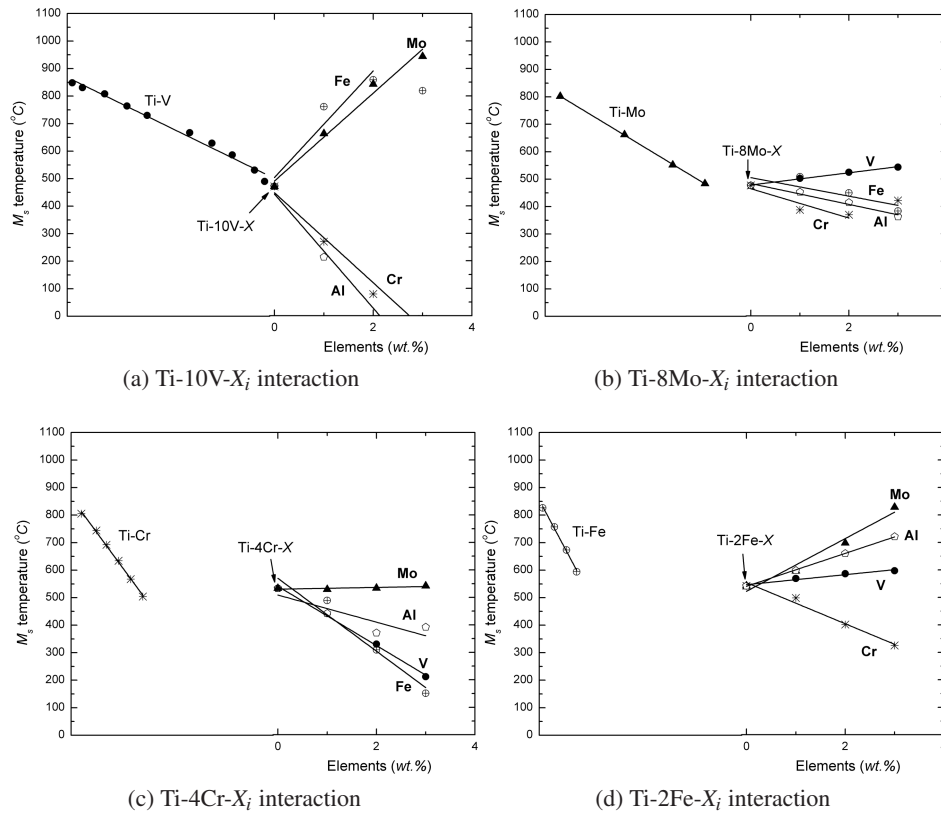


Figure 6.7: ANNs model M_s temperature variation as function of concentration of binary solutes in the defined system, and their interaction with varying concentrations of other ternary solutes.

the interaction of the ternary solutes obtained using both the updated ANN model and the linearized TD model (equation 4.10 of *Chapter 4*) along with the nature of their interactions. The TD model shows the expected influence on the basis of the simple linear superposition of the binary dependencies. By comparing the expected slope (TD model) to the observed slope (ANNs model) the nature of the interaction effect due to addition of that particular element is deduced.

From the Figures and Tables, it is clear that the interactions are present, and they alter the M_s of the considered systems to a certain magnitude. The observations show (Fig. 6.7c and Table 6.4) that the Cr exhibit little or no interaction effects, and the behaviour of the ternary Ti-4Cr- X_i systems is as predicted by the

Table 6.2: The ternary interactions effect on M_s in the Ti-10V- X_i systems.

Ti-10V- X_i	ANN M_s slope / %	TD M_s slope / %	Interaction effect
Fe	65	-50	-
Cr	-55	-25	0
Mo	53	-8	-
Al	-69	2	-

Table 6.3: The ternary interactions effect on M_s in the Ti-8Mo- X_i systems.

Ti-8Mo- X_i	ANN M_s slope / %	TD M_s slope / %	Interaction effect
Fe	-11	-50	0
Cr	-18	-25	0
V	7	-7	0/-
Al	-13	2	0/-

Table 6.4: The ternary interactions effect on M_s in the Ti-4Cr- X_i systems.

Ti-4Cr- X_i	ANN M_s slope / %	TD M_s slope / %	Interaction effect
Fe	-44	-50	0
Mo	1	-7	0
V	-36	-7	0
Al	-16	2	0/-

Table 6.5: The ternary interactions effect on M_s in the Ti-2Fe- X_i systems.

Ti-2Fe- X_i	ANN M_s slope / %	TD M_s slope / %	Interaction effect
Cr	-25	-25	0
Mo	32	-7	-
V	6	-7	0/-
Al	20	2	0

additivity rule. Figures 6.7a, 6.7c, 6.7d and Tables 6.2, 6.4, 6.5 show that the addition of Mo leads to an increase in M_s rather than the predicted decrease. Clearly there is a very strong interaction between Mo, on the one hand and V, Fe and Cr. However, for higher Mo contents (Fig. 6.7b and Table 6.3) the interactions seemed weaker. Figures 6.7a, 6.7d and Tables 6.2, 6.5 also point a noticeable interaction effects for Fe-V and Al-V. The rest other interactions seemed weaker.

The above observations clearly imply that interaction terms among the solute elements involving Fe, Mo, V and Al have to be considered for β multicomponent Ti systems in order to estimate their M_s temperature with better precision. Not considering this aspect in the TD model design of the new multicomponent metastable β Ti alloy, Ti-10V-5Al-5Cr-1Mo (*Ti10551*), involving the solute elements that influence the M_s temperature due to their interactions, might well be one of the reasons for not observing the PiTTi effect in the new alloy. It can be contemplated that such strong interactions could have decreased the alloy M_s temperature to the observed well-below room temperature levels, which may have resulted in β reaching the highly stable state that was observed for the new alloy.

6.5 Conclusions

The newly updated ANN model M_s predictions are in good agreement with the literature experimental values for both the binary and multicomponent systems. Such ANN model have been used as an additional validation tool to the thermodynamic based M_s model predictions. For binary Ti systems, the predictions of both models

are quite comparable and fall within the acceptable scatter range of ± 50 °C. However, for multicomponent systems the M_s equation predictions are quite anomalous and were not in agreement with the ANN predictions.

Using the updated ANN model, the existence of interactions among the main solutes Fe, Cr, Mo, V and Al has been identified. It can be concluded that strong interaction effects exist for Mo-(Fe, V), Fe-V and V-Al that can significantly influence the M_s temperature of any related systems. Based on this study the interaction effects for Cr with other elements seemed negligible. It should be pointed out that the above conclusions are based on the ANN model trained with data from relatively few multicomponent alloys, and should be regarded as indicative at this moment.

Summary

Titanium alloys possess good corrosion properties, high temperature stability and high strength-to-weight ratio. However, they fall short in providing the optimum strength-ductility relation in the most demanding structural applications, including the aerospace sector. Inspired by the possibility of enhancing the strength-ductility relation in steels through the TRIP effect, this thesis elucidates at identifying and quantifying the key factors that effectively control and/or promote such effect (termed here as Plasticity induced Transformation in Titanium alloys (PiTTi)), and exploring the plausible property improvements it may lead in metastable β titanium alloys. Controlling the key factors that effectively promote such effect through experimentation, and a novel theoretical alloy design methodology could lead to new grades of titanium alloys.

The current trends in improving the existing property limits of titanium alloys are reviewed in *Chapter 1*. The possibility of applying the deformation induced martensitic transformation concept to explore for the potential property improvements it may lead in titanium alloys, specifically metastable β alloys, is highlighted in reference to the successful TRIP category of ferrous alloys.

The occurrence of plasticity induced martensitic transformation and their effect on tailoring mechanical properties is demonstrated in *Chapter 2*. Detailed characterization on two commercial metastable β alloys (*Ti – 1023* and $\beta – Cez$) is performed. The microstructural features of the considered β alloys has been modified via various solution treatment conditions. Experimental investigations distinctly show the occurrence of PiTTi in the commercial near β type *Ti – 1023* alloy system. Such formation of martensite is reflected with a double yield-point

like behaviour in the compressive stress-strain curves. Strength improvements up to $\sim 20\%$ were achieved due to PiTTi in *Ti* – 1023. The solution treatment parameters promoting the capability to undergo such hardening via martensite formation upon loading have been identified and usually involve a β solutionizing. However, the β – *Cez* alloy does not show a distinct presence of PiTTi effect for the various solution treatment conditions considered. Moreover, the different microstructural features after various solution treatments do not result in any noticeable variation or improvement in compressive properties. The tunability of the microstructure is necessary to understand further the controlling factors of PiTTi effect in β – *Cez*. Further experimentation in *Ti* – 1023 lead to the understanding of the indentation and tribological characteristics of the PiTTi promoting phases for the different solution treatment conditions.

In *Chapter 3*, the various key factors that control and/or promote the stress induced martensite formation have been identified for *Ti* – 1023 alloy for the various solution treated conditions considered in *Chapter 2*. The solute partitioning of the elements among the α and β phase is quite evident and alters the M_s temperature locally for various solution treatment conditions. It may be postulated that solution treatments: i) involving above β transus temperatures result in a partially transformed and compositionally homogenized microstructure, though the nominal V content is not reached; ii) involving below β transus temperatures (*i.e.* below 795 °C), result in diffusional formation of α , which rejects V and Fe while absorbs Al. Given the large fraction of α formation at low temperatures, the retained small β domains contain β stabilizers (V) and eutectoid (Fe) elements; increasing their stability such that martensite is not formed upon quenching. The reduction of grain size down to the range of 100 to 200 μm by selection of lower solution treatment temperatures and shorter times at just above β transus (820 °C for 15 *min*) resulted in a moderate improvement of alloy ductility while retaining the same strength level as obtained through PiTTi effect. However, the smaller grain size did not affect the two critical stress levels in SIM formation. Similarly, increasing the α phase fraction by a solution treatment involving longer soaking time at below β phase regime (900 °C for 15 *min* followed by 700 °C for 60 *min*) precludes the martensite formation and thereby the improvement in PiTTi properties. Furthermore, the temperature dependence of the strength improvements stemming from PiTTi effect

is evident. However, the PiTTi formation capability, upon compression, disappears with an increase in deformation temperature, as demonstrated from X-ray measurements. The temperature at which the effect disappears is identified as 233 °C, which is comparable to the predicted M_s value of 240 °C for *Ti* – 1023 using the developed M_s prediction model.

Considering the critical role of the athermal M_s temperature on PiTTi effect, in *Chapter 4*, a thermodynamic model to predict the martensite start temperature (M_s) as function of solute concentration was developed for β Ti alloys. Following Olson and Cohen's theory on martensite nucleation and Ghosh-Olson's approach, a model representing the compositional dependence of the critical energy for martensite formation for Ti alloys involving BCC to HCP lattice transformation energetics has been developed. The model successfully reflects the energy contribution of each binary element towards the martensite formation. It was found that the solute-dependent exponent is 1.5 for Ti-binary systems but the data can also be approximated reasonably well using a linear dependence, to allow comparison to the Mo equivalence equation. It agrees well with that of the BCC to HCP transformations. The model has been successfully applied to binary systems of Ti with Fe, Mn, Cr, Mo, Cu, Ni, V, Nb, Zr and Al, and reproduced quite well the reported M_s data within an accuracy of ± 50 K. Extending further the binary M_s predictions to generic multicomponent β systems, an equation is postulated assuming non-linear dependence with solute concentrations. The equation ignores the interaction between solute elements and β grain size dependence. A linear relation has been observed between the postulated M_s equation and the already established and frequently employed Mo equivalence criterion for β Ti alloys, effectively validating the proposed equation for Ti-multicomponent systems. The application of the developed thermodynamic based M_s model equation to the above β (900°C - 60 min) solution treated condition of *Ti* – 1023 alloy show athermal martensite formation in accord to the M_s prediction value. However, for the below β conditions the equation predicts martensite formation against observations mainly due to neglecting the grain size effect, which is critical for smaller β domains.

In *Chapter 5*, a novel alloy design methodology, based on the developed M_s equation and the established β stability requirements of *Chapter 4*, is proposed wherein the respective parameters like M_s temperature and Mo eq. are optimized

to desired values for designing new alloy compositions. Such approach was applied to propose a new alloy grade of metastable β Ti alloy, Ti-10V-5Al-5Cr-1Mo (*Ti10551*) alloy, fulfilling the desired criteria of at or around room temperature M_s with adequate β metastability, for potential PiTTi effect. The other new alloy composition is: Ti-10V-2Fe-3Al-0.1B (*Ti1023 – B*), where the B is considered to realize the prior β grain size reduction and its eventual influence on PiTTi properties. The prototype new alloy compositions were fabricated. Detailed characterization of the two new alloys for plasticity induced martensitic transformation after various solution treatments has been performed. The *Ti1023 – B* alloy exhibited the PiTTi effect clearly with similar characteristics, and comparable properties as *Ti – 1023* alloy except for the presence of hard TiB particles. However, the random distribution of TiB needles did not result in the intended prior β grain size reduction in the as-received sample. Further homogenizing treatment at 1500 °C for 2 h i.e. above the solvus of TiB did result in redistribution and segregation of the TiB particles along grain boundaries. However the grain refinement was not realized. *Ti10551* alloy states studied did not exhibit the PiTTi effect for the considered solution treatments. The achieved β seem to be highly stable precluding any transformation upon loading at room temperature. However, the alloy microstructure is altered resulting in improved mechanical properties. As a further validation to the developed model, the commercial β – 21S alloy is characterized for martensite formation. Though the stress-strain curve behaviour is different for above β involved treatments, it does not show a clear evidence of the typical double yield phenomenon corresponding to PiTTi effect.

In *Chapter 6*, additional validation of thermodynamic (TD) based M_s model predictions is performed. The TD results are compared with the most powerful statistical based neural network model present in the literature. This ANNs model was first updated with the gathered M_s vs. composition database of several Ti-X binary systems resulting in a newly updated ANN model. The new ANN model predictions are in good agreement with the literature experimental values for both the binary and multicomponent systems. Additional validation of thermodynamic based M_s model predictions with such newly updated ANN model predictions have been performed. For binary Ti systems, the predictions of both models are quite comparable and fall within the acceptable scatter range of ± 50 °C. However, for

multicomponent systems the M_s equation predictions are quite anomalous and were not in agreement with the updated ANN predictions. Using the updated ANN model, the existence of interactions among the main solutes Fe, Cr, Mo, V and Al has been identified. It can be concluded that strong interaction effects exist for Mo-(Fe, V), Fe-V and V-Al that can significantly influence the M_s temperature of any related systems. Based on this study the interaction effects for Cr with other elements seemed negligible.

In conclusion, the thesis explains the following key points: i) Identifying the conditions and main factors for occurrence and tailoring of PiTTi effect in metastable β alloys for strength improvements than the existing levels with clear illustration using *Ti – 1023* alloy; ii) proposing a thermodynamic based model for prediction of martensite formation (*i.e.*, M_s temperature) in both binary and multi-component β titanium alloys with effective validation; and iii) proposing a novel alloy design methodology for designing new grades of titanium alloys meeting the at or around room temperature M_s and ample β metastability requirements for potential PiTTi effect.

Finally, the achieved property improvements due to PiTTi effect in *Ti – 1023* can be extended to generic metastable β systems given that a proper control of the proposed factors, and a more refined model for the M_s temperature of multi-component systems, taking into account solute interaction effects, are established. Optimizing the microstructure while being able to manipulate the morphology of the existing phases on the basis of integrated kinetics model will allow further fine tuning of the conditions for $\beta \rightarrow$ martensite transformation. Implementing the microstructural features into the developed M_s model can lead to simultaneous optimization of the alloy compositions and the heat treatment parameters. Finally, addressing the mentioned points shall lead to development of new grades of titanium alloys with tailored properties for applications in the aerospace and related fields involving high strength and formability requirements.

Samenvatting

Titanium legeringen hebben normaliter goede corrosie eigenschappen, een hoge temperatuurstabiliteit en een hoge specifieke sterkte. Ze schieten echter tekort op de combinatie van sterkte en vervormbaarheid voor een aantal veeleisende toepassingen, zoals die gevonden worden in de lucht- en ruimtevaart. Geïnspireerd door de mogelijkheid om in staal de sterkte/vervormbaarheidsverhouding te verhogen door het zgn TRIP effect, tracht dit proefschrift de belangrijkste factoren voor het optreden van plastische vervorming geïnduceerde transformatie (in dit proefschrift benoemd als het PiTTi effect) in titanium legeringen te identificeren en daar waar mogelijk te kwantificeren. Voldoende kennis van deze factoren en bijpassende nieuwe legeringsontwerp-strategieën zou kunnen leiden tot nieuwe titaniumlegeringen met verbeterde mechanische eigenschappen.

De huidige methodieken voor het verbeteren van bestaande titaniumlegeringen is samengevat in *Hoofdstuk 1*. Speciale aandacht wordt besteed aan de mogelijkheid om via plastische vervorming geïnduceerde transformatie de eigenschappen van titanium legeringen verder te verbeteren, onder verwijzing naar de gerealiseerde verbeteringen in TRIP staalsoorten.

Het optreden van plastische vervorming geïnduceerde transformaties in titaniumlegeringen en het effect op de mechanische eigenschappen is beschreven in *Hoofdstuk 2*. Daarin wordt ook een gedetailleerde studie naar de microstructuur en eigenschappen van 2 commerciële legeringen ($Ti - 1023$ en $\beta - Cez$) gepresenteerd. De microstructuur werd bepaald via diverse oplosbehandelingen. De experimentele resultaten laten duidelijk zien dat positieve PiTTi effecten op kunnen treden in $Ti - 1023$ legeringen. De vorming van martensiet leidt tot een kenmerk-

ende kracht-rek kromme met een dubbele vloeigrens. Toenames van 20 % in de compressie sterkte werden via deze methode gerealiseerd. Soortgelijke effecten werden in β -Cez legeringen niet waargenomen, niet tegenstaande een soortgelijke microstructuur verandering. Aanvullende experimenten leidde tot een verbeterd inzicht in de indentatie- en tribologische eigenschappen van de verschillende fasen die door de warmtebehandeling gevormd werden.

In *Hoofdstuk 3* worden de belangrijkste factoren voor het optreden van het PiTTi effect nogmaals bestudeerd. Het optreden van lokale herverdeling van legeringselementen tijdens de oplosgloeibehandeling bleek cruciaal omdat dit leidt tot lokale verschuivingen in de martensiet-start temperatuur, M_s . Op basis van de experimenten wordt geconcludeerd dat i) gloeibehandelingen boven de β -transus temperatuur leiden tot lokale element-herverdelingen, waarbij het legeringselement V zijn evenwichtswaarde nog niet bereikt, ii) gloeibehandelingen onder de β -transus temperatuur leiden verdere groei van de α -fase en verlaging van het lokale V en Fe gehalte en verhoging van het Al-gehalte. De verkleining van de gemiddelde korrelgrootte tot circa 100 μm leidde tot een beperkte verbeteringen van de vervormbaarheid met behoud van de compressiesterkte. De kleinere korrelgrootte had geen effect op de twee kritische spanningsniveaus voor de vorming van spannings-geïnduceerde martensiet (SIM). Verlenging van de gloeibehandeling leidde tot een verdwijnen van de martensietvorming en een verlies van het PiTTi effect. De temperatuursafhankelijkheid van het PiTTi effect is vastgesteld en bleek zeer significant te zijn. Het effect verdwijnt bij hogere temperaturen, hetgeen door onafhankelijke aanvullende Röntgendiffractie metingen werd bevestigd. De kritische temperatuur voor het PiTTi effect werd bepaald op 293 °C wat goed overeenkomt met de voorspelde M_s temperatuur van 240 °C.

Gelet op het grote belang van het optreden van een martensitische transformatie en daarmee het belang van de M_s temperatuur, wordt in *Hoofdstuk 4* een model voor de martensiet start temperatuur als functie van de legeringssamenstelling gepresenteerd. Het model is gebaseerd op de Ghosh-Olson methodiek voor het voorspellen van de martensietovergang in staal. Het resulterende model voorspelt de legeringselement afhankelijkheid van de M_s in binaire legeringen met zeer goede nauwkeurigheid. Anders dan in het geval van ijzer-legeringen bleek de verschuiving van de M_s te schalen met de concentratie $X^{1.5}$. De M_s temperaturen

konden binnen ± 50 °C nauwkeurig voorspeld worden voor de legeringselementen Fe, Mn, Cr, Mo, Cu, Ni, V, Nb, Zr en Al. De binaire elementbijdrages werden vervolgens gesommeerd in een eenvoudig model voor M_s van meervoudige legeringen, met verwaarlozing van elementinteracties en korrelgrootte effecten. Niet tegenstaande zijn eenvoud werd een goede lineaire relatie tussen de berekende M_s temperatuur en het zgn. Molybdeen equivalentiegetal gevonden. Toepassing van het model op de boven de β -transus temperatuur gegloeide materialen leidde tot een correcte voorspelling van het optreden van de martensiet transformatie.

In *Hoofdstuk 5* wordt een nieuwe legeringsoptimalisatiemethodiek op basis van het M_s -samenstellings model van *Hoofdstuk 4* gepresenteerd. Deze methodiek leidde tot een metastabiele legering Ti-10V-5Al-5Cr-1Mo (*Ti10551*) welke voldeed aan de eis van een M_s temperatuur rond kamertemperatuur en voldoende β -stabiliteit. Een andere nieuwe legering is de Ti-10V-2Fe-3Al-0.1B (*Ti1023 – B*) legering waarbij de toevoeging van Borium geacht wordt te kunnen leiden tot substantiële korrelgrootteverfijning. Deze experimentele legeringen werden vervolgens extern vervaardigd en in de context van dit proefschrift uitvoerig bestudeerd. De *Ti1023 – B* legering vertoonde soortgelijke karakteristieken als de B-vrije variant. Als gevolg van de vorming van grote B-houdende uitscheidingen werd de beoogde korrelgrootte reductie niet gerealiseerd, ook niet na een extra oplosbehandeling op 1500 °C. De tevens geproduceerde *Ti10551* legering vertoonde echter voor geen van de warmtebehandelingen het beoogde PiTTi effect. De afwezigheid van dit effect wordt toegeschreven aan een te hoge stabiliteit van de ingevroren β -fase. Aanvullende metingen aan de commerciële $\beta - 21S$ legeringen lieten wel een andersoortige kracht-rek kromme zien, maar niet het beoogde deformatie geïnduceerde transformatie gedrag.

In *Hoofdstuk 6* wordt het eerdere thermodynamica gebaseerde model voor de M_s van binaire legeringen nader onderzocht door de voorspellingen te vergelijken met die van een statistisch Kunstmatig Neuraal Netwerk (ANN) model. Dit model was eerst bijgewerkt met de resultaten van de binaire legeringen waaraan het thermodynamische model gevalideerd was. Zowel het thermodynamische model als het ANN model gaven een nauwkeurige voorspelling van de M_s temperatuur van de binaire legeringen maar uit de analyse voor multicomponent legeringen bleek dat legeringselement-interacties, met name die tussen Mo-(Fe, V), Fe-V en

V-Al een significant effect op de M_s hebben. Daarentegen bleek Cr nauwelijks een interactie-effect met andere leveringselementen te hebben.

Kort samengevat: dit proefschrift beschrijft de condities leidend tot vervorming geïnduceerde martensietvorming in Titanium legeringen, presenteert een thermodynamica gebaseerd model voor de Martensiet start temperatuur M_s in binaire Ti-X legeringen en beschrijft een nieuwe methodiek voor het ontwerpen van verbeterde Titanium legeringen.

De gerealiseerde verbeteringen in de eigenschappen van $Ti - 1023$ legeringen leidden tot een generiek model voor betere metastabiele β -legeringen. In de toekomst dient het onderliggende model uitgebreid te worden met de effecten van legeringselement-interacties en microstructurele effecten. Uiteindelijk kan deze methodiek en het onderliggende model leiden tot nieuwe titanium legeringen met aantrekkelijker eigenschappen voor toepassingen in de lucht- en ruimtevaart, waarbij een hoge strekte gekoppeld dient te zijn aan een hoge vervormbaarheid.

Bibliography

- [1] C. Leyens and M. Peters: Titanium and Titanium alloys: Fundamentals and applications, Wiley-VCH (2004)
- [2] G. Lütjering and J.C. Williams: Titanium (Springer-Verlag Publications, Germany), (2003)
- [3] E.W. Collings: Physical metallurgy of Titanium alloys, ASM (1984)
- [4] M. Niinomi and T. Kobayashi: ISIJ Intl., 31 (1991) 848
- [5] H. Margolin, J.C. Williams, J.C. Chesnutt and G. Lütjering: Proc. of 4th Intl. Conf. on Ti, (1980) p. 169
- [6] K. Sakurai, Y. Itabashi and A. Komatsu: Titanium '80, Science and Technology, AIME, Warrendale, USA (1980) p. 299
- [7] R. Boyer, G. Welsch and E.W. Collings, eds.: Materials properties Handbook: Titanium Alloys, ASM, Materials Park, USA (1994) p. 228
- [8] R. Boyer, G. Welsch and E.W. Collings, eds.: Materials properties Handbook: Titanium Alloys, ASM, Materials Park, USA (1994)
- [9] R.W. Schutz and D.E. Thomas: Corrosion, Metals Handbook, 9th Edn., Vol.13, ASM, Metals Park, USA (1987) p. 669
- [10] D. Eylon and S.R. Seagle: Titanium '99, Science and Technology, CRISM "Prometey", St. Petersburg, Russia (2000) p. 37
- [11] R.R. Boyer: Mater. Sci. Eng. A, A213 (1996) 103

- [12] R.R. Boyer, J.C. Williams and N.E. Paton: Titanium '99, Science and Technology, CRISM "Prometey", St. Petersburg, Russia (2000) p. 1007
- [13] T. Kobayashi and M. Niinomi: J. Soc. Mater. Sci. Jpn., 36 (1987) 831
- [14] G. Lütjering, A. Gysler and L. Wagner: 6th World conference on Titanium, Les Editions de Physique, Les Ulis, France (1988) p. 71
- [15] M. Peters and G. Lütjering: Titanium '80, Science and Technology, AIME, Warrendale, USA (1980) p. 925
- [16] G. Lütjering, J. Albrecht and O.M. Invasishin: Microstructure/Property relationships of Ti alloys, TMS, Warrendale, USA (1994) p. 65
- [17] G. Lütjering, J. Albrecht and O.M. Invasishin: Titanium '95, Science and Technology, Cambridge University Press, Cambridge, UK (1996) p. 1163
- [18] O.M. Invasishin and G. Lütjering: Titanium '99, Science and Technology, CRISM "Prometey", St. Petersburg, Russia (2000) p. 441
- [19] M. Peters, A. Gysler and G. Lütjering: Titanium '80, Science and Technology, AIME, Warrendale, USA (1980) p. 1777
- [20] G. Wegmann, J. Albrecht, G. Lütjering, K.D. Folkers and C. Liesner: Z. Metallkunde, 88 (1997) 764
- [21] G. Schroeder, J. Albrecht and G. Lütjering: Titanium '99, Science and Technology, CRISM "Prometey", St. Petersburg, Russia (2000) p. 545
- [22] ASM Materials Properties Handbook: Titanium alloys, ASM International (1994)
- [23] S. Tamirisakandala, R.B. Bhat, J.S. Tiley and D. B. Miracle: Scripta Mater., 53 (2005) 1421
- [24] J. Zhu, A. Kamiya, T. Yamada, W. Shi and K. Naganuma: Mater. Sci. Eng. A, A339 (2003) 53
- [25] O.O. Bilous, L.V. Artyukh, A.A. Bondar and S.O. Firstov: Mater. Sci. Eng. A, A402 (2005) 76

- [26] T. Furuhashi, S. Annaka, Y. Tomio and T. Maki: *Mater. Sci. Eng. A*, A438-440 (2006) 825
- [27] P.J. Bania: *Beta Titanium alloys in 1990's*, The Minerals, Metals and Materials Society (ed. by D.Eylon, R.R.Boyer and D.A. Koss), Warrendale, USA, (1993) p. 6
- [28] A. Bhattacharjee, S. Bhargava, V.K. Varma, S.V. Kamat and A.K. Gogia: *Scripta Mater.*, 53 (2005) 195
- [29] T.W. Duerig, J. Albrecht, D. Richter and P. Fischer: *Acta Metall.*, 30 (1982) 2161
- [30] T.J. Headley and H.J. Rack: *Metall. Trans. A*, 10A (1979) 909
- [31] S. Ankem: *Metall. Trans. A*, 18A (1987) 2015
- [32] Alain Vassel: *Beta Titanium alloys in 1990's*, The Minerals, Metals & Materials Society (ed. by D.Eylon, R.R.Boyer and D.A. Koss), (1993) p. 173
- [33] Y. Kawabe and S. Muneki: *Beta Titanium alloys in 1990's*, The Minerals, Metals & Materials Society, (ed. by D.Eylon, R.R.Boyer and D.A. Koss), (1993) p. 187
- [34] Y. Kawabe and S. Muneki: *ISIJ Intl.*, 31 (1991) 147
- [35] C. Ouchi, H. Suenaga and Y. Kohsaka: *Proc. 6th Intl. Conf. on Ti*, ed. by P. Lacombe, R. Tricot, G. Beranger, Paris, (1989) p. 819
- [36] J.D. Cotton, J.F. Bingert, P.S. Dunn and R.A. Patterson: *Metall. Mater. Trans. A*, 25A (1994) 461
- [37] H.M. Otte: *The Sci. Tech. and Appln. of Titanium*, Pergamon Press, Oxford, UK, (1970) p. 645
- [38] W.G. Burgers: *Physica*, 1 (1934) 561
- [39] J.B. Newkirk and A.H. Geisler: *Acta Metall.*, 1 (1953) 370
- [40] M. Peters, G. Lütjering and G. Ziegler: *Z. Metallkunde*, 74 (1983) 274

- [41] T. Ahmed and H.J. Rack: *Mater. Sci. Eng. A*, A243 (1998) 206
- [42] S. Bein and J. Bechet: *J.de Phys. IV*, 6 (1996) C1-99
- [43] P. Laheurte, A. Eberhardt and M.J. Philippe: *Mater. Sci. Eng. A*, A396 (2005) 223
- [44] H.M. Flower: *Proc. 5th Intl. Conf. on Titanium*, (eds. G. Lutjering, U. Zwicker and W. Bunk), Munich, Germany, DGM, 3 (1984) p. 1651
- [45] J.C. Williams, B.S. Hickman and H.L. Marcus: *Metall. Trans. A*, 2 (1971) 1913
- [46] T.W. Duerig and J.C. Williams: *Beta Ti alloys in the 1980's*, (AIME, Warrendale, PA), (1984) p. 19
- [47] G.M. Pennock, H.M. Flower and D.R.F. West: *Titanium'80 Sci. and Tech.*, (AIME, Warrendale, PA), 2 (1980) 1343
- [48] T.W. Duerig, G.T. Terlinde and J.C. Williams: *Metall. Trans. A*, 11A (1980) 1987
- [49] O.M. Ivasishin, A.I. Ustinov, V.S. Skorodzievskii, M.S. Kosenko, Y.V. Matviychuk and F.I. Azamatova: *Scripta Mater.*, 37 (1997) 883
- [50] E.S. Kumar Menon and R. Krishnan: *J. Mater. Sci.*, 18 (1983) 365
- [51] E. Galvao da Silva and U. Gonser: *Acta Metall.*, 29 (1981) 903
- [52] T. Ahmed and H.J. Rack: *J. Mater. Sci.*, 31 (1996) 4267
- [53] K.S. Jepson, A.R.G. Brown and J.A. Gray: *The Sci. Tech and Appln. of Ti*, ed. by R.I. Jaffee and N. Promisel, Pergamon press, (1970) p. 677
- [54] A.R.G. Brown, D. Clark, J. Eastbrook and K.S. Jespon: *Nature*, 201 (1964) 914
- [55] B.A. Hatt and V.G. Rivlin: *Br. J. Appl. Phys.*, 1 (1968) 1145
- [56] A.R.G. Brown and K.S. Jespon: *Mem. Sci. Rev. Metall.*, 63 (1966) 575

- [57] A.V. Dobromyslov and V.A. Elkin: *Scripta Mater.*, 44 (2001) 905
- [58] J.C. Williams: *Titanium Sci. and Tech.*, Plenum press, New York, USA, (1973) p. 1433
- [59] G. Lütjering, J.C. Williams, and A. Gysler: *Microstructure and Mech. Props. of Ti alloys*, 1
- [60] R. Davis, H.M. Flower and D.R.F. West: *J. Mater. Sci.*, 14 (1979) 712
- [61] P. Jacques, Q. Furnemont, A. Mertens and F. Delannay: *Phil. Mag. A*, 81 (2001) 1789
- [62] F.D. Fischer, Q.P. Sun and K. Tanaka: *ASME Appl. Mech. Rev.*, 49 (1996) 317
- [63] G.W. Greenwood and R.H. Johnson: *Proc. Roy. Soc.*, A283 (1965) 403
- [64] E. Gautier and A. Simon: *Int. Conf. on Phase Transformations '87*, Lorimer, G.W. (Ed.), The Inst. of Metals, London (1988) p. 285
- [65] F.D. Fischer, G. Reisner, E. Werner, K. Tanaka, G. Cailletaud and T. Antretter: *Intl. Jl. of Plasticity*, 16 (2000) 723
- [66] Q. Furnémont, M. Kempf, P.J. Jacques, M. Göken and F. Delannay: *Mater. Sci. Eng. A*, A328 (2002) 26
- [67] K. Otsuka and T. Kakeshita: *MRS Bulletin*, (2002) 91
- [68] K. Otsuka and X. Ren: *Prog. Mater. Sci.*, 50 (2005) 511
- [69] K. Sugimoto, N. Usui, M. Kobayashi and S. Hashimoto: *ISIJ Intl.*, 32 (1992) 1311
- [70] O. Matsumura, Y. Sakura and H. Takechi: *Scripta Metall.*, 21 (1987) 1301
- [71] P. Jacques, A. Mertens, E. Girault, J. Ladriere and F. Delannay: *Metall. Trans. A*, 32A (2001) 2759
- [72] P. Jacques, F. Delannay, X. Cornet, P. Harlet and J. Ladriere: *Metall. Mater. Trans. A*, 29A (1998) 2383

- [73] G.R. Chanani, V.F. Zackay and E.R. Parker: *Metall. Trans. A*, 2 (1971) 133
- [74] G.B. Olson and M. Azrin: *Metall. Trans. A*, 9 (1978) 713
- [75] T. Grosdidier, Y. Combres, E. Gautier and M.J. Philippe: *Metall. Mater. Trans. A*, 31A (2000) 1095
- [76] A. Paradkar, S.V. Kamat, A.K. Gogia and B.P. Kashyap: *Mater. Sci. Eng. A*, A520 (2009) 168
- [77] H. Ohyama and T. Nishimura: *ISIJ Intl.*, 35 (1995) 927
- [78] S. Ishiyama, S. Hanada and O. Izumi: *ISIJ Intl.*, 31 (1991) 807
- [79] H.M. Flower, A.I.P.N. Wobu and D.R.F. West: *Proc. of the 5th Intl. Conf. on Ti*, (1984) p. 1026
- [80] R.M. Middleton and C.R. Hickey: *Titanium and Titanium alloys*, Plenum press, 2 (1982) 1567
- [81] T.W. Duerig, D.F. Richter and J. Albrecht: *Scripta Metall.*, 16 (1982) 957
- [82] T. Grosdidier and M.J. Philippe: *Mater. Sci. Eng. A*, A291 (2000) 218
- [83] T. Grosdidier, C. Roubaud, M.J. Philippe and Y. Combres: *Scripta Mater.*, 36 (1997) 21
- [84] T. Grosdidier, C. Roubaud, M.J. Philippe, S. Zaeferrer, M. Zandona, E. Gautier and Y. Combres: *Jl. de Phys. IV*, 6 (1996) C1-435
- [85] A. Paradkar, S.V. Kamat, A.K. Gogia and B.P. Kashyap: *Metall. Mater. Trans. A*, 39A (2008) 551
- [86] Q.Y. Sun, S.J. Song, R.H. Zhu and H.C. Gu: *J. Mater. Sci.*, 37 (2002) 2543
- [87] S. Ishiyama and S. Hanada: *The Sumitomo Search*, 54 (1993) 41
- [88] S. Hanada and O. Izumi: *Metall. Trans. A*, 17A (1986) 1409
- [89] S. Hanada and O. Izumi: *Metall. Trans. A*, 11A (1980) 1447

- [90] S. Hanada and O. Izumi: *Metall. Trans. A*, 18A (1987) 265
- [91] S. Zaeferrer, J. Ohlert and W. Bleck: *Acta Mater.*, 52 (2004) 2765
- [92] B.V.N. Rao and M.S. Rashid: *Mater. Char.*, 39 (1997) 435
- [93] V.V. Balasubrahmanyam and Y.V.R.K. Prasad: *Mater. Sci. Technol.*, 17 (2001) 1222
- [94] M.Jackson, R.J. Dashwood, L. Christodoulou and H.M. Flower: *Mater. Sci. Technol.*, 16 (2000) 1437
- [95] D. Grandemange, Y. Combres and D. Eylon: *Beta Titanium alloys in 1990's*, The Minerals, Metals & Materials Society (ed. by D. Eylon, R.R. Boyer and D.A. Koss), (1993) p. 227
- [96] G. Dieter: *Mechanical metallurgy*, McGraw-Hill, New York, (1986) p. 275-324
- [97] T.O. Sato, S. Hukai and Y.C. Huang: *J. Aust. Inst. of metals*, 5 (1960) 149
- [98] P. Duwez: *Trans. ASM*, 45 (1953) 934
- [99] K.S. Jepson, A.R.G. Brown and J.A. Gray: *The Science, technology and application of Titanium*, Pergamon Press, London, (ed. by R.I. Jaffee and N. Promisel), (1970) p. 677
- [100] J.Ö. Andersson, T. Helander, L. Hoglund, P. Shi and B. Sundman: *Calphad*, 26 (2002) 273
- [101] TTTI3—Thermotech Titanium Alloys Database (Version 3.0, January 2006), Thermotech Ltd., Guildford, UK and Thermo-Calc software AB, Stockholm, Sweden
- [102] G. Lutjering and J.C. Williams: *Titanium* (Springer-Verlag Publications, Germany), (2003) p. 289
- [103] MDI Jade Software, Version 5
- [104] K.W. Andrews: *J. Iron Steel Inst.*, 203 (1965) 721

- [105] T. Sourmail and C. Garcia-Mateo: *Comp. Mater. Sci.*, 34 (2005) 323
- [106] W.G. Vermeulen, P.F. Morris, A.P. de Weijer and S. van der Zwaag: *Iron making and Steel making*, 23 (1996) 433
- [107] J.J. Wang, P.J. van der Wolk and S. van der Zwaag: *Mater. Trans. JIM*, 41 (2000) 761
- [108] G. Ghosh and G.B. Olson: *Acta Metall. Mater.*, 42 (1994) 3361
- [109] S. Malinov, W. Sha and Z. Guo: *Mater. Sci. Eng. A*, A283 (2000) 1
- [110] S. Malinov and W. Sha: *Comp. Mater. Sci.*, 28 (2003) 179
- [111] R.R. Boyer, E.W. Collings and G.E. Welsch: *Materials Properties Handbook - Titanium Alloys*, ASM International, Materials Park, OH, (2004) p. 6
- [112] G.B. Olson and M. Cohen: *Metall. Trans. A*, 7A (1976) 1897
- [113] G.B. Olson and M. Cohen: *Metall. Trans. A*, 7A (1976) 1905
- [114] H.K.D.H. Bhadeshia: *Metal Sci.*, 15 (1981) 175
- [115] H.K.D.H. Bhadeshia: *Metal Sci.*, 15 (1981) 178
- [116] G. Ghosh and G.B. Olson: *Acta Metall.*, 42 (1994) 3371
- [117] G. Ghosh and G.B. Olson: *Jl. Ph. Equilib.*, 22 (2001) 199
- [118] G. Ghosh and G.B. Olson: *Acta Mater.*, 50 (2002) 2655
- [119] J.W. Christian: *Intl. Symp. On New Aspects of Martensitic Transformation*, Japan Inst. Met., (1976) p. 21
- [120] G.B. Olson and M. Cohen: *Ann. Rev. Mater. Sci.*, 11 (1981) 1
- [121] L.A. Gypen and A. Deruyttere: *J. Mater. Sci.*, 12 (1977) 1028
- [122] J. Friedrichs and P. Haasen: *Phil. Mag. A*, 31 (1975) 863
- [123] G. Ghosh: *Solid-Solid phase transformations*, (Ed. by W.C. Johnson, J.M. Howe, D.E. Laughlin and W. A. Soffa), TMS, (1994) p. 691

- [124] P. Pietrokowsky and P. Duwez: *Trans. AIME*, 194 (1952) 627
- [125] Y.C. Huang, S. Suzuki, H. Kaneko and T. Sato: *The Science Technology and application of Titanium*, ed. by R.I. Jaffee and N. Promisel, Pergamon Press, London, (1970) p. 691
- [126] T. Zhou, M. Aindow, S. P. Alpay, M. J. Blackburn and M. H. Wu: *Scripta Mater.* 50 (2004) 343
- [127] Z.X. Li and C. C. Cao: *Intermetallics*, 13 (2005) 251
- [128] T.T. Cheng: *Intermetallics*, 8 (2000) 29
- [129] M.J. Bermingham, S.D. McDonald, K. Nogita, D.H. St. John and M.S. Dargusch: *Scripta Mater.*, 59 (2008) 538
- [130] B. Cherukuri, R. Srinivasan, S. Tamirisakandala and D.B. Miracle: *Scripta Mater.*, 60 (2009) 496
- [131] S. Tamirisakandala, R.B. Bhat, J.S. Tiley and D. B. Miracle: *J. Mater. Eng. Perform.*, 14 (2005) 741
- [132] N.G. Jones, R.J. Dashwood, D.Dye and M. Jackson: *Mater. Sci. Eng. A*, A490 (2008) 369
- [133] R.R. Boyer and R.D. Briggs: *J. Mater. Eng. Perform.*, 14 (2005) 681
- [134] N.G. Jones, R.J. Dashwood, D.Dye and M. Jackson: *Metall. Mater. Trans. A*, 40A (2009) 1944
- [135] N.G. Jones, R.J. Dashwood, M. Jackson and D.Dye: *Acta Mater.*, 57 (2009) 3830
- [136] S. Nag, R. Banerjee, J.Y. Hwang, M. Harper and H.L. Fraser: *Phil. Mag. A*, 89 (2009) 535
- [137] C. Zener, quoted in C.S. Smith: *Trans. Met. Soc. AIME*, 175 (1948) 15
- [138] S. Malinov, W. Sha and P. Markovsky: *J. Alloys and Comp.*, 348 (2003) 110

- [139] S. Malinov, W. Sha, Z. Guo, C.C. Tang and A.E. Long: *Mater. Char.*, 48 (2002) 279
- [140] K. Chaudhuri and J.H. Perepezko: *Metall. Mater. Trans. A*, 25A (1994) 1109
- [141] H.K.D.H. Bhadeshia: *ISIJ Intl.*, 39 (1999) 966
- [142] P.J. van der Wolk, J.J. Wang, J. Sietsma and S. van der Zwaag: *Z. Metallkunde*, 93 (2002) 1208
- [143] S. Malinov and W. Sha: *Mater. Sci. Eng. A*, A365 (2004) 202
- [144] Z. Guo, S. Malinov and W. Sha: *Comp. Mater. Sci.*, 32 (2005) 1
- [145] S. Malinov, W. Sha and J.J. McKeown: *Comp. Mater. Sci.*, 21 (2001) 375
- [146] M.T. Hagan and M. Menhaj: *IEEE Trans. Neural Netw.*, 5 (1994) 989
- [147] D.J.C. MacKay: *Neural Comput.* 4 (1992) 415
- [148] T.P. Vogl, J.K. Mangis, A.K. Rigler, W.T. Zink and D.L. Alkon: *Biol. Cybern.*, 59 (1988) 256

Acknowledgements

This thesis would not have been possible without the guidance, help, support and understanding of many persons involved directly or indirectly. I would like to thank one and all who helped me to achieve this.

I like to express my sincere gratitude to my promoter Prof. dr. ir. Sybrand van der Zwaag and daily supervisor Dr. Pedro Rivera for providing me with an opportunity to pursue a doctoral degree at Delft University of Technology. Their invaluable guidance throughout my PhD journey has been a pleasant learning experience. A lot of inspiration has come from Prof. van der Zwaag for his continuous support, encouragement and willingness to address the queries whenever I knocked on his door. Dr. Pedro Rivera's knowledge, inputs and regular discussions have been very instrumental all through this research. He has always been around to help me both professionally and personally. I am grateful for what he has been, at times more a friend, than simply a supervisor. I greatly appreciate the support provided by M2i and the industrial partner SKF during the course of this work.

I am extremely thankful to my former colleague, Dr. David San Martin (presently in CENIM, Spain), who played an important and a continuous role in terms of interesting discussions, suggestions and experimental help at different stages of this work. I also thank Prof. Elizabeth Gautier, for providing me with the β - *Cez* material used in this study. I thank Dr. Erik Vegter of SKF, Nieuweigen for allowing and helping me in carrying out nano-indentation measurements at their facilities. I also thank Mr. M.Valefi and Prof. dr. ir. D.J.Schipper of the tribology group in University of Twente for performing the tribological measurements at their group. I am grateful to Prof. dr. ir. Jilt Sietsma for interesting discussions during various

M2i cluster meetings. A special word of thanks to Dr. Emre Tasci for his close association during the work performed on the electronic contribution to martensitic transformation, not reported in this thesis. I would like to express my deep gratitude to Dr. Savko Malinov and Prof. Wei Sha for providing the $\beta - 21S$ material, and the updated neural network model without which the *Chapter 6* of this thesis might have been left undone.

The kind experimental help provided by Mr. Nico, Mr. Erik, Mr. Kees, Mr. Tim, Mr. Hans, Mr. Pascal, Mr. Ruud and Dr. Guiming from 3mE, Mr. Frans, Mr. Bob, Mr. Niels and Mr. Kees from LR, Mr. Leon (EWI) and several others is greatly appreciated. A very special thanks to the master students Paolo di Napoli, Maarten Rijs and Mathilde Forget for their contributions at the various stages of this work. Especially, Mathilde's work on characterization of various aspects of the new alloys is highly appreciated.

I was lucky to be a part of our research group, which has the most international blend one could think of. I always have had an opportunity to learn a lot about cultures, cuisines, etc., apart from science. My profound thanks to all former and present colleagues for making my stay in the NovAM (formerly, FAM) group a fruitful and memorable one: Wei Xu for being a nice office-mate, and for all the (non-) technical discussions that we had was sure very informative; Alwin, Steven for all Dutch culture and language related clarifications; Huang, David for helping me in many aspects, especially during my initial days in Holland; Laura, Geeta and Shanta for helping me in all the administrative related issues; Fabrizio, Chris, Hartmut, Alex, Pim, Doty, Rahul, Sanna, Sang woo, Meiji, Bui, Yanmin, Guiming, Mazhar, Theo, Santiago, Arek, Jie, Maruti, Jason, Li, Hao, Stephane, Natalia, Girish, Daniel, Maarten and Rangan for all the group related activities.

After all, life is not only about doing a PhD. There are many other aspects for which I had the pleasure of sharing great company with Muru, Ram, Raghu, Navin, Madan, Prem, Sid, Sampath, Joe, Chai, Then, Kanag, Maruti, Sarav, Shree-kant, Kapil and many other friends in the AVS building, in the Netherlands and in India. My heartfelt thanks to each and everyone of you for all the help, fun, dinners, playing cricket, badminton, tennis, snooker, squash, bowling and travelling together during these years.

Finally, I owe lot more than a word of 'Thanks' to my family: my dad, mom, brothers, sister-in-laws, sisters, wife...for their continuous support, encouragement and confidence on me; without them I would not have made it this far. They all stood beside me in each and every step of my hitherto career. Special thanks to my parents for understanding and accepting all the important and independent decisions that I made, including coming to the Netherlands. Thanks to my brothers and sisters for their care and support. Last, but definitely not the least, a very special thanks to my dear wife Vijayalatha, not only for her unwavering love, support, caring and encouragement but more for her patience and understanding for all that we had to undergo during the final stages of my PhD, and coincidentally the initial stages of our married life together.

Suresh Neelakantan (Delft, May 2010)

Curriculum Vitae

Suresh Neelakantan

born on 22 April, 1980
in Chengalpattu, Tamilnadu province, India

Sept. 1997 - Jun. 2001

Bachelor of Engineering in Metallurgical Engineering, Department of Metallurgy,
Government College of Engineering, University of Madras, Salem, India

Jan. 2002 - Apr. 2004

Master of Science in Metallurgical Engineering, Department of Material Science,
Indian Institute of Science, Bangalore, India

May 2004 - Apr. 2005

Project Scientist in National Aerospace Laboratories, Bangalore, India

May 2005 - Nov. 2005

Research Associate, Department of Material Science, Indian Institute of Science,
Bangalore, India

Dec. 2005 - June 2010

PhD Researcher in the Novel Aerospace Materials (formerly, Fundamentals of Ad-
vanced Materials) group, Faculty of Aerospace Engineering, Delft University of
Technology, Delft, The Netherlands under the supervision of Prof. dr. ir. Sybrand
van der Zwaag and Dr. P.E.J. Rivera-Díaz-del-Castillo

List of Publications

Journal

- **Suresh Neelakantan**, D. San Martin, J. Chao, P.E.J. Rivera-Díaz-del-Castillo and S. van der Zwaag: Temperature Dependence of Stress Induced Martensite Formation in a Metastable β Ti-10V-2Fe-3Al alloy. *Scripta Materialia*, to be submitted.
- **Suresh Neelakantan**, P.E.J. Rivera-Díaz-del-Castillo, S. Malinov and S. van der Zwaag: Comparison of Thermodynamic and Neural Network Predictions of M_s in Ti alloys. *Scripta Materialia*, to be submitted.
- **Suresh Neelakantan**, P.E.J. Rivera-Díaz-del-Castillo and S. van der Zwaag: Design of Titanium Alloys Showing Plasticity Induced Transformation, *Advanced Materials Research*, 2010, 89-91, pp. 405-410.
- **Suresh Neelakantan**, P.E.J. Rivera-Díaz-del-Castillo and S. van der Zwaag: Prediction of the Martensite Start Temperature for β Titanium Alloys as a Function of Composition, *Scripta Materialia*, 2009, 60 (8), pp. 611-614.
- **Suresh Neelakantan**, D. San Martin, P.E.J. Rivera-Díaz-del-Castillo and S. van der Zwaag: Plasticity Induced Transformation in a Metastable β Ti-1023 Alloy by Controlled Heat Treatments, *Materials Science and Technology*, 2009, 25 (11), pp. 1351-1358.

Conference

- **Suresh Neelakantan**, P.E.J. Rivera-Díaz-del-Castillo and S. van der Zwaag: Thermodynamic design of ultra-strong Ti alloys undergoing plasticity induced martensitic transformations, Proceedings of TMS 2010 Annual Meeting and Exhibition, Seattle, USA, February 14-18, 2010, pp.203-210.
- **Suresh Neelakantan**, P.E.J. Rivera-Díaz-del-Castillo and S. van der Zwaag: Design of highly formable and strong titanium alloys through plasticity induced transformation, Proceedings of TMS 2008 Annual Meeting and Exhibition, Volume I: Mechanical behavior, microstructure, and modeling of Ti and its alloys, New Orleans, USA, March 9-13, 2008, pp. 357-362.
- **Suresh Neelakantan**, M. Rijs, P.E.J. Rivera-Díaz-del-Castillo, D. San Martin and S. van der Zwaag: Ductility optimization through plasticity induced martensitic transformation in Ti-10V-2Fe-3Al and Ti-5Al-2Sn-4Zr-4Mo-2Cr-1Fe alloys, Proceedings of Ti-2007 science and technology, The Japan Institute of Metals, Kyoto, Japan, June 3-7, 2007, pp. 575-578.
- P.E.J. Rivera-Díaz-del-Castillo, P. Di Napoli, **Suresh Neelakantan**, and S. van der Zwaag: Phase kinetics modelling of titanium alloys undergoing plasticity induced transformation, Proceedings of Ti-2007 science and technology, The Japan Institute of Metals, Kyoto, Japan, June 3-7, 2007, pp. 479-482.